PhD degree in Medical Nanotechnology

European School of Molecular Medicine (SEMM)

University of Milan

Faculty of Medicine

Settore disciplinare: FIS/03

DESIGN OF VASCULARIZABLE SCAFFOLDS FOR LARGE TISSUE ENGINEERING

Alessandro Tocchio

IFOM-IEO Campus, Milan

Matricola n. R08886

Supervisor: Prof. Paolo Milani

University of Milan, Milan

Anno accademico 2012-2013

Design of vascularizable scaffolds for large tissue engineering

Alessandro Tocchio

Ph.D. thesis in Medical Nanotechnology
European School of Molecular Medicine, Milan, Italy
Università Degli Studi Di Milano, Milan, Italy
February 2014

Supervisor: PAOLO MILANI
Internal Co-supervisor: CRISTINA LENARDI
External Co-supervisor: IVAN MARTIN

The research in this thesis was carried out from 2010 until 2014 in the research group Advanced Biomaterials of the Fondazione Filarete for Biosciences and Innovation in collaboration with The Interdisciplinary Centre for Nanostructured Materials and Interfaces (CIMAINA) of the University of Milan.

Table of Contents

General introduction

Alessandro Tocchio[1,2]

[1]Fondazione Filarete, Viale Ortles 22/4, 20139 Milano, Italy; [2]SEMM, European School of Molecular Medicine, Campus IFOM-IEO, Via Adamello 16, 20139 Milano.

Background

The emerging field of tissue engineering is dedicated to restore, maintain or improve the functions of damaged or lost human tissues [1]. Current tissue engineering approaches include: i) the use of cells isolated from the patient and then injected in a desired location of the body, ii) the use of injected or implanted biomaterials and iii) their combination to create *in vitro* functional tissues to be used as transplants or *in vitro* test systems [2, 3]. In the latter, cells are firstly isolated from the patient and subsequently expanded in-vitro. When the sufficient amount of cells is reached, they are seeded and cultured on a biomimetic scaffold in a controlled culture environment. Once the construct become mature, it is implanted in the desired site of the patient's body to complete the tissue regeneration [4]. In this method the scaffold acts as a support for tissue growth and maturation both *in vitro* and when implanted *in vivo*, degrading as cells deposit their extracellular matrix [5]. However, despite significant successes have been achieved with this approach over the last 20 years, a number of challenges still remain, preventing a pervasive clinical application of tissue engineering [6,7]. Among all the scientific issues,

one of the main challenges is the development of biomaterials able both to support and guide cell growth, providing the appropriate biochemical and mechanical stimuli for the specific engineered tissue [8,9]. Another key issue lays in the design of biomaterials with a complex three-dimensional architecture [5] able to match the requirements of hierarchical porosity and roughness, and which mimic the complexity of the *in vivo* milieu. A particular aspect of this problem is to overcome the mass transport limit by enabling the provision of sufficient nutrients to the engineered tissue, during *in vitro* growth, and enhancing the formation of blood vessels, after implantation [10]. In fact, any tissue that is more than a few 100 microns thick needs a vascular system because every cell requires to be close enough to capillaries to absorb the oxygen and vital nutrients that diffuse constantly out of these tiny vessels [7]. When this condition is not satisfied, cells quickly become irreparably damaged. Nowadays, only skin, cartilage and bladder grafts are successfully used in clinics [10–16] while cornea grafts are far ahead [17,18]. This is mainly thanks to their lower requirement for nutrients and oxygen that can be met by the host's vascularization. However, only few tissues can be successfully supplied via diffusion from distant blood vessel systems [19,20]. Indeed, this approach fails when applied to large and complex tissues [4]. This is due to the fact that the formation of new blood vessels is a slow phenomenon and the deficiency of nutrients supply rapidly causes widespread cell death in graft cores [21]. At present, diffusion limitation is reducing the size of the engineered tissues to smaller than clinically relevant dimensions. For this reason, overcoming the current inability to engineer tissue with controlled blood vessel systems architecture, mimicking the branched vascular system of the human body [22], is critical to create large and complex *in vitro* tissues [23] and to transfer tissue engineered constructs to the clinic [4,24,25].

Aim of study

In the light of this overview, it is evident that the main scientific challenge in tissue engineering lays in satisfying cellular demands both in terms of scaffolding materials, providing adequate biochemical and mechanical stimuli, and also in terms of three-dimensional architecture, mimicking the complex organization of natural cellular microenvironment. The aim of this PhD work, merging the study of novel biomaterials and the development of original micro and nanofabrication methods, is to create enabling technologies towards the design of innovative scaffolds for thick and complex tissues engineering.

Outline

In this work, customizable biocompatible hydrogels were combined with innovative fabrication approaches to engineer scaffolds with controlled chemical, mechanical and biological features and a hierarchical three-dimensional architecture. The abilities of these scaffolds to supply nutrient perfusion and mass transport, and to promote *in vitro* vascularization in large constructs are evaluated and discussed in detail.

In **Chapter 2** the design of novel RGD-mimetic poly(amidoamine) (PAA) based hydrogels with wide and controlled degradation rate and improved mechanical and biological properties for biomedical applications is presented. The results presented in this study indicate that PAA hydrogels are excellent biomaterials for the fabrication of tissue engineering scaffolds.

In **Chapter 3** PAA hydrogels were further investigated to design a novel photopolymerizable matrix for three-dimensional cell encapsulation and

microfluidic applications. The results support the use of PAA hydrogels as tunable and inexpensive biomaterials for the creation of complex cell-laden microengineered constructs.

In **Chapter 4** PAA hydrogels were fabricated in to macro porous foams with the aim to recreate the complex microarchitecture of natural extracellular matrix. An extensive screening of the biological, chemical and mechanical properties was performed. The results confirmed that macroporous PAAs hydrogels are able to support and enhance three-dimensional cell growth and can be considered an optimal scaffold for soft tissue engineering.

In **Chapter 5** the development of innovative fabrication approaches to engineer scaffolds with a perfusable microfluidic network is presented [28]. Branched microfluidic networks were embedded within hydrogel matrices through an innovative method based on sacrificial templates. Results demonstrated that perfused microfluidic networks are able to sustain the cell viability of murine fibroblast in the core of PAA hydrogel cell-laden constructs and, when seeded with endothelial cells, to form branched endothelialized networks.

In **Chapter 6**, there is a general review of the results obtained in this work.

The **Appendix** explores issues involved in technological transfer of nanomedicine products [29]. A detailed analysis of market, competitors and investors in the sector has been performed. This overview aims to help scientists, startup mangers and investors to understand the key dynamics and successful cases in the transfer of nanotechnology in medicine.

References

[1] Langer R, Vacanti JP. (May 1993). Tissue engineering. Science 1993;260(5110): 920–926.

[2] Korossis SA, Bolland F, Kearney JN, Fisher J, Ingham E. Topics in Tissue Engineering In: Ashammakhi N, Reis RL; 2005. Volume 2, chapter 8.

[3] Pallua N, Suschek CV. Tissue Engineering: From Lab to Clinic. Springer;2010.

[4] Atala A, Kasper FK, Mikos AG. Engineering Complex Tissues. Sci Transl Med 2012;4(160):160rv12.

[5] Lanza RP, Langer R, Vacanti JP. Principles of tissue engineering, San Diego: Academic Press; 2007.

[6] Viswanathan S, Joshi C. Regenerative Medicine: Challenges and Perspectives for Successful Therapies. Current Topics in Microbiology and Immunology 2013;367:101-112.

[7] Khademhosseini A, Langer R, Borenstein J, Vacanti JP. Microscale technologies for tissue engineering and biology, Proc Natl Acad Sci USA 2006;103(8):2480-87.

[8] Geckil H, Xu F, Zhang X, Moon S, Demirci U. Engineering hydrogels as extracellular matrix mimics. Nanomedicine 2010;5(3):469-484.

[9] Borenstein JT, Weinberg EJ, Orrick BK, Sundback C, Kaazempur-Mofrad MR, Vacanti JP. Microfabrication of three-dimensional engineered scaffolds. Tissue Engineering 2007;13(8):1837-44.

[10] Safran MR, Seiber K. The evidence for surgical repair of articular cartilage in the knee. J Am Acad Orthop Surg 2010;18(5):259–266.

[11] MacNeil S. Progress and opportunities for tissue-engineered skin. Nature 2007; 445(7130):874-880.

[12] MacNeil S. Biomaterials for tissue engineering of skin. Materials Today 2008;11(5):26–35.

[13] Clar C, Cummins E, McIntyre L, Thomas S, Lamb J, Bain L, Jobanputra P, Waugh N. Clinical and cost-effectiveness of autologous chondrocyte implantation for cartilage defects in knee joints: systematic review and economic evaluation. Health technology assessment 2005;9(47):1–82.

[14] Ruano-Ravina A, Diaz MJ. Autologous chondrocyte implantation: a systematic review. Osteoarthritis Cartilage 2006;14:47–51.

[15] Safran MR, Seiber K. The evidence for surgical repair of articular cartilage in the knee. J Am Acad Orthop Surg 2010;18(5):259–266.

[16] Atala A, Bauer SB, Soker S, Yoo JJ, Retik AB. Tissue-engineered autologous

bladders for patients needing cystoplasty. Lancet 2006;367(9518):1241-46.

[17] Parikumar P, John S, Senthilkumar R, Manjunath S, Baskar S, Haraguchi K, Abraham S. Successful transplantation of in vitro expanded human corneal endothelial precursors to corneal endothelial surface using a nanocomposite sheets, J Stem Cells Regen Med 2011;7(2):94.

[18] ClinicalTrials.gov Identifier: NCT01765244. Allogeneic Tissue Engineering (Nanostructured Artificial Human Cornea) in Patients With Corneal Trophic Ulcers in Advanced Stages, Refractory to Conventional (Ophthalmic) Treatment.

[19] Santos MI, Reis RL. Vascularization in bone tissue engineering: physiology, current strat- egies, major hurdles and future challenges. Macromol Biosci 2010;10(1):12-27.

[20] Lovett M, Lee K, Edwards A, Kaplan DL. Vascularization strategies for tissue engineering. Tissue Eng Part B Rev 2009;15(3):353-370.

[21] Radisic M, Yang L, Boublik J, Cohen RJ, Langer R, Freed LE, Vunjak-Novakovic G. Medium perfusion enables engineering of compact and contractile cardiac tissue. Am J Physiol Heart Circ Physiol 2004;286(2):H507-H516.

[22] Novosel EC, Kleinhans C, Kluger PJ. Vascularization is the key challenge in tissue engineering. Advanced Drug Delivery Reviews 2011;63(4-5):300–311.

[23] Khademhosseini A, Vacanti JP, Langer R. Progress in tissue engineering. Sci Am 2009;300(5):64-71.

[24] Novosel EC, Kleinhans C, Kluger PJ. Vascularization is the key challenge in tissue engineering. Advanced Drug Delivery Reviews 2011;63(4-5):300–311.

[25] Laschke MW, Menger MD. Vascularization in tissue engineering: angiogenesis versus inosculation. Eur Surg Res 2012;48(2):85-92.

[26] Ferruti P, Bianchi S, Ranucci E, Chiellini F, Piras AM. Novel agmatine-containing poly(amidoamine) hydrogels as scaffolds for tissue engineering. Biomacromolecules 2005;6(4)2229-35.

[27] Martello F, Tocchio A, Tamplenizza M, Gerges I, Pistis V, Recenti R, Bortolin M, Del Fabbro M, Argentiere S, Milani P, Lenardi C. Poly(amidoamine)-based Hydrogels with Tailored Mechanical Properties and Degradation Rates for Tissue Engineering. Acta Biomaterialia 2014;10(3):1206–1215.

[28] Tocchio A, Lenardi C, Martello F. Method for producing three-dimensional monolithic microfluidic devices, WO 2012 164512.

[29] Morigi V, Tocchio A, Bellavite Pellegrini C, Sakamoto JH, Arnone M, Tasciotti E. Nanotechnology in medicine: from inception to market domination. J Drug Deliv 2012;389485.

Poly(amidoamine)-based hydrogels with tailored mechanical properties and degradation rates for tissue engineering

Alessandro Tocchio[a,b,1], Federico Martello[a,1] et al.

[a]Fondazione Filarete, Viale Ortles 22/4, 20139 Milano, Italy; [b]SEMM, European School of Molecular Medicine, Campus IFOM-IEO, Via Adamello 16, 20139 Milano, Italy; [1]These authors contributed equally to this work.

This chapter has been published: Martello F, Tocchio A, Tamplenizza M, Gerges M, Pistis V, Recenti V, Bortolin M, Del Fabbro M, Argentiere S, Milani P, Lenardi C. Poly(amidoamine)-based Hydrogels with Tailored Mechanical Properties and Degradation Rates for Tissue Engineering. Acta Biomaterialia 2014;10(3):1206–1215

1. Introduction

Hydrogels are defined as three-dimensional networks of hydrophilic polymers that are able to absorb up to hundreds of times its dry weight in water, thus acquiring biomechanical properties similar to the extracellular matrix (ECM) and allowing cells to adhere, proliferate and differentiate onto their surface. Several classes of hydrogels are characterized by excellent biocompatibility, minimal inflammatory reaction and tissue damage, which make them attractive materials for tissue engineering and regenerative medicine [1]. Hydrogels based on synthetic polymers, thanks to their versatility and low costs compared with natural biomaterials, have been successfully employed in a variety of biomedical applications,

ranging from ophthalmic and vascular prostheses to drug delivery and soft-tissue replacement [2-4]. In particular, hydrogels based on poly(2-hydroxyethylmethacrylate) (PHEMA) have shown to hold several advantages over other synthetic polymers [5]. Indeed, they display excellent biocompatibility *in vivo* and can be fabricated with different architectures and mechanical properties similar to natural tissue [6-9]. Even though PHEMA homopolymers cannot be degraded enzymatically or by acidic/alkaline solutions, copolymers containing HEMA were found to be biodegradable [8]. Another promising class of synthetic polymers for tissue engineering application are poly(amido-amine)s (PAAs) [10]. They are obtained by Michael-type addition of bis-acrylamides to primary amines and/or secondary diamines, under mild conditions. Different bioactive molecules can be incorporated in the PAA's backbone by covalent attachment during the synthetic process [11-13]. PAA-based hydrogels show good biocompatibility and are extremely versatile, being easily modifiable by introducing different comonomers that carry additional chemical functions such as carboxylic acids, thiols and amino groups [14-20]. Biological properties of synthetic materials can be further improved through surface/bulk modification with bioactive functional groups able to interact specifically with cell receptors [21,22]. For example, cell adhesion has been improved by introducing the tripeptide arginin-glycin-aspartic acid (RGD). The RGD motif is a structural element of many adhesion proteins, such as fibronectin, laminin, and vitronectin, which is specifically recognized by cell surface receptors, like integrins [23,24]. However, despite their good biological properties and low immunological reaction risk, RGD-modified hydrogels require complex synthetic procedure and high production costs [25]. To overcome these hurdles, Tanahashi and coworkers modified the surface of poly(propylene fumarate-co-ethylene glycol) hydrogels with 4-aminobutylguanidine (ABG)

units. Interestingly, he demonstrated that the increased fibroblast cell adhesion was related to the RGD-mimetic structure of the guanidine side groups [26]. The introduction of ABG units in a cross-linked amphoteric PAA hydrogel, as demonstrated by Ferruti and co-workers, resulted in an increased fibroblast cell adhesion [15]. However, PAA hydrogels displayed some drawbacks such as non controllable degradation rate, scarce mechanical properties and high risk of ruptures during hydrogel washing due to osmotic pressure [14-15, 27]. Since it has been demonstrated that the ABG residue in PAA hydrogels maintains cell adhesion promoting ability even when copolymerized with other monomers, we supposed that, by introducing HEMA as acrylic comonomer in the three-dimensional network, it would be possible to control degradation rate and enhance mechanical properties without hampering the cell adhesion efficiency [28]. Therefore, in order to develop reliable and effective supports for tissue engineering, we tested a library of PAA-based hydrogels, obtained by varying several synthetic parameters such as monomer ratio and reaction time (Fig. 1A and 1B). With the aim to improve mechanical properties and to control the degradation rate of PAAs hydrogels, PHEMA was grafted to PAA chains by free-radical polymerization. The obtained PAA-based hydrogels showed finely controllable degradation rate, high compressive strength, allowed a fast washing process and promoted cell adhesion and proliferation with MDCK cells.

2. Materials and Methods

2.1 Materials

4-aminobutylguanidine sulfate (ABG), ammonium persulfate (APS), 2-hydroxyethylmethacrylate (HEMA), 2-hydroxy-4-(2-hydroxyethoxy)-2-methylpropiophenone (HMP), lithium hydroxide monohydrate (LiOH),

hydrochloric acid (HCl), N,N-ethylendiamine (EDA), trichlorododecylsilane (TCS), and tetramethylethylenediamine (TEMED), potassium chloride (KCl), sodium chloride (NaCl), sodium phosphate dibasic (Na2HPO4), potassium phosphate monobasic (KH_2PO_4) were purchased from Sigma-Aldrich at the highest degree of purity available and used as received. Milli-Q grade water was used in all the experiments. The PBS buffer used in the experiments contained 2.69 mM KCl, 136.89 mM NaCl, 3.21 mM Na_2HPO_4, 1.47 mM KH_2PO_4. All solvents were purchased from Sigma Aldrich and used without further purifications. Finally, 2,2-bis(acrylamido)acetic acid (BAC) was prepared as previously reported and its purity (99.9%) determined both by acid-base titration and by NMR spectroscopy [29]. The reference PAA hydrogel was prepared according to literature (see “Preparation procedure for AGMA1-75 hydrogel”) [17].

2.2 Glass slide silanization and mold fabrication

Glass slides were silanized for fabricating cylindrical molds. Briefly, glass slides were washed with acetone, activated by plasma oxygen (70 W, 70 s) and immersed in a TCS solution (5% v/v in petroleum ether) for 10 minutes. Afterwards, glass slides were washed in succession with petroleum ether and ethanol, dried with gentle air flow and stored at room temperature (RT). Two types of mold were then prepared by interposing between two silanized glass slides a preformed silicone spacer of 0.3 or 1 mm thickness and 5 or 20 mm of internal diameter, respectively.

2.3 Synthesis of PAA (PAA-based hydrogels) and PAH (PAA-HEMA-based hydrogels) series

In a 50 mL round-bottom flask, BAC (1 eq), water, lithium hydroxide (1.2 eq) and ABG (specific amounts are reported in Table 1) are added in this order so as to obtain a BAC concentration of 3 mM. After 24 hours

stirring, 0.12 meq of APS (aqueous solution, 0.11 mM) was added in presence or absence of HEMA, to achieve PAH and PAA series, respectively. The resulting mixture was injected into the cylindrical mold, and allowed to react at RT for 24 hours. Then the hydrogels were recovered from the mold and washed (see "Hydrogel washing procedure" paragraph).

2.4 Synthesis of OPAA (PAA Oligomers-based hydrogels) and OPAH (PAA Oligomers-HEMA-based hydrogels) series

The mixture consisting of BAC, LiOH and ABG was prepared with the same procedure followed for PAA and PAH series (specific amounts are reported in Table 2), stirred for 72 h at RT, then diluted 1:50 with bi-distilled water and neutralized with 1.0 M hydrochloric acid. Subsequently, the solution was purified from unreacted BAC by ultrafiltration using a 1000 Da cut-off membrane until no sodium chloride was present in the eluates and subsequently freeze-dried (Telstar Cryodos 50). The purified PAA oligomers (yield, 70%) were dissolved in PBS buffer to obtain a 42% w/w oligomer concentration. The photoinitiator HMP (50% w/v in DMSO) was added to the oligomers solution to a final concentration of 0.5% (w/w) with or without HEMA, to achieve OPAH and OPAA series, respectively. The reacting mixture was stirred for 1 minute, injected in the glass mold and photopolymerized by exposure to long-wavelength UV light (365 nm, 10 mW/cm^2) for 7 min. Then the hydrogels were recovered from the mold and treated with the same procedure followed for PAA and PAH series. The oligomers' average molecular weight is shown in Table 2.

	ABG[a] [mmol]	HEMA[a] [mmol]	Reaction time[b]	Swelling ratio (%)
PAA 3a	0.25	-	3h	150%
PAA 3b	0.5	-	3h	170%
PAA 3c	0.9	-	3h	195%
PAA 24a	0.25	-	24h	210%
PAA 24b	0.5	-	24h	250%
PAA 24c	0.9	-	24h	263%
PAA 72a	0.25	-	72h	290%
PAA 72b	0.5	-	72h	340%
PAA 72c	0.9	-	72h	351%
PAH l3a	0.25	0.125	3h	148%
PAH l3b	0.5	0.15	3h	214%
PAH l3c	0.9	0.19	3h	227%
PAH l24a	0.25	0.125	24h	176%
PAH l24b	0.5	0.15	24h	256%
PAH l24c	0.9	0.19	24h	233%
PAH l72a	0.25	0.125	72h	190%
PAH l72b	0.5	0.15	72h	281%
PAH l72c	0.9	0.19	72h	257%
PAH m3a	0.25	0.313	3h	141%
PAH m3b	0.5	0.375	3h	155%
PAH m3c	0.9	0.475	3h	168%
PAH m24a	0.25	0.313	24h	164%
PAH m24b	0.5	0.375	24h	175%
PAH m24c	0.9	0.475	24h	179%
PAH m72a	0.25	0.313	72h	175%
PAH m72b	0.5	0.375	72h	182%
PAH m72c	0.9	0.475	72h	186%
PAH h3a	0.25	0.625	3h	124%
PAH h3b	0.5	0.75	3h	131%
PAH h3c	0.9	0.949	3h	143%
PAH h24a	0.25	0.625	24h	136%
PAH h24b	0.5	0.75	24h	146%
PAH h24c	0.9	0.949	24h	143%
PAH h72a	0.25	0.625	72h	149%
PAH h72b	0.5	0.75	72h	146%
PAH h72c	0.9	0.949	72h	166%

Table 1. Monomer molar amount, reaction specifications and swelling data related to PAA and PAH hydrogel series. [a]Starting reagent molar amounts related to 1 mmol of BAC. [b]Reaction time of the Michael-type addition reaction.

	ABG[a] [mmol]	HEMA[a] [mmol]	Oligomer[b] Mw/Mn	Swelling at 72h (%)
OPAA 1	0.515	-	1100/1000	235%
OPAA 2	0.724	-	2100/1900	290%
OPAA 4	0.852	-	4300/4100	363%
OPAA 8	0.923	-	8700/8200	416%
OPAH l1	0.515	0.242	1100/1000	219%
OPAH l2	0.724	0.276	2100/1900	275%
OPAH l4	0.852	0.296	4300/4100	338%
OPAH l8	0.923	0.308	8700/8200	378%
OPAH m2	0.724	0.552	1100/1000	240%
OPAH m4	0.852	0.593	4300/4100	325%
OPAH m8	0.923	0.615	8700/8200	343%
OPAH h2	0.724	0.845	1100/1000	205%
OPAH h4	0.852	0.907	4300/4100	279%
OPAH h8	0.923	0.942	8700/8200	330%

Table 2. Monomer molar amounts, reaction specifications, GPC and swelling data of OPAA and OPAH series. [a]Starting reagent molar amounts related to 1 mmol of BAC. [b]Purification has been carried out by ultrafiltration on 1000 Da cut-off membrane and subsequent freeze-drying.

2.5 Washing procedure of hydrogel slabs

In order to remove unreacted monomers and other impurities, hydrogel slabs were immersed in a water/ethanol solution under gentle stirring on an orbital shaker. The volume ratio of hydrogel to washing solution was 1:100. The washing solutions were different as a function of the hydrogel slabs to be purified. Reference PAA hydrogel: washing solutions were replaced after at least 3 hours using in sequence the following solutions: water/ethanol 6/4, 4/6, 3/7, 2/8, 1/9, ethanol 99% (twice),

water/ethanol 1/9, 2/8, 3/7, 4/6, 6/4, 7/3, 8/2, 9/1, bidistilled water (4 times). PAA series; washing solutions were replaced after at least 60 minutes using the same sequence of solutions indicated for the reference PAA hydrogel. PAH, OPAA and OPAH series; washing solutions were replaced after at least 60 minutes in the following order: water/ethanol 50/50, 25/75, ethanol 99% (twice), water/ethanol 25/75, 50/50, 75/25, bidistilled water (4 times). The wastewater resulting from the washing process was freeze-dried and the impurities recovered were analyzed by ^{1}H-NMR until no impurities were detected. The characterization of purified hydrogel slabs was performed within 24 hours after the last washing cycle.

2.6 Chemical characterization

Size exclusion chromatography (SEC) traces of PAA-based polymers were obtained with Toso-Haas 486 columns using 0.1 M Tris buffer pH 8.00±0.05 as a mobile phase, with a UV detector operating at 230 nm. Sample concentration: 10 mg/ml; flow rate: 1 ml/min. The molecular weight determination was based on pullulan standards. Proton nuclear magnetic resonance (^{1}H-NMR) spectra were run on a Bruker Advance 400 spectrometer operating at 400.132 MHz. Sample concentration: 30 mg of oligomer per mL of deuterium oxide (Sigma-Aldrich). ^{1}H-NMR spectra are given in the Supporting Information section. Fourier-transform infrared spectroscopy (FTIR) spectra of dry hydrogel samples were measured using a Jasco FTIR 300 spectrophotometer. Sample preparation: hydrogels disks of 0.3 mm height and 5 mm diameter were dried for 5 days under vacuum (10 mBar) and subsequently analyzed through an ATR-FTIR accessory with a Zn-Se crystal.

2.7 Mechanical characterization

The compressive strength was measured by using a testing machine equipped with a 100 N load cell (BR EMT503 A, MP Strumenti, Italy). The hydrogels were prepared by injection molding into 15 mm diameter, 15 mm height cylinders. Axial load was applied with a crosshead constant speed of 1 mm min-1 up to rupture. Six specimens of each sample were tested at 20 °C and 60% relative humidity.

2.8 Equilibrium swelling measurements

Hydrogels cylindrical slabs, having 0.5 cm diameter and 0.3 mm thickness, were previously dried at 20 °C and 0.1 Torr. Their weight was 40 mg ± 2 mg. Each specimen was placed inside a 10 mL tube containing 5 mL PBS (pH 7.0), incubated at 37 °C and weighed at regular intervals. The uptake of water was measured gravimetrically until the maximum mass was obtained. The percent amount of water absorbed was calculated using the following formula:

$$\text{Swelling (\%)} = W_t / W_d \times 100, \quad (1)$$

where W_t is the hydrogel sample's weight at time t and W_d is the weight of the dry sample at time zero.

2.9 Degradation study

Hydrogels cylindrical slabs having 0.5 cm diameter and 0.3 mm thickness, were placed inside a 10 mL test tube containing 5 mL PBS (pH 7.0) and incubated at 37 °C. At fixed time points they were freeze-dried and weighed. The percent degradation was calculated using the following:

$$\text{Degradation (\%)} = W_f / W_d \times 100, \quad (2)$$

where W_f is the dry weight at time t, W_d is described before.

2.10 Cell Culture

Madin-Darby Canine Kidney (MDCK) epithelial cells (NBL-2; ATCC) were maintained in Minimum Essential Medium with Earle's balanced Salts (MEM) supplemented with 10% fetal bovine serum (FBS), 2 mM L-glutamine, 100 units ml^{-1} penicillin, 100 µg ml-1 streptomycin, 1 mM pyruvic acid (sodium salt) in 5% CO2, 98% air-humidified incubator (Galaxy S, RS Biotech) at 37°C. Subcultures were routinely established every 48-72 h day.

2.11 2-D cell culture on hydrogel disks

MDCK (1.25 x 104 cells cm^{-2}) cells were seeded into 12 well plates containing UV-sterilized hydrogel discs (2 cm diameter and 1 mm thickness) containing dishes (12-24 wells) and were cultured for 24-48h monitoring their growth with an inverted microscope (Axiovert 40 CFL; Zeiss, Germany). Digital images were collected with an AxioCam ICm1.

2.12 Cell attachment/spreading assay

After 24 h, cells on discs were washed with PBS, fixed with 3% paraformaldehyde (15 minutes, RT), washed again and stained with BisBenzimide H 33258 (Hoechst) 5 µg/ml. Then, fluorescent nuclei digital images were collected (8 fields for disc, 10X) and their number was measured by ImageJ software.

2.13 Immunofluorescence staining

Experiments were performed after 48 hours from cell plating. Samples were fixed and immunostained for F-actin (the actin polymer form), vinculin (a membrane-cytoskeletal protein in focal adhesion plaques) and

nucleus. For cell staining we used the following: Monoclonal Anti-Vinculin primary antibody (clone hVIN-1), Alexa Fluor® 488 goat anti-mouse IgG1(γ1) secondary antibody (Invitrogen), Alexa Fluor® 555 phalloidin (Invitrogen) and nuclei were counterstained with DAPI (4'-6-Diamidino-2-phenylindole). Briefly, at room temperature cells were rinsed twice with PBS and fixed with 4% paraformaldehyde in PBS for 15 min; after washing, cells were treated with a permeabilization buffer containing 0.2% BSA (Albumin from Bovine Serum, Fraction V, Biochemical) and 0.1% Triton X-100 for 10 min, blocked with 2% BSA, stained with anti-vinculin, washed with 2% BSA, stained with Alex488-anti-mouse secondary antibody and Alexa555-phalloidin in 2% BSA for 45 min, washed twice in PBS and stained with DAPI. Samples were rinsed twice with PBS and mounted with Mowiol 4-88 (Calbiochem).

2.14 Cytotoxicity assay

MDCK (1.25 x 104 cells cm^{-2}) cells were seeded into dishes adding PBS recovered from hydrogels degradation test after 16 weeks and incubated at 37°C in 5% CO2 and 98% air-humidified for 48 h. Then a MTT colorimetric assay (Roche) for measuring enzymes activity was performed (see company data sheet for details). Formazane product absorbance (550 nm) was measured (Tecan sunrise).

2.15 Statistical Analysis

Each hydrogel type was tested at least 5 times with similar results. All data are expressed as 100*sample arithmetic mean/control arithmetic mean ± S.E.M.. Significance of differences was determined using Student's t-test ($p<0.05$).

3. Results

3.1 Hydrogel synthesis

In this work, four different series of amphoteric PAA hydrogels containing ABG as RGD-mimetic unit were prepared by a two-step synthesis. At first, a Michael-type addition was carried out in presence of ABG and an excess of BAC, to achieve diacrylamide-terminated homobifunctional PAA oligomers [30]. In the second step, the reaction mixture containing the PAA oligomers and unreacted BAC was polymerized by free-radical polymerization in presence or absence of HEMA, to obtain PAH (PAA-HEMA-based hydrogels) and PAA (PAA based hydrogels) series, respectively. Alternatively, PAA oligomers were purified from unreacted BAC by ultrafiltration, and then UV-induced photopolymerization was run either with or without HEMA, thus obtaining OPAH (PAA Oligomers-HEMA-based hydrogels) and OPAA (PAA Oligomers-based hydrogels) series (Fig. 1A).

The ratio of acrylic to PAA chains ratio was correlated to water uptake, degradation rate in physiological conditions, compressive strength and biological response with MDCK cells. Moreover, to assess the role of acrylic chains in the above-mentioned physico-chemical and biological properties of the synthesized hydrogels, a PAA hydrogel without acrylic chains was prepared according to the literature method and used as reference [17].

In order to study the effect of the PAA chains length in the hydrogel, diacrylamide-terminated homobifunctional PAA oligomers of controlled molecular weight ranging from 1000 to 8000 Da were synthesized by varying the amount of BAC added into the reaction mixture. The chemical structure of the synthesized oligomers was verified by ^{1}H-NMR

spectroscopy and FT-IR. The data related to monomers ratios, reaction time, GPC data and the equilibrium swelling of the PAA-based hydrogels obtained in the presence or absence of unreacted BAC are shown in Table 1 and 2, respectively.

In all preparations, the relative amounts of the monomers were adjusted in order to balance the total numbers of aminic hydrogens and the acrylamido functions. The main factors affecting the average molecular weight of the final oligomers are the reaction time and the ratio of the total numbers of aminic hydrogens with the acrylamido functions. The average molecular weight of the starting PAA oligomers is inversely proportional to the hydrogel's cross-linking degree [10].

The hydrogels' optical transparency was qualitatively evaluated to assess their suitability for *in vitro* experiments. The transparency was found higher by increasing the reaction time of the Michael-type addition step, the ABG/BAC ratio and the concentration of HEMA (Fig. 2). FT-IR analyses of dry hydrogels confirmed that the polymer composition was consistent with their ratio in the starting reagent mixture (data not shown).

A critical point in hydrogel preparation is the purification from unreacted monomers or other impurities. Usually, this step requires large amounts of water and time-consuming procedures, which can take more than 10 days. However, such an extensive extractions can cause hydrogels ruptures due to internal mechanical stress caused by swelling. In this study, the hydrogels synthesized showed an improved resistance to osmotic shock, allowing a fast washing process ranging from 2 (PAH, OPAA and OPAH series) to 3 working days (PAA series).

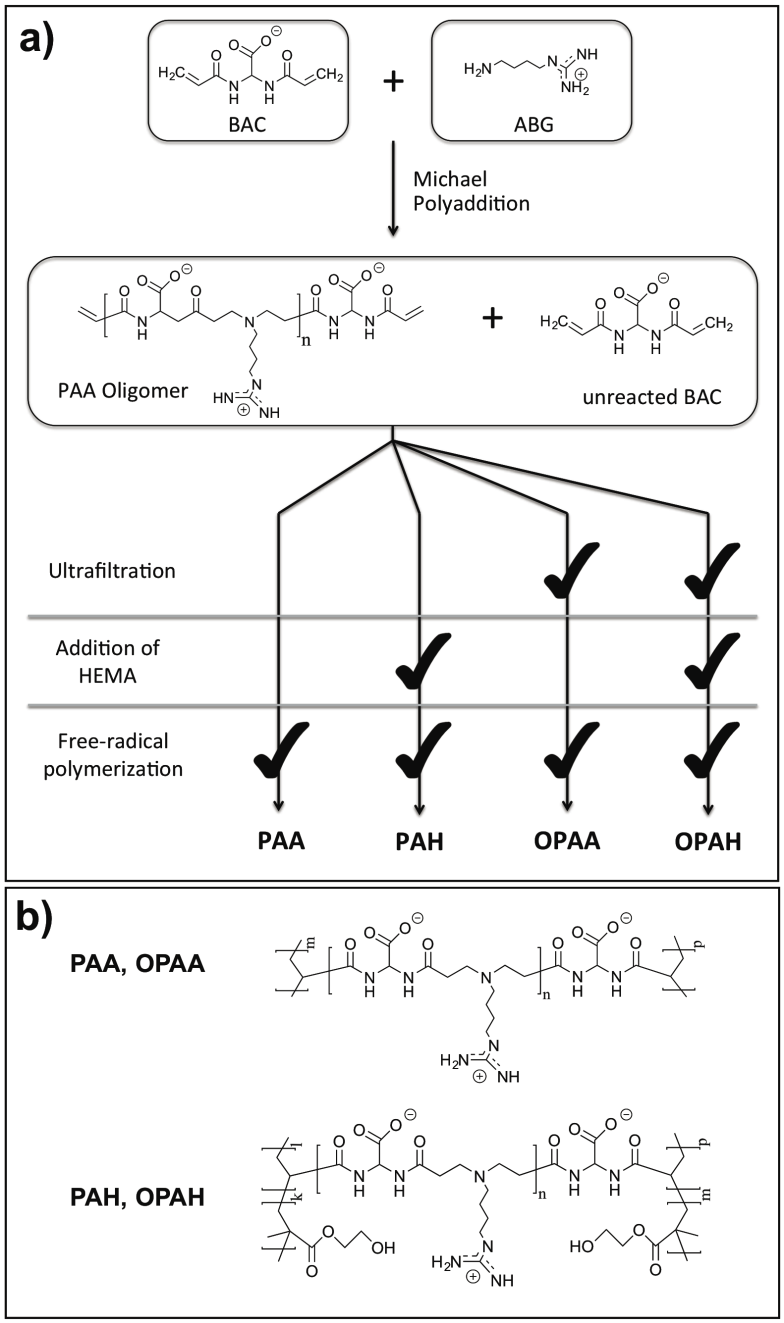

Figure 1. (a) Synthetic scheme of PAA, OPAA, PAH and OPAH hydrogel series [30]; (b) chemical structure of the synthesized hydrogels.

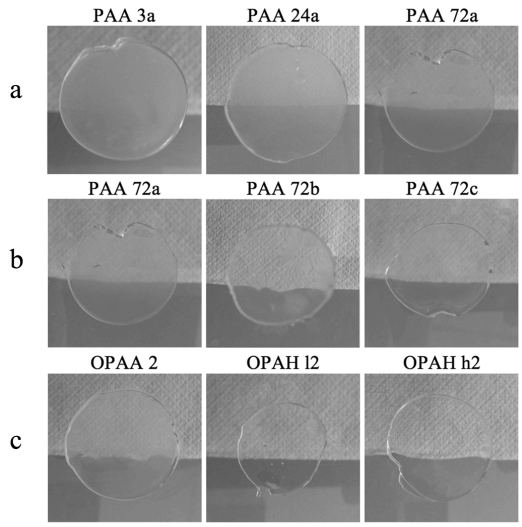

Figure 2. Comparison of the optical transparency of selected hydrogels as a function of the following parameters, increasing from left to right: (a) Michael-type addition reaction time, (PAA 3a, PAA 24a and PAA72a); (b) ABG/BAC molar ratio, (PAA 72a, PAA 72b and PAA 72c); (c) concentration of HEMA, (OPAA 2, OPAH l2 and OPAH h2).

3.2 Hydrogel characterization

The equilibrium swelling ratio was systematically examined as a function of the starting reagents composition (Table 1 and 2). As expected, the PAA and PAH hydrogels displayed a lower swelling ratio compared to OPAA and OPAH because of the higher degree of cross-linking. Further, the presence of HEMA generally decreased the swelling ratio, which could be due to the lower hydrophilicity of PHEMA compared to PAA chain. In confirmation of this, it was noted that PAH and OPAH series showed higher swelling ratio in ethanol, compared to PAA and OPAA series [31].

A major hurdle in the development of PAA hydrogels for tissue engineering is their brittleness when external forces are applied, especially during washing and handling steps [15,32]. The hydrogels synthesized in this study showed improved compressive strength, thanks to the presence of cross-linked acrylic chains within the three dimensional PAA polymeric

network. To assess the mechanical properties of the synthesized hydrogels compressive strength measurements were performed on selected samples representing the four developed hydrogels series and the reference PAA hydrogel lacking acrylic chains. As shown in Fig. 3, the compressive strength was clearly enhanced in all the PAA-based hydrogels compared to reference PAA hydrogel. The difference between PAA/PAH series and the OPAA/OPAH series is due to the different cross-linking density, since in the latter case the excess of unreacted bisacrylamide was removed by ultrafiltration, thus decreasing the number of bifunctional monomers in the reacting mixture and thus the degree of cross-linking. The inclusion of HEMA does not affect the rupture strain, whereas plays a key role in the compression strength, being negative for the PAH and positive for OPAH hydrogels. This is likely due to the fact that the mechanical behavior of the HEMA containing PAA hydrogels tend to approach those of pure PHEMA hydrogels [33].

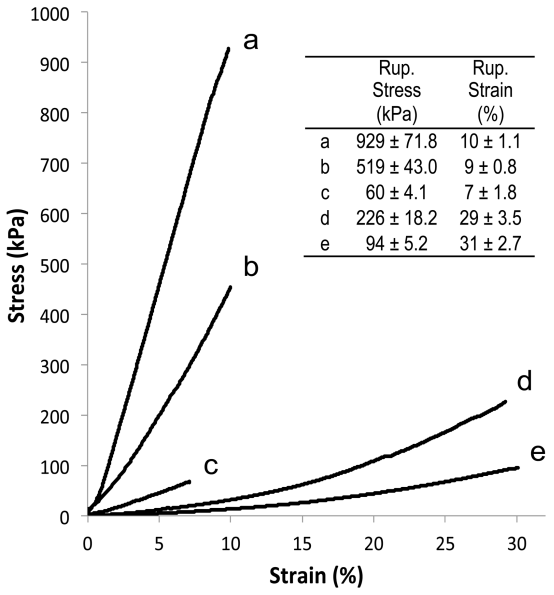

	Rup. Stress (kPa)	Rup. Strain (%)
a	929 ± 71.8	10 ± 1.1
b	519 ± 43.0	9 ± 0.8
c	60 ± 4.1	7 ± 1.8
d	226 ± 18.2	29 ± 3.5
e	94 ± 5.2	31 ± 2.7

Figure 3. Representative stress-strain curves of PAA 24a (a), PAH h24a (b), reference PAA hydrogel (c), OPAH h2 (d) and OPAA 2 (e). In the inset table, mean values of stress and strain at rupture point are presented ± standard deviation on six samples.

3.3 Degradation rate

The degradation rate was found to increase with the starting PAA oligomers' average molecular weight as expected due to PAAs' degradation mechanism involving hydrolytic cleavage of the amidic bond [10]. Moreover, the time required for a complete degradation was higher if compared to the reference PAA hydrogel lacking acrylic chains [15]. The PAA and PAH hydrogels displayed a lower degradation rate compared with OPAA and OPAH hydrogels (Fig. 4) because of their higher crosslinking density and the fact that the amides of the Michael-type adduct are more easily hydrolysable than those of the bisacrylamide itself. Interestingly, the degradation rate of OPAA and OPAH was high at the beginning (25-37% of the hydrogel dry weight lost in the first 20 days) and moderate in the following weeks, resulting in the range of 49-82% after six months.

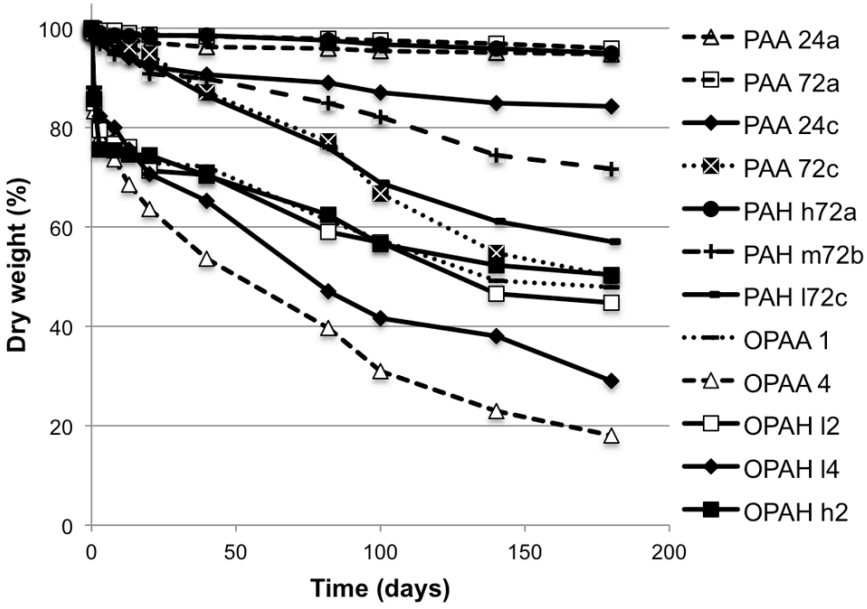

Figure 4. Degradation behavior over time of selected synthesized hydrogels representing PAA, PAH, OPAA and OPAH series (lines are added for clarity). Experimental data are presented as mean ± standard deviation.

On the contrary, the PAA and PAH showed a slower and more linear degradation rate, leading to loss of dry weight in the range 5% - 50% after six months. The presence of HEMA monomer units in the PAA polymeric network reduced the hydrogel degradation rate, which is consistent with the lower swelling degree of PAH/OPAH towards PAA/OPAA. Indeed the lower was the quantity of water absorbed by the macromolecular network the lower the degradation rate.

3.4 Biological behavior

To assess the adhesion and proliferation efficiency of the PAA-based hydrogels, Madin-Darby Canine Kidney (MDCK) cells were chosen as a model epithelial cell line. The hydrogels were seeded at a cell density of 10,000 cells cm^{-2} and observed for 96 hours, when generally confluence was reached. As shown in Fig. 5 and 6, all the tested hydrogels were shown to promote cell adhesion. Moreover, no toxic substances were released in the environment during cell culture, as a high number of viable cells was found adherent to the Tissue Culture Polystyrene (TCPS) well bottom. After 2 hours, cells on both the hydrogels and control glass appear to be mainly round and pearly. After 4 hours a substantial amount of cells on samples PAA 24b, PAH m24a, OPAA 1, OPAH l2 and control glass started to show a polygonal-like morphology typical of the phenotype of adherent MDCK cells. On the same hydrogels, at 24 and 48 hours after seeding, cells start to form a monolayer, which was already complete, whereas on the control glass it needed 72 hours to reach confluence. On all the remaining hydrogels confluence was reached after 72 to 96 hours. MDCK cells grown on the reference PAA hydrogel without acrylic chain exhibited modest adhesion and a proliferation comparable with the glass control (data not shown).

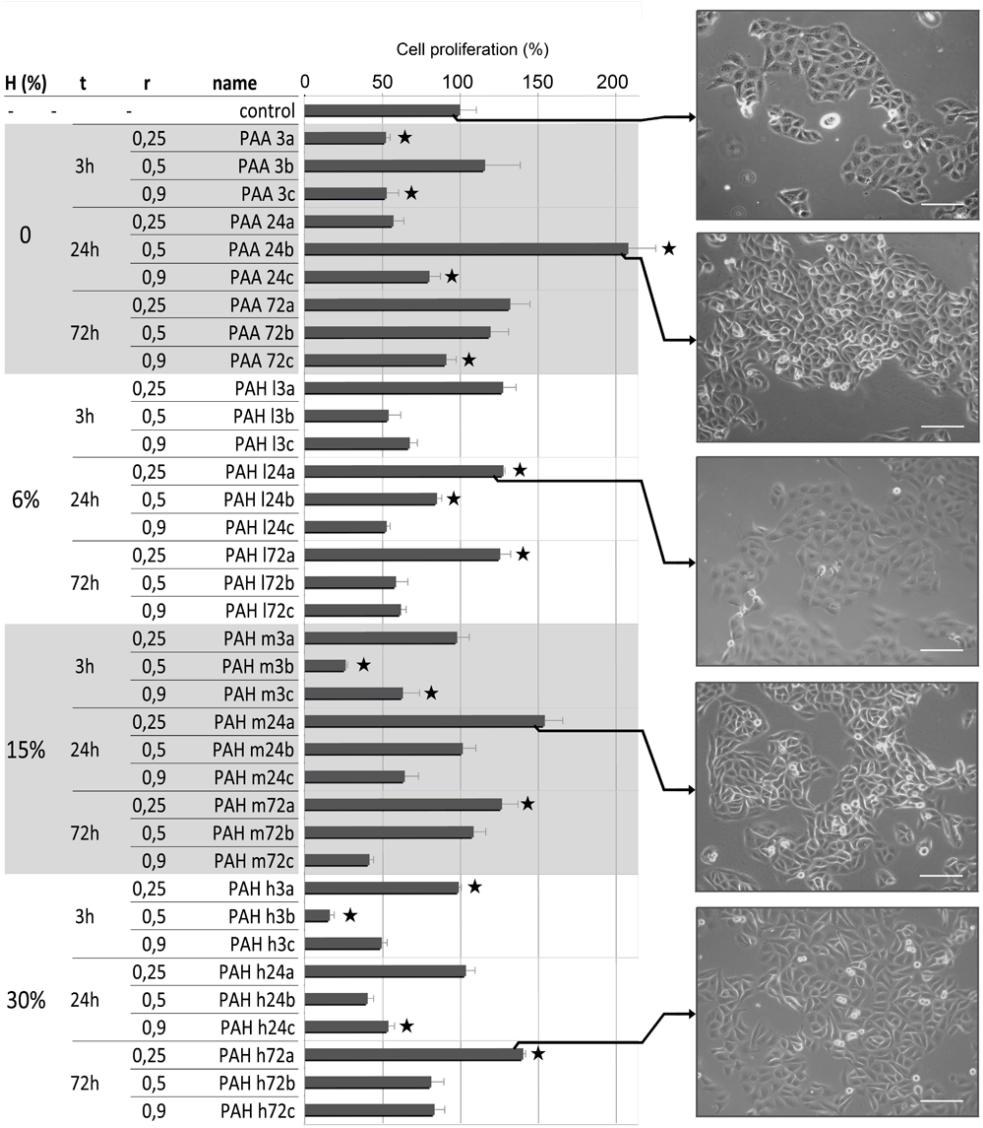

Figure 5. Cell proliferation at 48h after cell seeding of the PAA and PAH hydrogels series compared with glass control. In the table on the left side, "H" is the molar percentage of HEMA over the sum of BAC and ABG in the polymerizing mixture; "t" is referred to the reaction time of the Michael-type addition step; "r" is the ABG/BAC molar ratio. Horizontal bars are referred to the corresponding hydrogel in the table and represent the proliferation efficiency. The symbol "★" represents statistical significance by students T-test ($p<0.05$), comparing each sample against control. Optical images of the hydrogels with the highest proliferation at 48h are shown on the right side (scale bar, 150 μm).

Interestingly, the introduction of HEMA moieties seemed not to hamper the adhesion properties of PAA hydrogels. In particular, PAH hydrogels with r = 0.25 showed higher cell adhesion and proliferation compared to the sample with r = 0.5 and 0.9 for all the reaction time tested. Among all the tested hydrogels, PAA 24b displayed the highest proliferation; the hydrogels obtained after 48 and 72 h reaction time appear to perform generally better than those synthesized after 24 h reaction time. This could be related to the surface chemistry, whose changes depend on starting monomer ratio and the Michael-type addition reaction time [10].

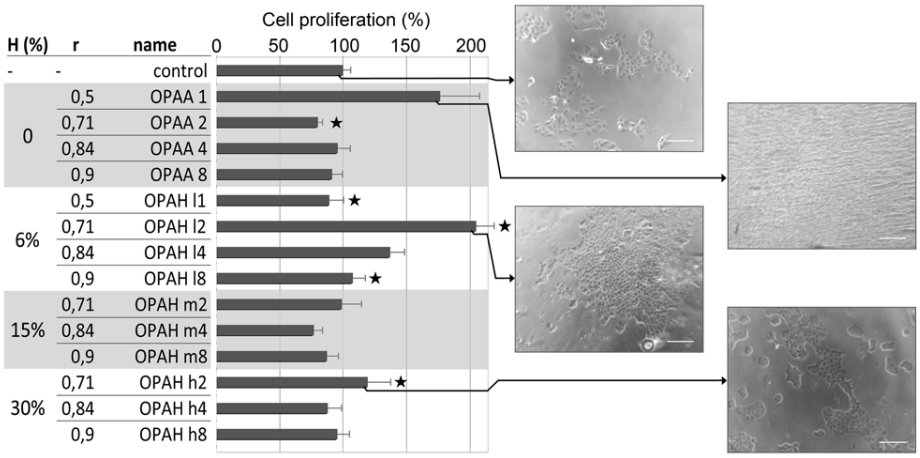

Figure 6. Cell proliferation efficiency at 48h after cell seeding of the OPAA and OPAH hydrogels series compared with glass control. In the table on the left side, "H" is the molar percentage of HEMA over the sum of BAC and ABG in the polymerizing mixture; "r" is the ABG/BAC molar ratio. Horizontal bars are referred to the corresponding hydrogel in the table and represent the proliferation efficiency as measured by MTT assay. The symbol "★" represents statistical significance by students T-test ($p<0.05$), comparing each sample against control. Optical images of the hydrogels with the highest proliferation at 48h are shown on the right side (scale bar, 150 μm).

On average, the OPAA and OPAH hydrogels showed a higher proliferation than the PAA and PAH hydrogels. The inclusion of HEMA chains into the OPAH hydrogels slightly improved the cellular adhesion and proliferation, with the exception of OPAH l1, showing lower proliferation than OPAA 1,

probably due to unfavorable effects of stiffness and surface chemistry (Fig. 6). The results obtained for OPAA and OPAH showed that the lower the starting oligomer's molecular weight, the higher was the cell proliferation. However, the cellular morphology seems to be somewhat rounded (Fig. 7). Finally, the cytotoxicity of the degradation products was measured by MTT assay. The MDCK cells were mixed with solutions retrieved from degradation tests after 16 weeks, and no evident toxicity of the degradation products was observed.

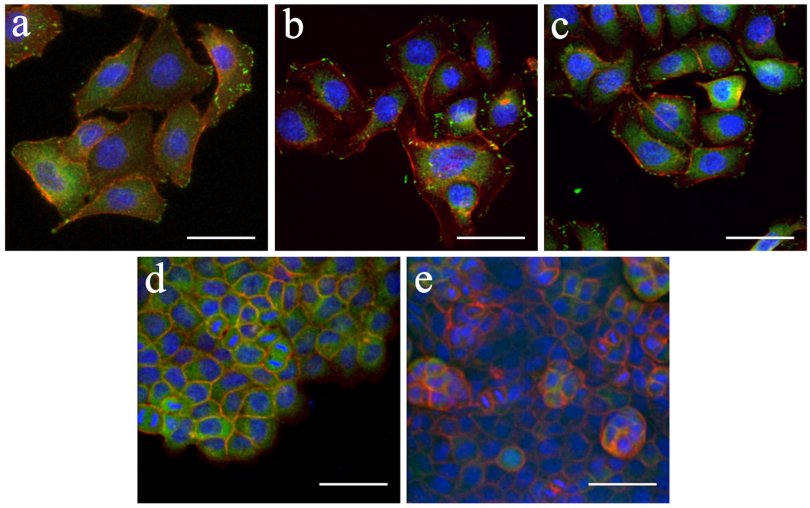

Figure 7. Adhesion complexes and actin organization of adherent MDCK cells after 48h from seeding on glass (a), PAA 24b (b), PAH I24a (c), OPAA 1 (d) OPAH I2 (e). Vinculin (green), actin (red) and nucleus (blue) fluorescent staining (scale bar, 50 μm).

4. Discussion

Here, a thorough investigation on the mechanical and biological properties of PAA-based hydrogel has been performed to design tailorable scaffolds for tissue engineering. Four different series of hydrogels were synthesized by varying the following parameters: reaction time of the Michael-type addition, ABG/BAC molar ratio and, only for PAH and OPAH

series, HEMA/(BAC+ABG) molar ratio. We investigated the effect of these experimental parameters on several hydrogel properties, including swelling degree, transparency, compressive strength, degradation rate, as well as cellular adhesion and proliferation. Based on the current knowledge on PAAs, both the ABG/BAC ratio and the Michael-type addition reaction time affect the average molecular weight of the PAA oligomers [10]. These oligomers were further reacted by radical polymerization to achieve hydrogels. The PAA oligomers' average molecular weight affected in turn surface chemistry and mesh size of the resulting hydrogels. The HEMA concentration in the polymerizing mixture was found to influence different features such as hydrophilicity, transparency and mechanical properties. The UV-induced photopolymerization was found to be successful in the preparation of OPAA and OPAH series, whereas PAA and PAH were obtained by redox-initiated polymerization. The photo-induction was ineffective for the latters probably because of the lower transparency of the starting liquid mixture. The synthesized hydrogels showed generally high versatility and excellent resistance to mechanical stress during washing steps, resulting in a faster washing process compared to reference PAA hydrogel. However, the hydrogel transparency was inversely proportional to the (HEMA + unreacted BAC)/PAA oligomers weight ratio before the radical polymerization step. This can be addressed to the phase separation following the appearance of acrylic chains in the polymerizing mixture [34]. We carried out a characterization of the mechanical properties by compressive strength measurement of selected samples representing the four studied hydrogel series in comparison with the reference PAA hydrogel. Thanks to the inherent mechanical properties of the acrylic chains within the polymer network, PAA-based hydrogels showed enhanced compressive strength and deformation capacity compared with

the reference PAA hydrogel. In particular, PAA and PAH hydrogels showed higher rupture load, whereas OPAA and OPAH displayed a much higher rupture strain compared to the reference PAA hydrogel, that is addressable to cross-linking density, which is, respectively, higher in the former and lower in the latter [35]. The equilibrium swelling degree was found inversely proportional to the HEMA/(BAC+ABG) ratio, due to the lower hydrophilicity of PHEMA chains. To assess the correlation between the acrylic-PAA chain balance and the degradability of the hydrogel, degradation tests of selected hydrogels representing the four studied series were carried out in physiologic environment at 37 °C. The degradation rate was found to be linearly dependent on the ratio of acrylic to PAA chains. Indeed, the higher the number of acrylic (i.e., non degradable) chains, the lower was the degradation rate. Accordingly, PAA and PAH hydrogels were characterized by lower degradation rate compared to OPAA and OPAH hydrogels. The mechanical and degradation tests demonstrated that it is possible to achieve a fine control of both compressive strength and degradation rate by varying the amount of BAC reacted in the radical polymerization. According to these results, the synthesized PAA-based hydrogels can match the requirements of different *in vitro* and *in vivo* applications, such us cell culture substrate, 3D matrix for tissue engineering and controlled drug release. Finally, extensive *in vitro* adhesion and proliferation tests with MDCK cells were carried out to correlate the biological properties with the investigated physico-chemical parameters. In particular cell proliferation onto the PAA-based hydrogels was up to 208% compared to glass control. By comparing the proliferation efficiency with the theoretical r ratio, it was evident that hydrogels with lower ABG/BAC ratio, showed better biological properties. This cellular response could be mainly due to the surface chemistry variation, with the contribution of stiffness variation. In fact, hydrogels

with higher cross-linking degree, which, at fixed ABG/BAC ratio, is higher for lower Michael-type addition reaction time, showed a poorer cellular proliferation. Interestingly, the presence of increasing concentration of HEMA did not result in decreased cell adhesion, despite the anti-fouling properties of PHEMA toward proteins, that could hinder the formation of an adequate protein substrate for cell adhesion [36]. This outcome enables the variation of HEMA concentration in PAA hydrogels to adjust transparency and mechanical properties, without hampering the optimal performances as substrate for cell culture.

	Compressive Strength	Transparency	Degradation rate	Swelling degree	MDCK Proliferation
PAA/PAH					
- r (ABG/BAC ratio)	↓	↑	↑	↑	↓
- reaction time	↓	↑	↑	↑	×
- HEMA/ (BAC+ABG) ratio	↓	↑	↓	↓	×
OPAA/OPAH					
- r (ABG/BAC ratio)	↓	↑	↑	↑	↓
- HEMA/(BAC+ABG) ratio	↑	↑	↓	↓	×

Table 3. Final assumptions on the observed correlations between the reaction parameters and the studied physico-chemical and biological properties. The symbol "↑" indicates direct proportionality; the symbol "↓" indicates inverse proportionality; the symbol "×" indicates that no linear relation could be determined between the variables.

The morphology after 48 hours of cells cultured on PAA and PAH hydrogels was similar to the control, whereas cells cultured on OPAA and OPAH were smaller and round shaped despite showing high proliferation. This could be explained by considering the difference in substrate stiffness between OPAA/OPAH and PAA/PAH hydrogels, that affects the cells spreading to the hydrogel's surface [37]. The complex inter-relation of monomers' ratios and reaction time with mechanical properties,

transparency, degradation rate, swelling degree and cellular proliferation are shown in Table 3.

5. Conclusions

The aim of the present study was to investigate the correlation of selected synthetic parameters such as monomer ratio, Michael-type addition reaction time and presence of various amounts of HEMA, to the physico-chemical and biological properties of the PAA-based hydrogels in order to develop a versatile platform for tissue engineering. Four series of innovative, biodegradable and biomimetic hydrogels based on poly(amidoamine)s with tailorable mechanical properties and degradation rate were successfully designed, synthesized and characterized. The introduction, through free-radical polymerization, of acrylic chains in the PAA macromolecular network improved cell adhesion and allowed the control of their mechanical properties and degradation rate. Even though the presence of PHEMA chains (up to 30%mol) in the PAA macromolecular network did not influence the adhesion and proliferation ability of the hydrogels, it was found to affect the swelling degree, the degradation rate and the mechanical properties, as well as to improve the transparency. Tailoring the swelling behavior may be useful for the application of PAA-based hydrogels as sensors or in microfluidics. Thanks to their mechanical properties, the PAA and PAH hydrogels seemed more suitable for *in vitro* culture and research purposes, whereas the OPAA and OPAH hydrogels would be more useful for *in vivo* applications as well as for cell encapsulation and hydrogel 3D printing applications, due to the mild conditions of the photopolymerization process and the higher degradation rate. Our results show that this class of hydrogels represents a very promising platform for the development of biomaterials and technologies for Tissue Engineering applications.

References

[1] Drury JL, Mooney DJ. Hydrogels for tissue engineering: scaffold design variables and applications. Biomaterials 2003;24(24):4337-51.

[2] Lee KY, Mooney DJ. Hydrogels for tissue engineering. Chem Rev 2001;101(7):1869-79.

[3] Mann BK. Biologic gels in tissue engineering. Clin Plast Surg 2003;30(4):601-609.

[4] Mather ML, Tomlins PE. Hydrogels in regenerative medicine: towards understanding structure-function relationships. Regen Med 2010;5(5):809-821.

[5] Montheard J, Chatzopoulos, M, Chappard, D. 2-hydroxyethylmethacrylate (HEMA) – Chemical Properties and Applications in Biomedical Fields. J Macromol Sci R M C 1992;32:1-34.

[6] Clayton AB, Chirila TV, Dalton PD. Hydrophilic sponges based on 2-hydroxyethyl methacrylate. 3. Effect of incorporating a hydrophilic crosslinking agent on the equilibrium water content and pore structure. Polym Int 1997;42(1):45-56.

[7] Dalton PD, Flynn L, Shoichet MS. Manufacture of poly(2-hydroxyethyl methacrylate-co-methyl methacrylate) hydrogel tubes for use as nerve guidance channels. Biomaterials 2002;23(18):3843-51.

[8] Atzet S, Curtin S, Trinh P, Bryant S, Ratner B. Degradable poly(2-hydroxyethyl methacrylate)-co-polycaprolactone hydrogels for tissue engineering scaffolds. Biomacromolecules 2008;9(12):3370-77.

[9] Filmon R, Grizon F, Basle MF, Chappaard D. Effects of negatively charged groups (carboxymethyl) on the calcification of poly(2-hydroxyethyl methacrylate). Biomaterials 2002;23(14):3053-59.

[10] Ferruti P, Marchisio MA, Duncan R. Poly(amido-amine)s: Biomedical applications. Macromolecular Rapid Communications 2002;23(5-6):332-355.

[11] Jain R, Standley SM, Frechet JMJ. Synthesis and degradation of pH-sensitive linear poly(amidoamine)s. Macromolecules 2007;40(3):452-457.

[12] Emilitri E, Ranucci E, Ferruti P. New poly(amidoamine)s containing disulfide linkages in their main chain. J Polym Sci Pol Chem 2005;43(7):1404-16.

[13] Lavignac N, Lazenby M, Franchini J, Ferruti P, Duncan R. Synthesis and preliminary evaluation of poly(amidoamine)-melittin conjugates as endosomolytic polymers and/or potential anticancer therapeutics. Int J Pharm 2005;300(1-2):102-112.

[14] Magnaghi V, Conte V, Procacci P, Pivato G, Cortese P, Cavalli E, Pajardi G, Ranucci E, Fenili F, Manfredi A, Ferruti P. Biological performance of a novel biodegradable

polyamidoamine hydrogel as guide for peripheral nerve regeneration. J Biomed Mater Res A 2011;98(1):19-30.

[15] Ferruti P, Bianchi S, Ranucci E, Chiellini F, Piras AM. Novel agmatine-containing poly(amidoamine) hydrogels as scaffolds for tissue engineering. Biomacromolecules 2005;6(4):2229-35.

[16] Lin C, Zhong Z, Lok MC, Jiang X, Hennink WE, Feijen J, Engbersen JF. Novel bioreducible poly(amido amine)s for highly efficient gene delivery. Bioconjug Chem 2007;18(1):138-145.

[17] Emilitri E, Guizzardi F, Lenardi C, Suardi M, Ranucci E, Ferruti P. Novel Poly(amidoamine)-Based Hydrogels as Scaffolds for Tissue Engineering. Macromol Symp 2008;266(1):41-47.

[18] Dos Reis G, Fenili F, Gianfelice A, Bongiorno G, Marchesi D, Scopelliti PE, Borgonovo A, Podestà A, Indrieri M, Ranucci E, Ferruti P, Lenardi C, Milani P. Direct Microfabrication of Topographical and Chemical Cues for the Guided Growth of Neural Cell Networks on Polyamidoamine Hydrogels. Macromol Biosci 2010;10(8):842-852.

[19] Martello F, Piest M, Engbersen JF, Ferruti P. Effects of branched or linear architecture of bioreducible poly(amido amine)s on their in vitro gene delivery properties. J Control Release 2012;164(3):372-379.

[20] Mauro N, Ranucci E, Procacci P, Laus M, Antonioli D, Mantovani C, Magnaghi V, Ferruti P. Degradable Poly(amidoamine) Hydrogels as Scaffolds for In Vitro Culturing of Peripheral Nervous System Cells. Macromol Biosci 2013;13(3):332-347.

[21] Chan WD, Goldberg HA, Hunter GK, Dixon SJ, Rizkalla AS. Modification of polymer networks with bone sialoprotein promotes cell attachment and spreading. J Biomed Mater Res A 2010;94(3):945-952.

[22] Shin H, Jo S, Mikos AG. Biomimetic materials for tissue engineering. Biomaterials 2003;24(24):4353-64.

[23] Zhang Z, Lai, YX, Yu, L, Ding, J. Effects of immobilizing sites of RGD peptides in amphiphilic block copolymers on efficacy of cell adhesion. Biomaterials 2010;31(31):7873-82.

[24] Massia SP, Hubbell JA. An RGD spacing of 440 nm is sufficient for integrin alpha V beta 3-mediated fibroblast spreading and 140 nm for focal contact and stress fiber formation. J Cell Biol 1991;114(5):1089-100.

[25] Ferruti P, Ranucci E, Trotta M. Biocompatible Polymers of Bisacrylamides and Aminoacids. PCT n°W02008152475 2008.

[26] Tanahashi K, Jo S, Mikos AG. Synthesis and characterization of biodegradable cationic poly(propylene fumarate-co-ethylene glycol) copolymer hydrogels modified with agmatine for enhanced cell adhesion. Biomacromolecules 2002;3(5):1030-37.

[27] Ferruti P, Bianchi S, Ranucci E, Chiellini F, Caruso V. Novel Poly(amido-amine)-Based Hydrogels as Scaffolds for Tissue Engineering. Macromol Biosci 2005;5:613–22.

[28] Franchini J, Ranucci E, Ferruti P, Rossi M, Cavalli R. Synthesis, physicochemical properties, and preliminary biological characterizations of a novel amphoteric agmatine-based poly(amidoamine) with RGD-like repeating units. Biomacromolecules 2006;7(4):1215-22.

[29] Ferruti P, Ranucci E, Trotta F, Gianasi E, Evagorou EG, Wasil M, Wilson G, Duncan R. Synthesis, characterisation and antitumour activity of platinum(II) complexes of novel functionalised poly(amido amine)s. Macromol Chem Physic 1999;200(7):1644-54.

[30] Franchini J, Ranucci E, Ferruti P. Synthesis, Physicochemical Properties, and Preliminary Biological Characterizations of a Novel Amphoteric Agmatine-Based Poly(amidoamine) with RGD-Like Repeating Units. Biomacromolecules 2006; 7:1215-22.

[31] Mukae, K, Sakurai M, Sawamura S Makino K Kim SW, Ueda I, Shirahama K. Swelling of poly(N-isopropylacrylamide) gels in water-alcohol (C1-C4) mixed-solvents. J Phys Chem-Us 1993;97(3):737-41.

[32] Jacchetti E, Emilitri E, Rodighiero S, Indrieri M, Gianfelice A, Lenardi C, Podestà A, Ranucci E, Ferruti P, Milani P. Biomimetic poly(amidoamine) hydrogels as synthetic materials for cell culture. J Nanobiotechnology 2008;6:14.

[33] Zhao W, Lenardi C, Webb P, Liu C, Santaniello T, Gassa F. A methodology to analyse and simulate mechanical characteristics of poly(2-hydroxyethyl methacrylate) hydrogel. Polym Int 2013;62:1059-67.

[34] Karpushkin E, Duskova-Smrckova, M, Remmler, T, Lapcikova, M, Dusek, K. Rheological properties of homogeneous and heterogeneous poly(2-hydroxyethyl methacrylate) hydrogels. Polym Int 2012;61(2):328-336.

[35] Guiseppi-Elie A, Dong C, Dinu CZ. Crosslink density of a biomimetic poly(HEMA)-based hydrogel influences growth and proliferation of attachment dependent RMS 13 cells. J Mater Chem 2012;22:19529-39.

[36] Goli KK, Rojas OJ, Genzer J. Formation and antifouling properties of amphiphilic coatings on polypropylene fibers. Biomacromolecules 2012;13(11):3769-79.

[37] Yeung T, Georges PC, Flanagan LA, Marg B, Ortiz M, Funaki M, Zahir N, Ming W, Weaver V, Janmey PA. Effects of substrate stiffness on cell morphology, cytoskeletal structure, and adhesion. Cell Motil Cytoskeleton 2005;60(1):24-34.

Biomimetic poly(amidoamine)-based hydrogel for 3D cell culture

Alessandro Tocchio[a,b,1] et al.

[a]Fondazione Filarete, Viale Ortles 22/4, 20139 Milano, Italy; [b]SEMM, European School of Molecular Medicine, Campus IFOM-IEO, Via Adamello 16, 20139 Milano, Italy;

1. Introduction

In recent years three-dimensional (3D) cell culture is receiving increased attention as a tool for *in vitro* biological experimentation [1]. In fact, researchers come to appreciate the different biological response between cells cultured in monolayer and 3D cell culture, more consistent to the environment in which cells physiologically operate [2,3]. In particular, as the complex relationships between cells and the extracellular matrix (ECM) *in vivo* plays a critical role in controlling their behavior and functioning [4], great efforts have been made to design synthetic ECMs, able to mimic the properties of the natural 3D cellular milieu, ensuring that cells cultured in vitro behave similarly to their counterparts *in vivo* [5]. The potential of 3D cell culture approach to create *in vitro* models, for toxicity/drug screening and disease or cellular studies [6,7], has encouraged the development of materials with controllable biological, chemical and mechanical properties [8,9], that are also able to recapitulate natural ECM microstructures, with the ultimate goal of achieving a precise control over cellular and tissue functions [5,10-13].

To this aim hydrogels have emerged as desirable biomaterial systems for guiding 3D cell behavior to specific functions [14]. Hydrogels offer numerous advantages such as high water content and biocompatibility. Naturally derived molecules were commonly used to create cell-laden hydrogels owing to their intrinsic bioactivity, biocompatibility, and biodegradability. In particular, cell-laden hydrogels have been created from a wide variety of native ECM molecules, including collagen [15], fibrin [16] [17], hyaluronic acid [18,19], Matrigel [20,21], and gelatin [22]. These biomolecules naturally contain cell-signaling attributes that enable high cellular viability and proliferation. Nevertheless, the same cues that allow cells to prosper in these materials are so abundant that become challenging to precisely control and assess their effects on cellular behavior. In addition, batch-to-batch variability generates hydrogels whose physico-chemical properties are difficult to reproduce and engineer [5]. This results in modest mechanical properties and in the inability to control their microarchitecture, limiting their use in the creation of durable cellular constructs. On the other hand, synthetic polymer-based hydrogels, in which the chemical and biophysical properties of the cell microenvironment can be easily tuned [8, 9, 12-14], are becoming increasingly attractive as 3D culture platforms. Poly(ethylene glycol) (PEG) is considered the gold standard for synthetic hydrogels thanks to its high hydrophilicity and its inert network resistant to protein adsorption [4,11]. However, the lack of cell-responsive features resulted in its inability to promote cellular proliferation and mobility, crucial for the creation of 3D organized cellular constructs. Modifications with binding motif Arg-Gly-Asp (RGD) [23-25], or physical mixing with ECM components [19], have been presented to increase cell adhesion and proliferation. PEG hydrogels, containing both cell binding RGD motifs and matrix metalloproteinase (MMP)-sensitive degradation regions [26-33],

have been shown to promote cell elongation, migration and interconnection *in vitro* with different cell lines. Their main drawback lies in the use of peptide sequences, which contribute to increase the cost and complexity of the synthesis and may weaken their micropatterning ability in comparison to unmodified photopolymerizable materials [22]. For these reasons, the use of PEG hydrogels is still limited to the creation of microscale *in vitro* tissue.

Another promising class of synthetic polymers for cell culture applications are poly(amidoamine)s (PAAs) [34]. They are obtained by Michael-type addition of bis-acrylamides to primary amines and/or secondary diamines, under mild conditions. Different bioactive molecules can be incorporated in the PAA's backbone by covalent attachment during the synthetic process [35-37]. PAA-based hydrogels show good biocompatibility and are extremely versatile, being easily modifiable by introducing different comonomers that carry additional chemical functions such as carboxylic acids, thiols and amino groups [38-43]. In order to improve cell adhesion properties of PAA hydrogels, Ferruti and co-workers developed an RGD-mimetic PAA with a repeating unit constituted by 2,2-bisacrylamidoacetic acid (BAC) and 4-aminobutylguanidine (ABG, Agmatine) [44]. The introduction of ABG units in a cross-linked amphoteric PAA hydrogel resulted in an increased fibroblast cell adhesion. However, PAA hydrogels displayed some drawbacks such as non-controllable degradation rate, poor mechanical properties and high risk of ruptures during washing due to osmotic pressure. Since it has been demonstrated that the ABG residue in PAA hydrogels maintains cell adhesion by promoting this ability even when copolymerized with other monomers, we supposed that, by copolymerizing the PAA-based ABG with Jeffamine® , it would be possible to obtain a hybrid hydrogel with optimal cell-adhesion and mechanical properties, avoiding the use of the

expensive RGD peptide. In this study, the synthesis of a new photocrosslinkable, biomimetic PAA-Jeffamine-PAA triblock copolymer (OAPAO) hydrogel is presented and its physico-chemical properties are extensively discussed. OAPAO hydrogel surface and 3D cell encapsulation behavior were deeply investigated. Additionally cell-laden OAPAO hydrogels were patterned with perfusable microchannels and seeded with endothelial cells, to investigate the potential use of OAPAO gels for micro tissue engineering applications.

2. Materials and Methods

2.1 Materials

4-aminobutylguanidine sulfate (ABG, agmatine), ammonium persulfate (APS), *O*,*O*′ - Bis (2 -aminopropyl) poly(propylene glycol)-*block*-poly(ethylene glycol)-*block*-poly(propylene glycol) with molecular weight of 600, 900 and 2000 (Jeffamine® 600, 900 and 2000, respectively), Poly(ethylene glycol) diacrylate 4000 (PEGDA), 2-hydroxy-1-(4-(hydroxyethoxy)phenyl)-2-methyl-1-propanone (Irgacure 2959, CIBA Chemicals), Dimethyl sulfoxide (DMSO), lithium hydroxide monohydrate (LiOH), hydrochloric acid (HCl), trichlorododecylsilane (TCS), and tetramethylethylenediamine (TEMED), sodium chloride (NaCl), sodium phosphate dibasic (Na_2HPO_4), potassium phosphate monobasic (KH_2PO_4) were purchased from Sigma-Aldrich at the highest degree of purity available and used as received. Milli-Q grade water was used in all the experiments. Phosphate buffered saline (PBS) used in the experiments contained 2.69 mM KCl, 136.89 mM NaCl, 3.21 mM Na_2HPO_4, 1.47 mM KH_2PO_4. Finally, 2,2-bis(acrylamido)acetic acid (BAC) was prepared as previously reported and its purity (99.9%) determined both by acid-base titration and by NMR spectroscopy [45].

2.2 Glass slides silanization and molds fabrication.

Glass slides were silanized for fabricating cylindrical molds. Briefly, glass slides were washed with acetone, activated by plasma oxygen (70 W, 70 s) and immersed in a TCS solution (5% v/v in petroleum ether) for 10 minutes. Afterwards, glass slides were washed in succession with petroleum ether and ethanol, dried with gentle air flow and stored at room temperature. Molds were then prepared by interposing between two silanized glass slides a preformed silicone spacer (0.3 and 1 mm thick). Into the preformed silicone spacers were previously cut void circles of internal diameter of 10 and 15 mm, respectively. The mold for microfluidic experiment was fabricated in a similar manner using two preformed silicone spacer of 1 mm thickness, cut to obtain a rectangular void area of 15X5 mm. In a different experimental setup a needle of 300 µm was placed between the two spacers.

2.3 PAA Oligomer synthesis

In a 50 mL round-bottom flask, BAC (200 mg, 1.0 mM), water (333 µL), lithium hydroxide (48.8mg, 1.14 mM) and ABG (for OPAA-2: 168.8 mg, 0.717 mM; for OPAA-4: 199.4 mg; for OPAA-6: 210.7 mg) were added in this order and the resulting mixture was stirred at 35°C for 7 days in the dark and under inert atmosphere. Afterwards, the mixture was diluted 1:50 with bi-distilled water and brought to pH 4.0 through addition of concentrated hydrochloric acid. The resulting solution was purified from unreacted BAC by ultrafiltration on membrane with a cut-off of 1000 (OPAA-2) or 3000 (OPAA-4 and OPAA-6) and subsequently freeze-dried (Telstar Cryodos 50). Yield: OPAA-2, 88%; OPAA-4, 82%; OPAA-6, 86%. GPC data: OPAA-2, Mn = 2100, d = 1.31; OPAA-4, Mn = 4300, d = 1.25; OPAA-6, Mn = 6400, d = 1.35. ^{1}HNMR spectra of all the synthesized oligomers showed the following characteristic peaks: ^{1}H NMR (400 MHz,

D_2O, 25°C, δ): 1.55 (br, $NHCH_2CH_2CH_2$), 1.71 (br, $NHCH_2CH_2$), 2.74 (br, $NHCOCH_2CH_2$), 3.13 (m, $NHCH_2$, NCH_2), 3.39 (br, $NHCOCH_2$), 5.51 (s, CHCOOH).

2.4 OAPAO oligomer synthesis

OAPAO diacrilamide terminated oligomers were synthesized by Michael-type addition of PAA to Jeffamine. In brief, in a 5 mL cuvette, PAA oligomers (600 mg, 0.3 mmol) water (884 µL), Jeffamine (for OAPAO-4, Jeffamine 500, 50.0 mg, 0.1 mmol; for OAPAO-5, Jeffamine 800, 80.0 mg, 0.1 mmol; for OAPAO-6, Jeffamine 2000, 195.0 mg, 0.1 mmol) and, only in the case of OAPAO-5 and OAPAO-6, 250 µL of ethylene glycol were added to improve reagents solubility. The pH of the resulting mixture was brought to 10.5 by addition of LiOH. The reactant solution was stirred at 35 °C for 24 hours under inert atmosphere and in the dark. The solution was then diluted 1:50 with bi-distilled water, acidified to pH 7.0 with a few drops of HCl (37 %), ultrafiltrated (5000 Da cut-off membrane) and freeze-dried. Yield: OAPAO-4, 87%; OAPAO-5, 70%; OAPAO-6, 57%.

2.5 Hydrogel preparation and characterization

Freeze-dried OAPAO and PEGDA oligomer was mixed into PBS. Irgacure 2959 (1000 mg/ml in 100% DMSO) was added, as a photoinitiator, to the hydrogel pre-polymer solution to yield final concentrations of 0.5% (w/v). The reacting mixture was stirred for 1 min, injected in the glass mold and photopolymerized by exposure to UV light (365 nm, 10 mW/cm^2) for 3 min. Then the hydrogels were recovered from the mold.

2.6 Chemical characterization

Size exclusion chromatography (SEC) traces of PAA-based polymers were obtained with Toso-Haas 486 columns using 0.1 M Tris buffer pH

8.00±0.05 as a mobile phase, with a UV detector operating at 230 nm. The molecular weight determination was based on pullulan standards. Proton nuclear magnetic resonance (^{1}HNMR) spectra were run on a Bruker Advance 400 spectrometer operating at 400.132 MHz. Fourier-transform infrared spectroscopy (FTIR) spectra of dry hydrogel samples were measured using a Jasco ATR-FTIR 300 spectrophotometer.

2.7 Mechanical characterization.

The compressive strength was measured using a testing machine equipped with a 100 N load cell (EMT503A, MP Strumenti, Pioltello (MI), Italy). Each measurement was run six times at 20 °C and 60 % relative humidity. Axial load was applied with a crosshead constant speed of 1 mm/min. The hydrogels were prepared 15 % (w/v) concentration by injection molding into 12 mm diameter, 7 mm height cylinders.

2.8 Swelling test

Hydrogels cylindrical samples, having 1.5 cm diameter and 0.3 cm thickness, were previously dried at 20 °C and 0.1 Torr. Their weight was 40 mg ± 2 mg. Each specimen was placed inside a 10 mL tube containing 5 mL PBS (pH 7.0), incubated at 37 °C and weighed at regular intervals. The uptake of water was measured until the maximum mass was obtained. The percent amount of water absorbed was calculated using the following formula:

$$\text{Swelling (\%)} = W_{wt} / W_d \times 100, \quad (1)$$

where W_{wt} is the water mass absorbed at time t and W_d is the mass of the dry sample at time zero.

2.9 Degradation test

Hydrogels cylindrical slabs having 1.5 cm diameter and 0.3 cm thickness, were placed inside a 10 mL test tube containing 5 mL PBS (pH 7.0) and incubated at 37°C. At fixed time point they were freeze-dried and weighed. The percent degradation was calculated using the following formula:

$$\text{Degradation (\%)} = W_f / W_d \times 100, \quad (2)$$

where W_f is the dry weight at time t, W_d is the mass of the dry sample at time zero.

2.10 Cell culture

NIH 3T3 murine embryonic fibroblasts (CRL-1658, ATCC, Manassas, Virginia) were kept at 37°C in 5% CO_2 98% air-humidified incubator. The cells were cultured in Dulbecco's Modified Eagle's Medium (DMEM) supplemented with 10% Fetal Bovine Serum (FBS), 2 mM L-Glutamine, 100 units/ml penicillin and 100 µg/ml–streptomycin. Once 80% confluent, the 25-cc flasks were passaged (subculture ratio 1:4 for multiple flasks) every 2-3 days for both experiments. Human umbilical vein endothelial cells (HUVECs) were obtained from PromoCell Gmbh (Heidelberg, Germany). The cells were cultured in M199 medium supplemented with 2 mM L-Glutamine, 100 units/ml penicillin and 100 µg/ml–streptomycin and freshly added with 20% FBS, 50 ng/ml ECGF and 100 µg/ml Heparin. In microfluidic experiments stable GFP expressing HUVECs (Pelobiotech, US) were used. They were perfused with endothelial cell growth media EBM-2 (Lonza) supplemented with EGM-2 singleQuot Kit Supplemets and Growth (Lonza), and they were used through passage 8. All products were purchased from Sigma Aldrich unless otherwise specified.

2.11 Cell adhesion

2-D cell culture on hydrogel discs.

3T3 and HUVEC (cell density: 10^4 cells/cm^2) cells were seeded on UV-sterilized hydrogel discs containing multiwell plate (24-48 wells) and incubated at 37°C in 5% CO_2 and 98% air-humidified. Cells were cultured for 24-48 h monitoring their growth with an inverted phase contrast microscope (Leica micro systems, Germany) equipped with a digital camera Leica DFC 295.

Cell attachment/spreading assay.

After 48h hydrogels discs cells were washed with PBS solution, fixed with 4% paraformaldehyde 15 minutes at room temperature, washed again with PBS and finally stained with BisBenzimide H 33258 (Hoechst) 5 µg/ml. Than, fluorescent nuclei digital images were collected with a Leica SP5 confocal microscope (5 fields for disc, 10x magnification zoom 2) and their number was measured by ImageJ software.

Fluorescence staining

After 48 h in culture, cells were fixed in situ with 4% paraformaldehyde, rinsed with PBS, permeabilized with 0.1% Triton X-100, blocked with 2% BSA and then incubated with Alexa fluor 555 directly conjugated to phalloidin, 0,11uM, (Invitrogen, Inc., Eugene, OR) for 40 min at room temperature for filamentous actin staining. After washing in PBS, cells were stained with Hoechst, 9.4uM. Images were captured along the channel length and channel depth (at 0.2–0.5mm depth intervals) using a Leica SP5 confocal microscope. All scaffolds were imaged through the glass cover slip wall. HUVEC cultured on gelatin-coated glass served as positive control.

2.12 Cell encapsulation

Murine fibroblasts were trypsinized, counted and suspended within PEGDA, OPAA-2 and OAPAO macromer solution containing 0.5% (w/v) photoinitiator at a concentration of $5x10^6$ cells/mL. Different macromer concentrations (5, 7.5, 10, 15% w/w) were tested. The cell-macromer solution was injected in the glass mold and photopolymerized by exposure to long-wavelength UV light (365 nm, 10 mW/cm^2) for 1 min. Agarose gel was used as a control. In this case low-melting point agarose was dissolved in sterile PBS (pH 7.4) to yield a final concentration of 2.5% (w/v) and heated to 70°C. NIH 3T3 fibroblasts were trypsinized, counted and suspended within the agarose solution at $5x10^6$ cells/mL that was cooled to ~42°C and pipetted to ensure even cell distribution. Agarose solution was injected in the glass mold and cooled to 4°C for 20 min. Hydrogels were then recovered from the mold and incubated in DMEM under standard culture conditions. Media was changed every 48 h. Murine fibroblast viability within the microgels was quantified by live/dead fluorescence assay (Calcein AM/Propidium Iodide, Life Technology) at different time points (0, 24, 48hours)

2.13 Microfluidic cell-laden hydrogel fabrication

To create perfusable microchannels, 200 mL of 15% (w/v) OAPAO-4 with 1% (w/v) of photoinitiator and containing $2x10^6$ cells/mL (NIH 3T3) was injected in the mold described in section 2.2. The mixture in the mold was evenly photopolymerized by exposure to long-wavelength UV light (365 nm, 10 mW/cm^2) for 1 min. The rectangular gel was then demolded and the needle was gently withdrawn. Perfusion studies were performed using fluorescent nanoparticles (Latex beads, amine-modified polystyrene, fluorescent blue aqueous suspension, 0.05 μm mean particle size) and connecting the microfluidic gel to a peristaltic pump

with small silicon tubing to enable perfusion. For cell perfusion experiments, 20 µl GFP-HUVECs suspension ($5x10^6$ cells/ml) was injected into the channel. Microfluidic gels were immersed in media and placed at standard cell culture conditions. To perform a dual-color live imaging labeled 3T3 cells were used and constructs were visualized with Leica SP5 confocal microscope incubator equipped.

2.14 Statistical Analysis

Each hydrogel type was tested at least 5 times with similar results. All data are expressed as 100*sample arithmetic mean/control arithmetic mean ± S.E.M.. Significance of differences was determined using Student's t-test ($p<0.05$).

3. Results

3.1 Hydrogel preparation

Diacrylamido-terminated PAA oligomers with average molecular weight of 2000 (OPAA-2), 4000 (OPAA-4) and 6000 Da (OPAA-6) were synthesized by Michael-type addition between BAC and ABG and subsequently purified by ultrafiltration and freeze-drying. In order to obtain an OPAA-Jeffamine-OPAA triblock copolymer with different molecular weights and terminated with acrylamide functions, the synthesized PAA oligomers were coupled through Michael-type addition with Jeffamine (Fig. 1). The coupling reaction successfully occurs only when OPAA-2 was coupled with Jeffamine. In fact, mixtures of Jeffamine with OPAA-4 and OPAA-6 allowed poor coupling reaction resulting in phase's separation in a wide pH and temperature range. Three different triblock copolymers (OAPAO-4, OAPAO-5 and OAPAO-6) with molecular weight of 4600, 4900 and 6000 Da, respectively, were produced. After ultrafiltration and freeze-drying, the

final triblock oligomer was photopolymerized through free-radical polymerization to yield degradable hydrogels for cell encapsulation with RGD-mimetic monomeric units.

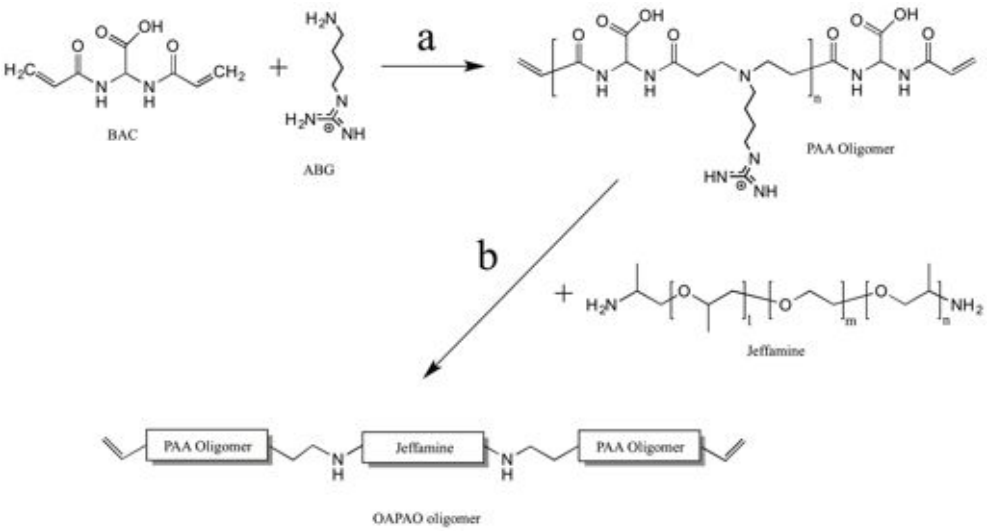

Figure 1. Synthetic scheme of the triblock diacrylamido-terminated (OAPAO) oligomer: a) water, 30°C, pH 9, inert atmosphere, 72h; b) water, 30°C, pH 10.5, inert atmosphere; 24h.

3.2 Mechanical properties

Mechanical properties of the extracellular environment have been shown to affect cell function and differentiation. To determine the effect of the oligomer's molecular weight on the mechanical properties of the OAPAO hydrogels, unconfined compression was performed on hydrogels of OAPAO-4, OAPAO-6 and the control PAA oligomers at the fixed concentration of 15% w/w. In general, increasing the molecular weight of the starting oligomer decreased stiffness and compressive modulus, due to lower crosslinking density. As illustrated in Figure 2a, hydrogels obtained from OAPAO are characterized by higher compressive elastic modulus (E') than those obtained from diacrylamide-terminated PAA

oligomers of the same average molecular weights. Such a characteristic is much evident in the case of OAPAO-4 hydrogels, where the elastic modulus was five times higher than the control hydrogel obtained from OPAA-4 oligomers. Following the same tendency, load failure was found to be higher for OAPAO-4 hydrogels (9.2 N) than OPAA-4 control (3.5 N). The enhanced elastic behavior of OAPAO hydrogels, compared to the control, underline the role that PEG segments play in the contrast of non-covalent interaction among PAA macro-domains, which is the main reason for PAA hydrogels fragility.

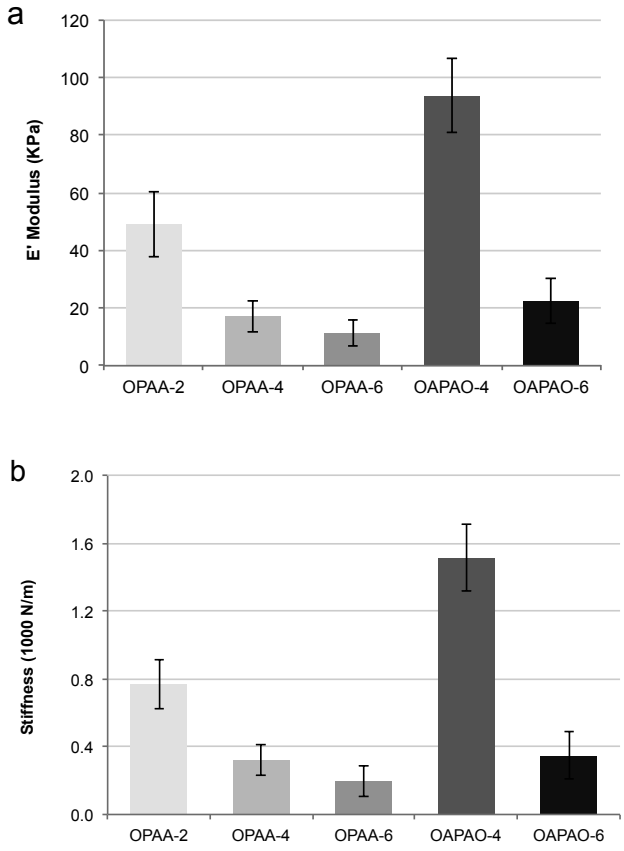

Figure 2. Compressive modulus (a) and stiffness (b) of the synthesized hydrogels. Error bars represent the SD of measurements performed on at least 3 samples.

3.3 Swelling and Degradation characteristics

The swelling characteristics of a polymer network are important in various applications as they affect solute diffusion, surface properties, mechanical properties, and surface mobility. The degree of gel swelling is dependent on the pore size of the polymer network and the interaction between the polymer and the solvent. As hydration can have a substantial effect on the physical properties of the resultant hydrogel, e.g. the replication fidelity of the desired micropattern, the change in the mass to swelling ratio of OAPAO was investigated relative to the hydrogel concentration. Hydrogels were made as described previously at 15% (w/v) OAPAO. Hydrogels were allowed to reach equilibrium over a 24 h incubation period in PBS at room temperature, then the mass swelling ratio of the swollen mass to the dry mass of polymer and the degradation rate in PBS at 37°C was calculated. Measured mass swelling ratio was 264 ± 2% for OPAA-2, 405 ± 5% for OAPAO-4 and 380 ± 5% for OAPAO-6. These data shows a higher mass to swelling ratio of OAPAO compared to OPAA-2, demonstrating that the conjugation Jeffamine had a significant effect on the material's ability for storing water within the polymer network. The degradation rate was higher for OAPAO hydrogels than for control OPAA-2 hydrogel, consistently with the higher swelling ratio of the studied polymers (Fig. 3). The degradation rate was found to increase with the oligomers' average molecular weight. In fact, among the OAPAO hydrogels, OAPAO-4 showed the highest rate of degradation reaching 45% of weight loss after approximately 120 days.

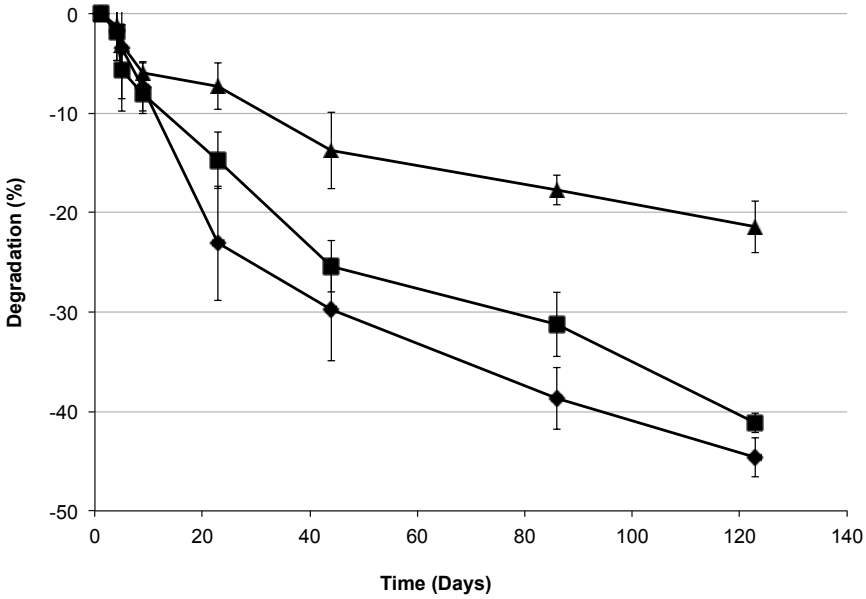

Figure 3. Degradation curves of 15% (w/v) OAPAO-4 (squares), OAPAO-6 (diamonds) and control OPAA-2 hydrogels (triangles).

3.4 3T3 Cell adhesion to 2D OAPAO surfaces

The ability of a scaffold to promote cell binding strongly affects cell behavior and is an essential requirement in tissue engineering [46]. In order to validate the use of OAPAO hydrogels for potential application in tissue engineering, we measured their cell adhesion properties using murine fibroblasts as a model cell type. Fibroblast adhesion was determined on different OAPAO hydrogels fixing the concentration at 15% (Fig. 4a) and 30% (w/v) (Fig. 4b) and varying the macromer molecular weight or increasing the concentrations at 7.5%, 10%, 15%, and 30% (w/v) at fixed molecular weight (Fig. 4c). Changes in the molecular weight of the OAPAO macromer was obtained by combining Jeffamine with increasing molecule weight to the same PAA oligomers. Cell adhesion was also investigated on pure PAA oligomers, PEGDA hydrogel and glass.

Pure PAA and PEDGA hydrogels represented, respectively, the highest concentration and the absence of RGD-mimetic sites. Glass was used as positive control. 3T3 readily bound to OAPAO surfaces of all concentrations with roughly the same affinity following initial seeding but after 48h some differences emerged. In Figure 4a is shown that OPAA-2 had the best adhesiveness as expected for the RGD-mimetic binding sites abundance (more than 3 times compared to glass) followed by OAPAO-4 and OAPAO-5 (more than 2 times compared to glass) and OAPAO-6 (almost comparable to glass). As expected, few cells adhered to PEGDA surfaces, as PEG is not cell adhesive, and adhesion was observed to decrease over time (results not shown). Doubling macromer concentration of OAPAO-4 from 15% to 30% (w/v) improved the performances showing the best result on OAPAO hydrogels (Fig. 4b). Interestingly, OAPAO-5 was prevented in its performance and decreased to glass control values. In order to better evaluate the performances of OAPAO-4 we measured cell adhesion at different OAPAO concentration (Fig. 4c). This experiment showed that OAPAO-4 has much better or at least the same performance as control glass in all the concentrations tested. Overall, these results confirmed that OAPAO-4 is best hydrogel for 2D cell culture.

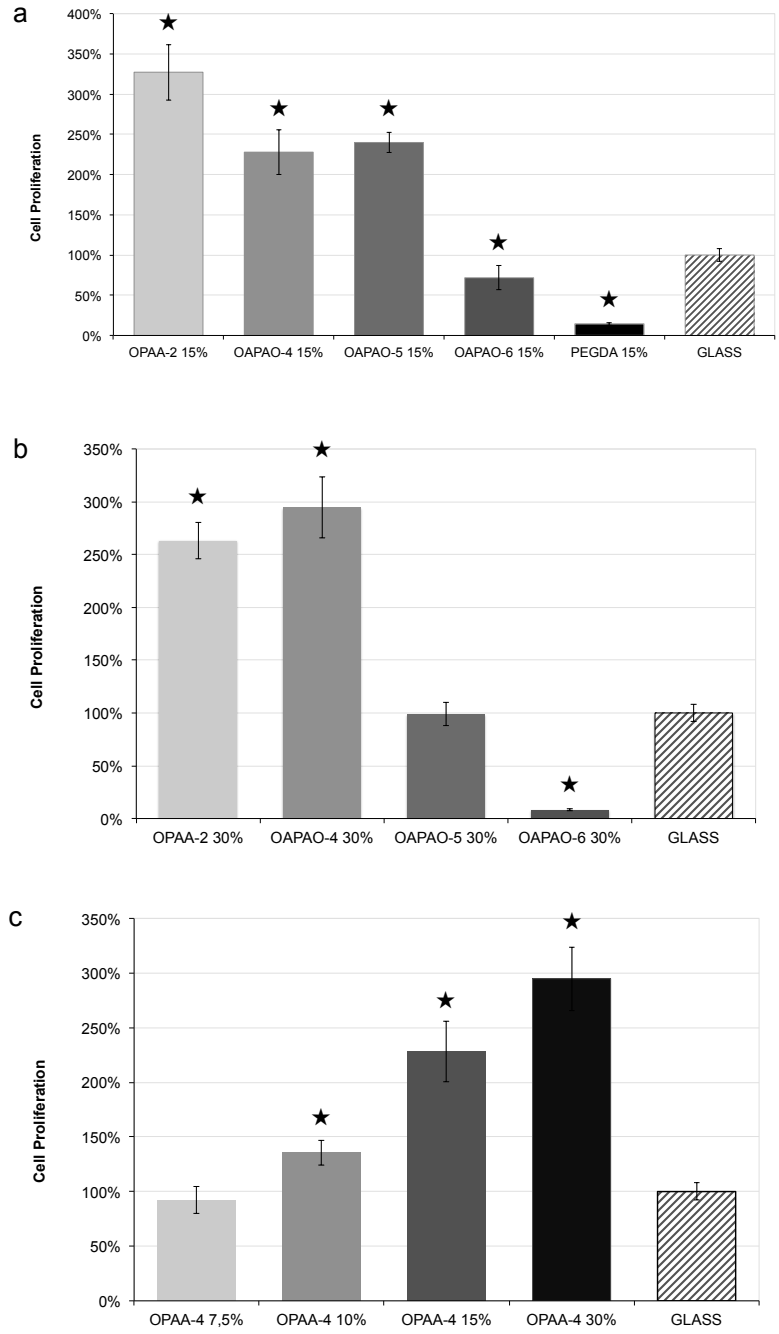

Figure 4. Cell proliferation values of 3T3 cells cultured for 48h on 2D hydrogels using glass slide as a control. The symbol "★" represents statistical significance by students T-test ($p<0.05$), comparing each sample against the control (GLASS).

3.5 HUVECs Cell adhesion to 2D OAPAO surfaces

Surface adhesion characteristics of OAPAO-4 were determined at 7.5%, 10%, 15%, and 30% (w/v) OAPAO-4 concentration (Fig. 5). The 4000 molecular weight was chosen as this formulation performed best in 3T3 cell adhesion experiments. HUVECs were chosen as a model cell type for potential application of OAPAO in vascularized tissue engineering, as well as to explore the compatibility of OAPAO with a human cell type.

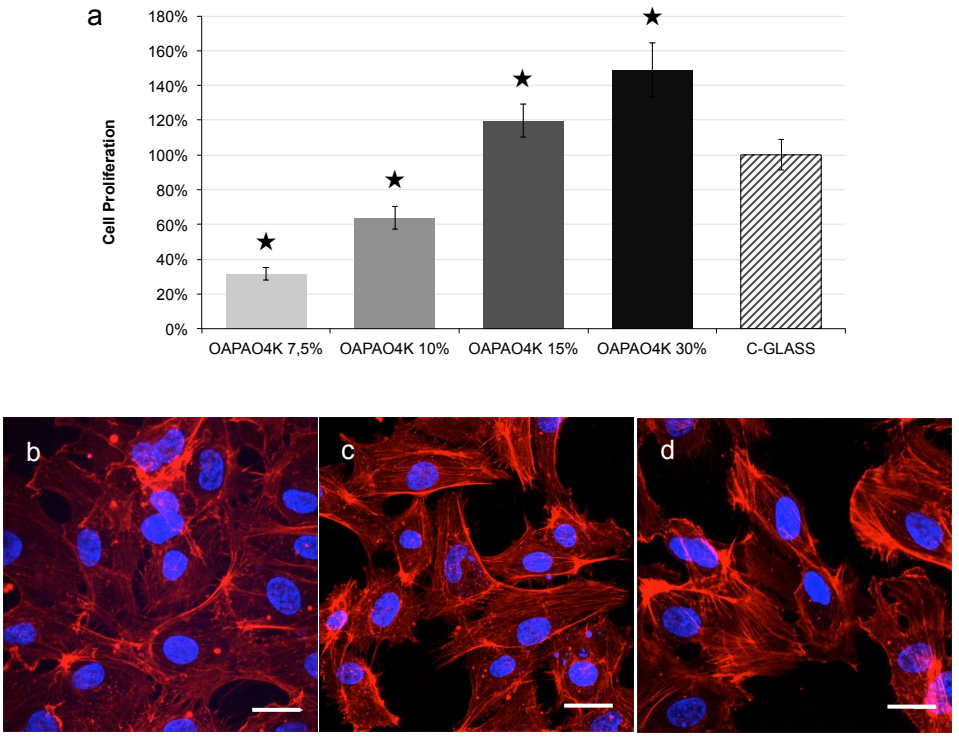

Figure 5. (a) Cell proliferation values of HUVECs cultured for 48h on 2D hydrogels of increasing OAPAO-4 concentration. The symbol "★" represents statistical significance by students T-test ($p<0.05$), comparing each sample against the control (C-GLASS). Confocal microscopy images of HUVECs conformation on OAPAO-4 at 15% (b) and 30% (w/v) (c) on glass (d) and (scale bar, 20μm).

Cells on OAPAO surfaces 15% and 30% attached and proliferated better than control, whereas on 10% and 7.5% less cells were found but still with a good morphology and viability (Fig. 5). Significant differences in the cell density, defined as the number of Hoechst positive cells per fixed area, demonstrated that cell density significantly increased with increased OAPAO concentration. These differences in cell behavior are likely due to a combination of variations in the stiffness of the OAPAO surfaces relative to the gel concentration, and increases in the density of bioactive sequences with increased macromer concentration.

3.6 3D cell encapsulation in OAPAO

To further demonstrate the use of OAPAO as a hydrogel for tissue engineering application, encapsulated cell behavior was studied within OAPAO hydrogel. In these experiments NIH 3T3 fibroblasts were encapsulated in 0.3 mm thickness and 10 mm diameter slab of OAPAO-4 at concentrations of 5%, 7.5%, 10% and 15% (w/v). OAPAO-4 gels performed similarly to PEG in terms of pattern replication accuracy and UV exposure time (data not shown). Viability at 4 h after encapsulation was 94 ± 1% in 5% OAPAO and 92 ± 1% in 7.5%, which were slightly higher than that in 10% (91% ± 1%) or 15% (91% ± 1%) (w/v) microgel samples. Initial viability was similar to that exhibited in agarose hydrogels (89 ± 3%), demonstrating that UV polymerization and micropatterning did not considerably alter cell viability. Consistently with these data, in previous works cell viability has been shown to decrease with macromer concentration in other hydrogel matrices [11,47]. This viability loss is due to encapsulation stress, nutrient limitations and swelling stress after polymerization. This behavior is more evident at 24 h when the viability was 85 ± 3% in 5% OAPAO-4 and 83 ± 3% in 7.5% OAPAO-4, which was higher than that in 10% (79% ± 3%) and 15% (72% ± 2%) (w/v) microgel

samples. Evolution of cell viability in bulk OAPAO until 15% was similar to the viability of agarose gel at all the time point whereas at more increased concentration showed reduced cell viability (Fig. 6f and g).

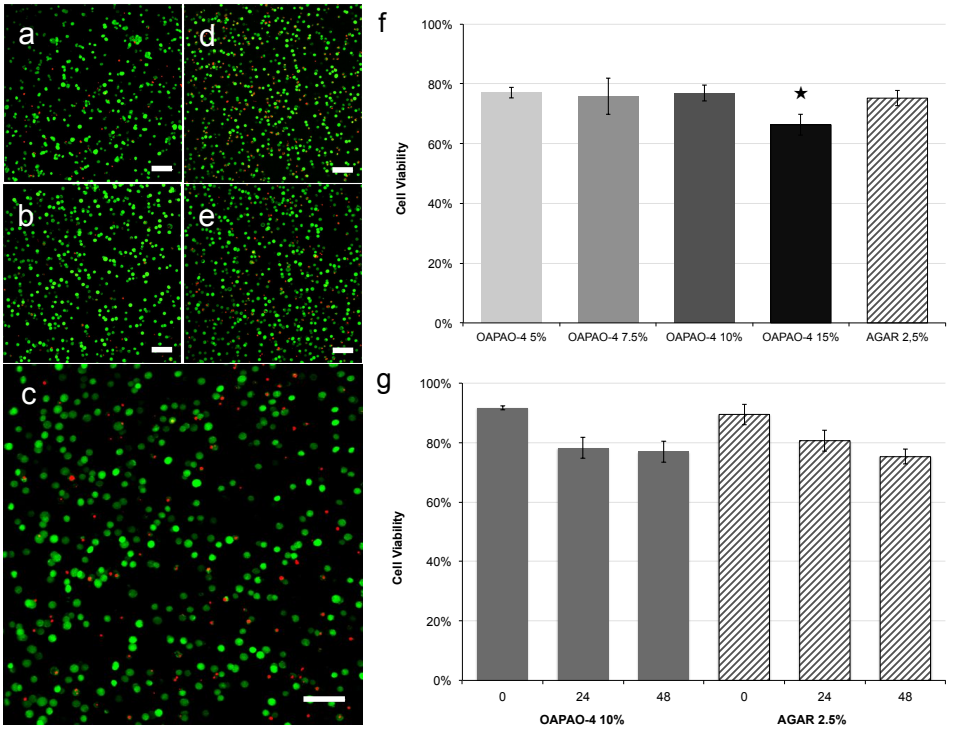

Figure 6. Characterization of encapsulated cell behavior. 3T3 fibroblasts embedded in OAPAO-4 at 5% (a), 7.5% (b), 10% (c), 15% (d) (w/v) and in agarose (e) microgel were stained with live/dead assay at 48 hours after encapsulation. Quantification of encapsulated cells cell viability for different OAPAO-4 concentration, at 48 hours (f) and different time points and fixed concentrations (g), demonstrated excellent cell survival at all conditions, compared to agarose. The symbol "★" represents statistical significance by students T-test ($p<0.05$), comparing each sample against the agarose control. Error bars represent the SD of averages obtained on 4 images from each of 6 independent samples per condition.

3.7 Endothelialized microfluidic channels in cell-laden OAPAO hydrogel.

To investigate the use of OAPAO for the creation of complex cell laden microengineered construct, labeled NIH 3T3 fibroblasts were embedded within microfluidic bulk OAPAO-4. In particular the mixture, containing

cells and macromers, was polymerized around a syringe needle, which, when removed, created a 300 μm perfusable channel in a cell-laden matrix (Fig. 7). In these experiment OAPAO-4 was used at 15% w/v concentration to reach an optimal compromise between encapsulated murine cell viability and HUVECs adhesion also ensuring enough gel stiffness needed for the perfusion of the microfluidic channel. Fluorescent nanoparticles were injected within the microchannel to demonstrate the ability to create defined microfluidic pathways within cell-laden OAPAO construct.

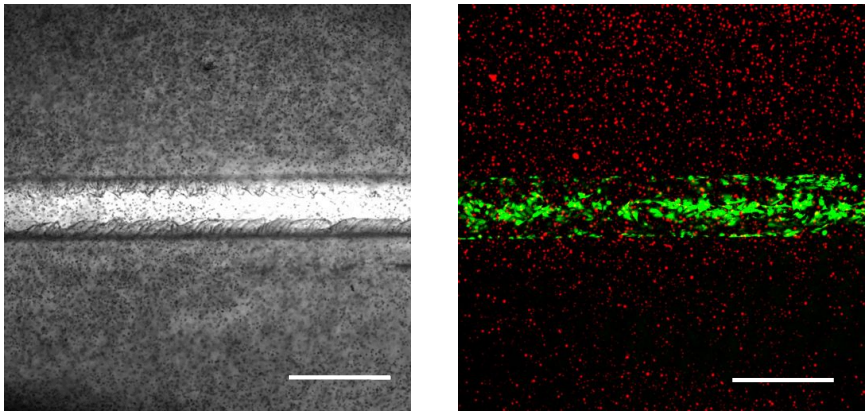

Figure 7. Optical (left) and confocal (right) images at 24h of endothelialized microfluidic channels in cell-laden OAPAO. Channels were created in OAPAO containing 3T3 fibroblasts (red) and seeded with GFP-HUVEC (green) cells demonstrating the ability to create cell-laden hydrogels with endothelial-lined, perfusable microvasculature (scale bar 500 μm).

To demonstrate the ability to create cell-laden structures with endothelialized microchannels, GFP-HUVECs were seeded into the channel of microfluidic OAPAO cell-laden hydrogel and allowed to adhere, as described in section 2.13. The microfluidic cell-laden gel was able to support HUVECs attachment, spreading and function also when externally perfused. The coculture of encapsulated 3T3 cells and HUVECs seeded on the surface of microchannel demonstrates the potential for making complex engineered microtissue with perfusable vascular networks.

4. Discussion

In this work, photo-crosslinkable PAA-based oligomers were synthesized as precursors of matrices for 3D cell culture and the physico-chemical and mechanical properties were studied in correlation to cell viability and proliferation with HUVECs cells in 2D (culture on hydrogel) and with NIH 3T3 fibroblasts in 2D and 3D (encapsulation) and their combination in a co-cultured construct. The produced oligomers contained the ABG-BAC monomeric unit, which acts both as an RGD-mimetic site and as a hydrolytically degradable function. These functions were inserted in diacrylamide-terminated oligomers able to yield soft hydrogels by photopolymerization compatible with the presence of cells. The oligomers used to obtain the studied hydrogels were synthesized through Michael-type addition of PAA and Jeffamine oligomers of selected molecular weight. In particular, PAA oligomers with molecular weights of 2000, 4000 and 6000 were tested for the Michael-type addition to Jeffamine. However, only the one type of PAA oligomer, OPAA-2, yielded the desired product, since shorter and longer PAA oligomers generated phase separation in presence of Jeffamine in water in a large temperature and pH ranges. The studied hydrogels were compared with the related products obtained by diacrylamido-terminated PAA oligomers, OPAA-2, OPAA-4 and OPAA-6. Compared to PAA-based control hydrogels, OAPAO hydrogels showed improved performances in terms of stiffness, storage and elastic modulus, equilibrium swelling ratio and degradation rate. In particular, extensive physico-chemical measurements revealed that the presence of Jeffamine segments in the PAA oligomer resulted into two main effects: (1) improvement of the mechanical properties, due to crystalline domains in the crosslinked network generated by Jeffamine segments increasing the hydrogel's stiffness [48]; (2) Increased swelling ratio, due to intrinsic hydrophilicity of Jeffamine, that resulted in a higher

degradation rate able to improve the limited degradation ability of PAA crosslinked by free-radical polymerization [38].

This study confirmed the superior OAPAO adhesion performance in 2D compared to the glass control, for both NIH 3T3 and HUVECs. High cell-binding properties are the result of RGD-mimetic binding sites abundantly present in the OAPAO macromer. OAPAO hydrogel was also employed for encapsulation of murine fibroblasts to form cell-laden hydrogels able to encourage cell viability *in vitro*. In particular, encapsulated cells showed cell viability comparable to the ones embedded in agarose gels. To our knowledge, this is the first study involving a 3D cell culture with a PAA based RGD-mimetic hydrogel. However, in all the encapsulation experiments cells did not migrate or degrade the OAPAO gels. This is due to the fact that OAPAO hydrogels are hydrolytically degradable, but lack of enzymatic degradation motifs. Without the possibility for cells to degrade and remodel the matrix, cell movement and organization in 3D is inhibited. In order to solve this limitation OAPAO hydrogels could be easily modified by incorporating protease-sensitive regions, similarly done in literature with PEG [26,28,31,33,49]. This will enable the use of OAPAO in most applications in which PEG has been successfully used, with comparable, or better performances as PEG containing cell binding and degradation motifs. Photopatterning ability of OAPAO was demonstrated in the fabrication of perfusable microfluidic channels. In these experiments OAPAO behaved similarly to PEGDA in terms of UV exposure time, fidelity and optical transparency. This indicates that OAPAO could potentially be used in most of the applications in which photopolymerizable PEG has been demonstrated in, with similar, or even better, performances. In order to demonstrate the potential of OAPAO in the creation of tissue-like structures, functional cells (NIH 3T3) were encapsulated in microfluidic OAPAO lined with endothelial cells (HUVECs)

and successfully characterized by confocal imaging. Cell-laden microvascular OAPAO has been shown to encourage cell-responsive behavior and surface binding. In the same experiment OAPAO hydrogels showed good mechanical stability when externally perfused (results not shown). Overall, these studies support the use of OAPAO hydrogels as tunable and inexpensive biomaterials for the creation of complex cell-laden constructs with features controllable on the microscale.

5. Conclusions

In the present study we demonstrated, for the first time, the use of PAA for 3D cell culture applications, highlighting the unique properties that make OAPAO an attractive material for creating cell-laden micro construct. The physico-chemical properties of OAPAO were demonstrated to be controllable through the variation of the molecular weight and the gel concentration yielding a tunable range of mechanical, swelling and degradation properties for different applications. Similarly to other synthetic hydrogel, OAPAO was easily patterned to fabricate consistent cell-laden hydrogels that can be used as monolithic microfluidic device. Unlike other synthetic UV crosslinkable hydrogels, cells rapidly adhered and proliferated on OAPAO surface, remaining viable when encapsulated in 3D. Overall these data suggest that OAPAO could be used for many applications where other synthetic hydrogels are too expensive or not appropriate, such as for creating endothelialized vascular network within engineered tissues. We envision that OAPAO hydrogels could ultimately become a tool for the creation tissue-like structures to be used as improved *in vitro* models to enhance the efficacy of drug screening and clinical treatments.

References

[1] Abbott A. Cell culture: biology's new dimension. Nature 2003;424:870-872.

[2] Cukierman E, Pankov R, Stevens DR, and Yamada KM. Taking cell-matrix adhesions to the third dimension. Science 2001;294:1708-12.

[3] Baker BM, Chen CS. Deconstructing the third dimension: how 3D culture microenvironments alter cellular cues. J Cell Sci 2012;125(13):3015-24.

[4] Khademhosseini A, Langer R, Borenstein J, Vacanti JP. Microscale technologies for tissue engineering and biology. Proc Natl Acad Sci USA 2006;103(8):2480-87.

[5] DeForest CA, Anseth KS. Advances in bioactive hydrogels to probe and direct cell fate. Annu Rev Chem Biomol Eng 2012;3:421-444.

[6] Astashkina A, Mann B, Grainger DW. A critical evaluation of in vitro cell culture models for high-throughput drug screening and toxicity. Pharmacol Ther 2012;134(1):82-106.

[7] Nyga A, Cheema U, Loizidou M. 3D tumour models: novel in vitro approaches to cancer studies. J Cell Commun Signal 2011;5(3):239-248.

[8] Engler AJ, Sweeney HL, Discher DE, Schwarzbauer JE. Extracellular matrix elasticity directs stem cell differentiation. J Musculoskelet Neuronal Interact 2007;7(4):335.

[9] Engler AJ, Sen S, Sweeney HL, Discher DE. Matrix elasticity directs stem cell lineage specification. Cell 2006;126(4):677-689.

[10] Tsang LV, Chen AA, Cho LM, Jadin KD, Sah RL, DeLong S, West JL, Bhatia SN. Fabrication of 3D hepatic tissues by additive photopatterning of cellular hydrogels. FASEB J 2007;21(3):790-801.

[11] Du Y, Lo E, Ali S, Khademhosseini A. Directed assembly of cell-laden microgels for fabrication of 3D tissue constructs. Proc Natl Acad Sci U S A 2008;105(28):9522-27.

[12] Murtuza B, Nichol JW, Khademhosseini A. Micro- and nanoscale control of the cardiac stem cell niche for tissue fabrication. Tissue Eng Part B Rev 2009;15(4):443-454.

[13] Burdick JA, Vunjak-Novakovic G. Engineered microenvironments for controlled stem cell differentiation. Tissue Eng Part A 2009;15(2):205-219.

[14] Huang G, Wang L, Wang S, Han Y, Wu J, Zhang Q, Xu F, Lu TJ. Engineering three-dimensional cell mechanical microenvironment with hydrogels. Biofabrication 2012;4(4):042001.

[15] Grinnell F. Fibroblast biology in three-dimensional collagen matrices. Trends Cell Biol 2003;13:264-269.

[16] Eyrich D, Brandl F, Appel B, Wiese H, Maier G. Long-term stable fibrin gels for cartilage engineering. Biomaterials 2007;28:55–65.

[17] Ho ST, Cool SM, Hui JH, Hutmacher DW. The influence of fibrin based hydrogels on the chondrogenic differentiation of human bone marrow stromal cells. Biomaterials 2010;31:38–47.

[18] Khademhosseini* A, Eng G, Yeh J, Fukuda J, Blumling J 3rd, Langer R, Burdick JA. Micromolding of photocrosslinkable hyaluronic acid for cell encapsulation and entrapment. J Biomed Mater Res A 2006;79(3):522-532.

[19] Brigham MD, Bick A, Lo E, Bendali A, Burdick JA, Khademhosseini A. Mechanically robust and bioadhesive collagen and photocrosslinkable hyaluronic acid semi-interpenetrating networks. Tissue Eng Part A 2009;15 (7):1645-53.

[20] Kleinman HK, Martin GR. Matrigel: basement membrane matrix with biological activity. Semin Cancer Biol 2005;15:378-386.

[21] Hughes CS, Postovit LM, Lajoie GA. Matrigel: a complex protein mixture required for optimal growth of cell culture. Proteomics 2010;10:1886–90.

[22] Nichol JW, Koshy ST, Bae H, Hwang CM, Yamanlar S, Khademhosseini A. Cell-laden microengineered gelatin methacrylate hydrogels. Biomaterials 2010;31(21):5536-44.

[23] Yeo Y, Geng W, Ito T, Kohane DS, Burdick JA, Radisic M. Photocrosslinkable hydrogel for myocyte cell culture and injection. J Biomed Mater Res B Appl Biomater 2007;81(2):312-322.

[24] Yang F, Williams CG, Wang DA, Lee H, Manson PN, Elisseeff J. The effect of incorporating RGD adhesive peptide in polyethylene glycoldiacrylate hydro- gel on osteogenesis of bone marrow stromal cells. Biomaterials 2005;26(30):5991-98.

[25] Ruoslahti E. RGD and other recognition sequences for integrins. Annu Rev Cell Dev Biol 1996;12:697-715.

[26] Mann BK, Gobin AS, Tsai AT, Schmedlen RH, West JL. Smooth muscle cell growth in photopolymerized hydrogels with cell adhesive and proteolytically degradable domains: synthetic ECM analogs for tissue engineering. Bioma- terials 2001;22(22):3045-51.

[27] Burdick JA, Anseth KS. Photoencapsulation of osteoblasts in injectable RGD-modified PEG hydrogels for bone tissue engineering. Biomaterials 2002;23:4315–23.

[28] Raeber GP, Lutolf MP, Hubbell JA. Molecularly engineered PEG hydrogels: a novel model system for proteolytically mediated cell migration. Biophys J 2005;89(2):1374-88.

[29] Miller JS, Shen CJ, Legant WR, Baranski JD, Blakely BL, Chen CS. Bioactive hydrogels made from step-growth derived PEG-peptide macromers. Biomaterials 2010;31:3736-43.

[30] Benton JA, Fairbanks BD, Anseth KS. Characterization of valvular interstitial cell function in three dimensional matrix metalloproteinase degradable PEG hydrogels. Biomaterials 2009;30(34):6593-03.

[31] Kraehenbuehl TP, Zammaretti P, Van der Vlies AJ, Schoenmakers RG, Lutolf MP, Jaconi ME, Hubbell JA. Three-dimensional extracellular matrix-directed cardioprogenitor differentiation: systematic modulation of a synthetic cell-responsive PEG-hydrogel. Biomaterials 2008;29(18):2757-66.

[32] Seliktar D, Zisch AH, Lutolf MP, Wrana JL, Hubbell JA. MMP-2 sensitive, VEGF-bearing bioactive hydrogels for promotion of vascular healing. J Biomed Mater Res A 2004;68(4):704-716.

[33] Lutolf MP, Weber FE, Schmoekel HG, Schense JC, Kohler T, Müller R, Hubbell JA. Repair of bone defects using synthetic mimetics of collagenous extracellular matrices. Nat Biotechnol 2003;21(5):513-518.

[34] Ferruti P, Marchisio MA, Duncan R. Poly(amido-amine)s: Biomedical applications. Macromolecular Rapid Communications 2002;23:332-355.

[35] Jain R, Standley SM, Frechet JMJ. Synthesis and degradation of pH-sensitive linear poly(amidoamine)s. Macromolecules 2007;40:452-457.

[36] Emilitri E, Ranucci E, Ferruti P. New poly(amidoamine)s containing disulfide linkages in their main chain. J Polym Sci Pol Chem 2005;43:1404-16.

[37] Lavignac N, Lazenby M, Franchini J, Ferruti P, Duncan R. Synthesis and preliminary evaluation of poly(amidoamine)-melittin conjugates as endosomolytic polymers and/or potential anticancer therapeutics. Int J Pharm 2005;300:102-112.

[38] Magnaghi V, Conte V, Procacci P, Pivato G, Cortese P, Cavalli E, Pajardi G, Ranucci E, Fenili F, Manfredi A, Ferruti P. Biological performance of a novel biodegradable polyamidoamine hydrogel as guide for peripheral nerve regeneration. J Biomed Mater Res 2011;98(1):19-30.

[39] Lin C, Zhong Z, Lok MC, Jiang X, Hennink WE, Feijen J, Engbersen JF. Novel bioreducible poly(amido amine)s for highly efficient gene delivery. Bioconjug Chem 2007;18:138-145.

[40] Emilitri E, Guizzardi F, Lenardi C, Suardi M, Ranucci E, Ferruti P. Novel Poly(amidoamine)-Based Hydrogels as Scaffolds for Tissue Engineering. Macromol Symp 2008;266:41-47.

[41] Dos Reis G, Fenili F, Gianfelice A, Bongiorno G, Marchesi D, Scopelliti PE, Borgonovo A, Podesta A, Indrieri M, Ranucci E, Ferruti P, Lenardi C, Milani P. Direct Microfabrication of Topographical and Chemical Cues for the Guided Growth of Neural Cell Networks on Polyamidoamine Hydrogels. Macromol Biosci 2010;10:842-852.

[42] Martello F, Piest M, Engbersen JF, Ferruti P. Effects of branched or linear architecture of bioreducible poly(amido amine)s on their in vitro gene delivery properties. J Control Release 2012;164:372-379.

[43] Mauro N, Ranucci E, Procacci P, Laus M, Antonioli D, Mantovani C, Magnaghi V, Ferruti P. Degradable Poly(amidoamine) Hydrogels as scaffolds for in vitro culturing of peripheral nervous system cells. Macromol Biosci 2012;13:332-347.

[44] Ferruti P, Bianchi S, Ranucci E, Chiellini F, Piras AM. Novel agmatine-containing poly(amidoamine) hydrogels as scaffolds for tissue engineering. Biomacromolecules 2005;6:2229-35.

[45] Ferruti P, Ranucci E, Trotta F, Gianasi E, Evagorou EG, Wasil M, Wilson G, Duncan R. Synthesis, characterisation and antitumour activity of platinum (II) complexes of novel functionalised poly(amido amine)s. Macromol Chem Physic 1999;200:1644-54.

[46] Khademhosseini A, Vacanti JP, Langer R. Progress in tissue engineering. Sci Am 2009;300(5):64-71.

[47] Yeh J, Ling Y, Karp JM, Gantz J, Chandawarkar A, Eng G, et al. Micromolding of shape-controlled, harvestable cell-laden hydrogels. Biomaterials 2006;27(31):5391e8.

[48] Sardon H, Engler AC, Chan JMW, Coady DJ, O'Brien JM, Mecerreyes D, Yangc YY, Hedrick JL, Homogeneous isocyanate- and catalyst-free synthesis of polyurethanes in aqueous media, Green Chem. 2013;15:1121-26

[49] Lutolf MP, Lauer-Fields JL, Schmoekel HG, Metters AT, Weber FE, Fields GB, Hubbell JA. Synthetic matrix metalloproteinase-sensitive hydrogels for the conduction of tissue regeneration: engineering cell-invasion characteristics. Proc Natl Acad Sci USA 2003;100(9):5413-8.

Chapter 4

Macroporous poly(amidoamine) foam for soft tissue regeneration

Alessandro Tocchio[a,b,1], Irini Gerges[a,1], Margherita Tamplenizza[a,1] et al.

[a]Fondazione Filarete, Viale Ortles 22/4, 20139 Milano, Italy; [b]SEMM, European School of Molecular Medicine, Campus IFOM-IEO, Via Adamello 16, 20139 Milano, Italy; [1]These authors contributed equally to this work.

1. Introduction

Tissue engineering is an emerging field that addresses the current clinical need of human tissues replacements [1]. Tissue substitutes are generally required after a trauma or tumor resection, or as a result of other pathologies [2]. Current autologous treatments for soft tissue defects still present a number of challenges and limitations, such as donor-site morbidity and volume loss over time [3]. Therefore there is still a strong need for alternative strategies to repair soft tissue like fat, nerves, blood vessel and fibrous tissue. The field of tissue engineering aims to address this problem providing novel strategies based on the development of bioactive tissue constructs *in vitro*, that can replace the tissue in both structure and function, when implanted *in vivo* [2]. The development of *in vitro* human tissue would offer a major innovation in soft tissue reconstruction strategies [4].

By serving as a temporary milieu for extracellular matrix (ECM) and providing the appropriate signals for growth and tissue formation, the

scaffold has become a fundamental element of tissue engineering processes [5,6]. Scaffolds for soft tissue engineering are typically designed to be highly porous with an interconnected open cell structure, to improve cellular infiltration and viability, to enable nutrients mass transport, to be structurally robust, and ideally, to promote angiogenesis and normal cell signaling processes [6-8].

Besides the 3D structure, the ability of a scaffold to promote cell adhesion and proliferation, due to cell-substrate interaction, is a success prerequisite for soft tissue engineering scaffolds [9,10]. In fact, the natural extracellular matrix (ECM) provides, not only mechanical support and surface adhesion, but also regulate cell function. Cells communicate with the ECM via integrins; signaling pathways through integrins can alter gene expression and result in cell migration, differentiation, proliferation or apoptosis [11,12]. Previous studies showed that surface modification of biomaterials with cell-recognition sites can enhance interaction between cells and matrix materials [13] and human umbilical vein endothelial cells (HUVECs), as an angiogenesis model, do not exempt [14,15]. Furthermore, peptide-modified biomaterials not only condition cell-matrix interaction *in vitro* but also influence the *in vivo* microenvironment on the molecular level, which is critical for tissue reconstruction [16,17]. As reported by Yu and co-workers [18], an Arg-Gly-Asp tripeptide (RGD) modified alginate can promote HUVECs viability and trigger new vessel formation. They suggest that integrin–ligand interaction may induce host tissue regeneration.

Growing interest had been paid toward the design of three dimensional macro porous structures, starting from natural origin biomaterials, such as collagen and gelatine, containing RGD motifs, which are well recognized by RGD-dependent integrin cell receptors and plays an important role in cell adhesion and proliferation [19-23]. Unfortunately,

the application of natural polymers in clinics is still hampered due to undesirable immune response, deriving from their allogenic or xenogenic origin, and the presence of impurities and endotoxins, depending on large-scale isolation techniques [24]. Unlike natural origin polymers, synthetic polymers gather a series of advantages like: versatility, controlled degradability and adequate mechanical properties. However, they need expensive surface or chemical modification, commonly using RGD peptide, in order to improve their cell adhesion capacity [25-29]. In order to improve cell adhesion of some synthetic polymers, Tanahashi and co-workers [30] pioneered chemical modification exploiting the co-polymerization with 4-(aminobutyl)guandine (Agmatine). They demonstrated that guanidine moieties are well recognized by RGD-dependent receptors, such as integrine, due to its similar chemical structure to RGD-tripeptide. This revolutionary approach boosted the use of synthetic polymers in tissue engineering offering an alternative solution to promote cell adhesion, avoiding expensive modification with RGD tripeptide.

Following the same approach, Ferruti and co-workers demonstrated that Agmatine-containing cross-linked poly(amido-amine)s (PAAs), show excellent capacity to promote cell adhesion and proliferation on its surface [31,32]. In a recent study carried out by our research group [33,34], we developed a wide library of Agmatine containing PAA based hydrogels, characterized by enhanced mechanical properties and degradation dynamics. Among these biomaterials, those obtained from free radical polymerization of diacrylamide-terminated poly(amido-amine)s oligomers (OPAA), containing RGD-mimetic repeating units, showed excellent capacity to promote Madin-Darby canine kidney (MDCK) epithelial cells adhesion on their surface.

In this work, we hypothesized that the excellent biological properties of Agmatine-containing PAA hydrogels could be exploited in tissue engineering, especially in soft tissue regeneration, when micro fabricated in a proper three-dimensional open-pore structure. We aimed to investigate how RGD-mimetic repeating units can orchestrate cell migration, proliferation and matrix deposition through macro porous constructs. A special attention was paid to evaluate the capacity of PAA open-pore foam (OPAAF), containing RGD-mimetic repeating units, to promote adipogenesis and in the stimulation of neovascularization *in vitro* and *in vivo*. In this work, we also investigated the effect of cross-linking density on chemical physics properties of PAA foams. To this aim, chemical physics and even biological characterizations were evaluated, starting from OPAA solutions, of two different concentrations: 25 and 38% (w/w). Both of the polymeric precursor solutions were cross-linked by free radical polymerization and obtained as open-pore structures by foaming before reaching their gel-point.

2. Materials and Methods

2.1 Materials

4-aminobutylguanidine sulfate (Agmatine), ammonium persulfate (APS), lithium hydroxide monohydrate (LiOH), hydrochloric acid (HCl), ammonium bicarbonate (NH_4HCO_3) and poly(ethylene glycol) sorbitan monolaurate (Tween® 20) were purchased from Sigma-Aldrich at the highest degree of purity available and used as received. Milli-Q grade water was used in all the experiments. Phosphate buffered saline (PBS) IX contained 2.69 mM KCl, 136.89 mM NaCl, 3.21 mM Na_2HPO_4 and 1.47 mM KH_2PO_4. All solvents were purchased from Sigma-Aldrich and used without further

purifications. 2,2-Bis(acrylamide)acetic acid (BAC) was prepared as previously reported [35] and its purity (99.9%) determined by acid-base titration and by NMR spectroscopy. All biological materials were purchased from Sigma-Aldrich unless otherwise specified.

2.2 Synthesis of diacrylamide-terminated poly(amido-amine)s *oligomer OPAA:*

In a 50 mL round-bottom flask, equipped with magnetic stirrer and nitrogen inlet, BAC (9g, 44.9mmol) and LiOH (2.2g, 51.3mmol) were dissolved in 15mL Milli-Q water. Agmatine (7.6g, 32.2mmol) was then added to the reacting mixture under magnetic stirring. The reaction was kept in dark and proceeded under inert atmosphere at 35°C for one week and stopped by acidification till pH=4 using HCl 1M solution. The product was purified by Utra-filtration, using 1000 cut off semi permeable membrane. OPAA was obtained as fine white powder after freeze-drying using Telstar Cryodos 50 lyophilizer. The reaction Yield was 84%. Average molecular weights (SEC-Pullulane standards): Mn=2000, Mw= 2600, P.D. Index= 1,3. *H NMR (D_2O)*: 1.57 (s, 2H, -C**H$_2$**-CH_2-NH-CNHNH_2); 1.70 (s, 2H, -N-CH_2-C**H$_2$**-); 2.71 (s, 2H, -C**H$_2$**-CONH); 3.07(s, 2H, -C**H$_2$**-NH-CNHNH_2); 3.14 (t, 2H, -N-C**H$_2$**-); 3.61 (m, 2H, -NH-C**H$_2$**-$(CH_2)_2$-NHCO-); 5.48-5.68 (m, 2H, C**H$_2$**=CH-CONH-); 6.18(m, 1H, CH_2=C**H**-CONH-)

2.3 OPAA foams (OPAAF) preparation

Foams were prepared by APS-initiated free radical polymerization of OPAA. Open cell foams have been obtained due thermal decomposition of NH_4HCO_3 at 60°C simultaneously to gelling reaction. Tween® 20 has been used as pore opening agent. Two open cell foams have been prepared

due to table 1. pH of the raw foams were adjusted to neutral, using 0,01M solution of citric acid. Discs of 10mm diameter and 3mm height have been cut and soaked at room temperature in 50% (w/w) ethanol aqueous solution for 2 days, and washed in Milli-Q water on orbital shaker for other 3 days, then dried from ethanol under reduced pressure (0,01bar) and UV-sterilized prior to cell seeding. Schematic representation of OPAA crosslinking through free radical polymerization is reported in Fig. 1.

2.4 Scanning electron microscopy

SEM images have been acquired using Carl ZEISS-Sigma scanning electron microscope, endowed with EDS-Brucker XFlash 5030-127eV detector.

2.5 Size Exclusion Chromatography

Traces were recorded using Toso-Haas 486 columns, Waters 515 HPLC pump and UV detector operating at 230 nm. The mobile phase was 0.1 M Tris buffer saline, pH 8.00±0.05. The follow rate was 1ml/min. OPAAs average molecular weights were calculated using Pullulane standards.

2.6 Nuclear magnetic resonance NMR

^{1}HNMR spectra were acquired on Bruker 8 Advance 400 spectrometer, operating at 400.133 MHz.

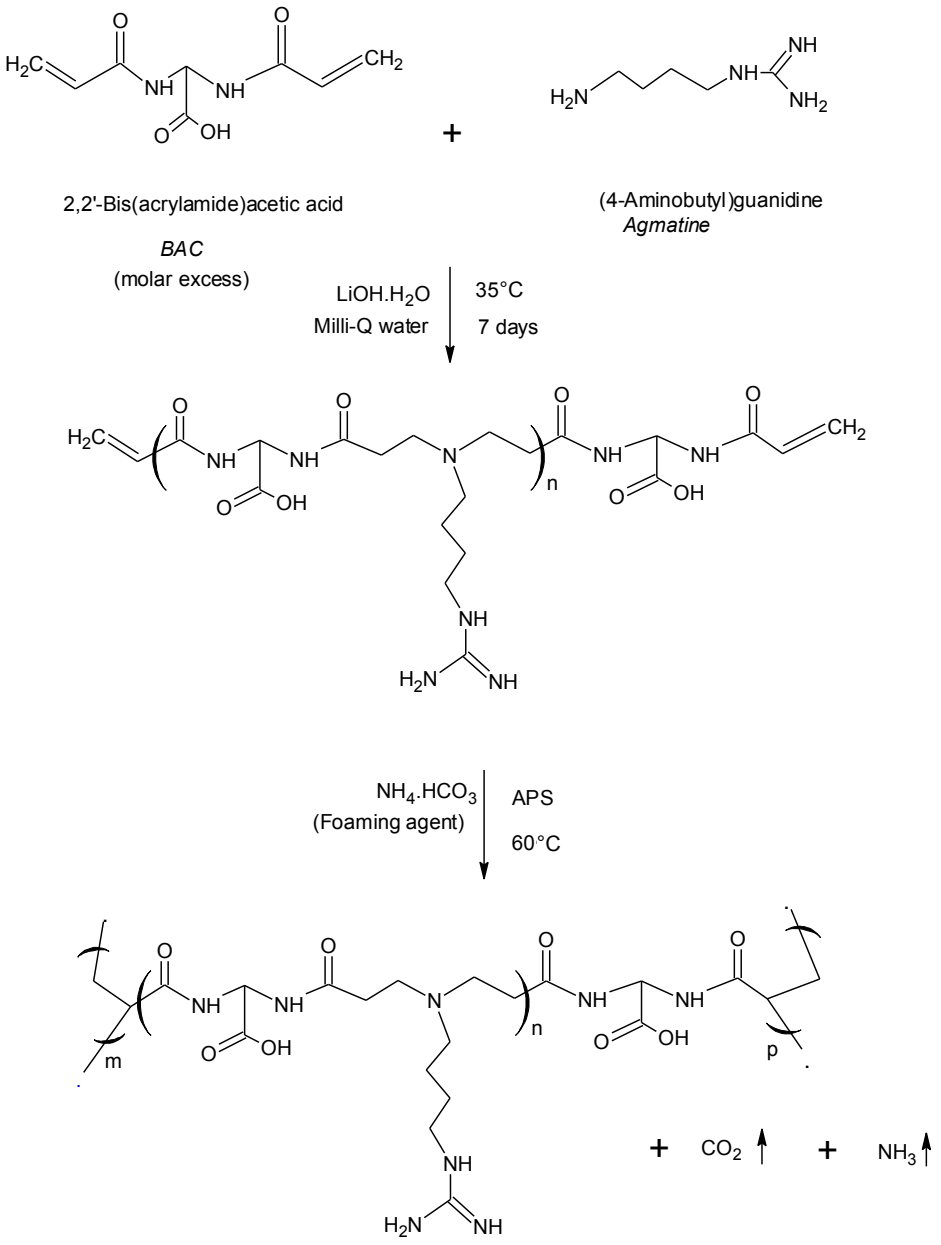

Figure 1. Schematic representation for OPAA foams syntheses

	OPAAF 25		OPAAF 38	
	g	weight %	g	weight %
OPAA	1	24.7	1	37
Milli-Q water	1.5	37	0.67	25
Tween®20	0.05	1.3	0.08	2.88
APS (0,1mM)	0.5	12.3	0.3	11
NH_4HCO_3	1	24.7	0.65	24

Table 1, composition of OPAA foams

2.7 Mechanical characterization

The mechanical properties of OPAA foams were studied with a dynamic mechanical analyzer (DMA mod. 2980, TA Instruments), using mechanical compression tests in frequency sweep and stress relaxation tests with subsequent strain recovery. All the mechanical tests were conducted on cylindrical specimens (ø = 5 mm, h = 3 mm) previously brought to a swelling plateau in distilled water. Six specimens were characterized for each formulation. Compression tests were performed in frequency sweep (f = 0,3, 1, 2, 3, 5 and 10Hz, n = 10 cycles) at a constant temperature (37°C) to obtain the complex modulus trend on variation of frequency. In particular, information can be obtained about the real component of the complex modulus, known as the conservative modulus (E'), which represents the energy accumulated in the material and consequently correlated with its elastic behavior, and the imaginary component, called the dissipative modulus (E"), which represents the dissipated energy linked to the viscous component of the material. The E"/E' ratio, called Tanδ, allows the contribution made by the two components to be evaluated on variation of the test parameters.

2.8 Equilibrium swelling and weight loss measurements

Tests were carried out in PBS 1X, using dry cylindrical samples of average weight 70 mg ± 10mg. Samples incubated at 37 °C and weighed at time at fixed time intervals. At each time point, the swollen samples were removed from PBS, blotted gently to remove excess PBS. For weight loss measurements, samples were washed in Milli-Q water, to remove PBS from the swollen foams, finally freeze dried and weighted. Swelling capacity and weight loss were calculated according to the following formulas:

$$\text{Swelling degree \%} = (W_s - W_0) * 100 / W_0 \quad \text{(Equation 1)}$$

$$\text{Weight loss \%} = (W_0 - W_d) * 100 / W_0 \quad \text{(Equation 2)}$$

Where W_0, W_s and W_d in equations 1 and 2 are the initial, swollen and dried weight respectively.

2.9 Cell culture and seeding

HUVECs were obtained from PromoCell Gmbh (Heidelberg, Germany). The cells were cultured in M199 medium (Sigma-Aldrich) supplemented with 2mM L-Glutamine, 100 units/ml penicillin and 100 µg/ml streptomycin and freshly added with 20% FBS (Sigma-Aldrich), 50 ng/ml β-endothelial cell growth factor (ECGF) and 100 µg/ml Heparin. HUVECs were harvested using 0.05% trypsin, centrifuged and resuspended in basal medium. Each scaffold, of 10mm diameter and 2mm thickness, was seeded with $1x10^6$cells, resuspended in 100 µl of basal medium. Scaffolds were seeded adding drop-wise cells suspension, then were placed in the incubator for 1 h to allow cell attachment. Thereafter, 1mL of corresponding medium was added to each well, and the plates were incubated at 37°C in 5% CO_2 95% air-humidified incubator.

2.10 Confocal microscopy

Cellular viability was investigated at 3 and 7 days of culture by using a live/dead assay solution consisting of Calcein-AM (1 μM) and Propidium Iodide (0.1 mM) prepared in PBS. Briefly, samples were rinsed in PBS, immersed in staining solution for 15-20 minutes and incubated at 37°C. Staining solution was removed, samples washed twice with PBS and immersed in PBS before imaging. Live imaging was performed using a confocal microscope (Leica Confocal Microscopy TCS SP5) incubator equipped using 490/515nm (excitation/emission) for Calcein-AM (Life Technologies) and 535/617nm (excitation/emission) for Propidium Iodide. Maximum intensity projection images were obtained using ImageJ software. Cell organization on scaffolds validated 3 times.

2.11 In vivo biocompatibility

Female CD1 mice (Charles River) aged 8 weeks (25-31 gr) were used for this study. Under general anesthesia, a 10 mm-long incision was made in the skin of the medial femoral region. Scaffolds (3 for type and time point) were placed subcutaneously, over the femoral artery, between the inguinal ligament and hiatus adductorius, keeping the perfusion of the distal leg intact. The incision was closed with interrupted 6/0 single filament ethilon (Biomedica Greto) sutures. Mice were sacrificed 51 days post implant, and scaffolds together with surrounding tissues were excised, and fixed in 10% neutral buffered formalin. Formalin-fixed samples were embedded in paraffin wax, sectioned at 4μm thickness, routinely stained with hematoxylin and eosin (HE), and evaluated under a light microscope for the assessment of host reaction and tissue ingrowth.

3. Results and Discussion

Foaming, compared to other common micro fabrication techniques such as solvent casting and particulate leaching, is the preferred choice for hydrogels obtained from free radical polymerization of water-soluble polymeric precursors. In fact it does not require the use of organic or toxic solvents, neither the complicated steps necessary for the elimination of porogen [28]. In this work, foaming of OPAA cross linked hydrogels took place thanks to the thermal decomposition of NH_4HCO_3, which release carbon dioxide and ammonia gas in the liquid polymeric solution, before and during cross-linking. Tween® 20 were added to achieve homogenous pore size distribution and open cell structure. The average pore size, from 50 to 400 μm, is in the same range for both scaffold types, however, the pore structure of the OPAAF 25 scaffolds is characterized by higher interconnection, whereas the OPAAF 38 appear less interconnected with small and randomly distributed pores (Fig. 2).

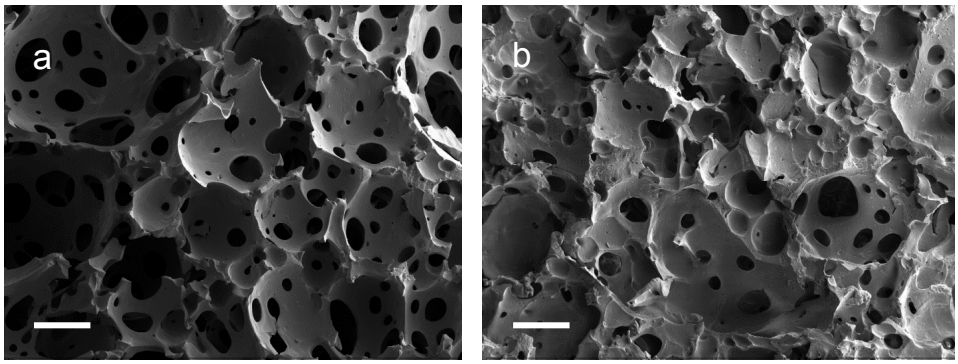

Figure 2. SEM images micrographs for OPAAF 25 (a) and OPAAF 38 (b) respectively (scale bar 200 μm)

Swelling kinetics of OPAA foams are graphically represented in Fig. 3. Both OPAAF 25 and OPAAF 38 reached the maximum swelling capacity "Plateau" in the first hour. Interestingly, OPAAF 25 swells twice than OPAAF 38. This difference reflects the effect of the cross-linking degree, the macromolecular mesh size and the foams architecture (pore structure and dimension). Degradation kinetics of OPAA based hydrogels, previously studied by Martello et al. 2013 [34], showed 25% weight loss during the first month of incubation, and proceeded gradually to reach 60% within the sixth month of incubation in PBS at 37°C.

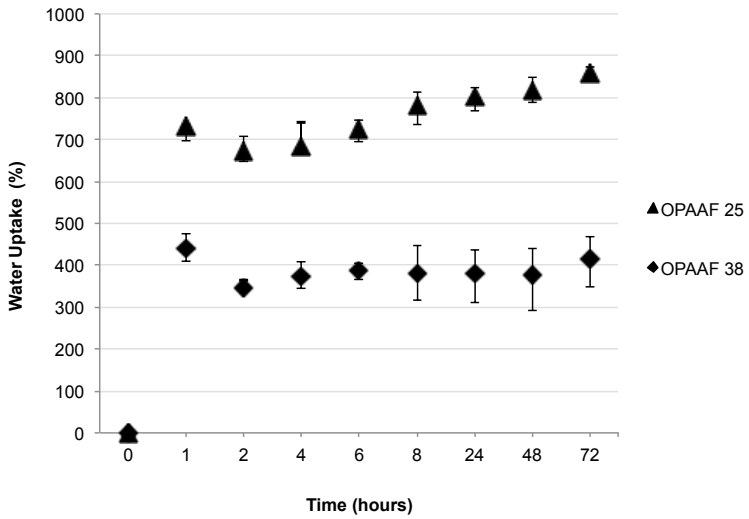

Figure 3. Swelling kinetics of OPAA foams in PBS 1X at 37°C

Mechanical characterization of OPAA foams (Fig. 4) shows remarkable relation between the elastic modulus E' and OPAA concentration, in each formulation. The higher the OPAA concentration, the stiffer the foam. This characteristic is directly related to the difference in their cross linking density. We observed that E' values were maintained invariable as frequency increased gradually from 0.3 to 10Hz (Fig. 4a).

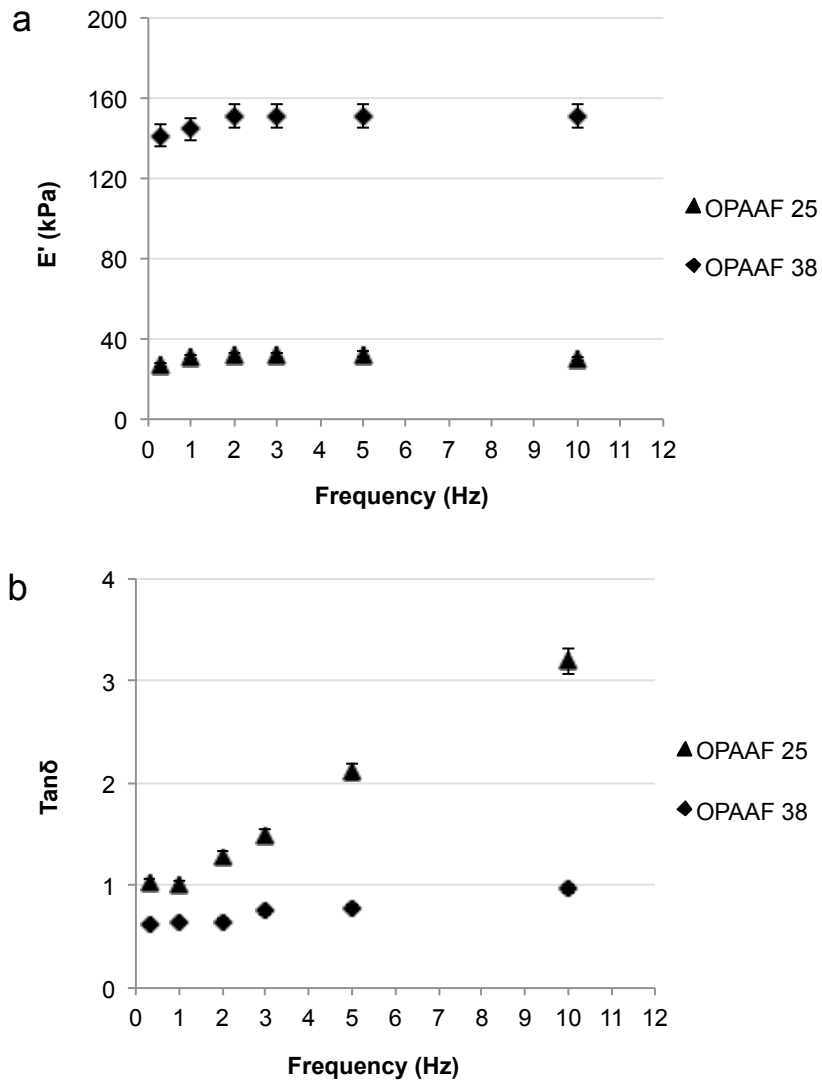

Figure 4. (a) Compressive elastic modulus E' (kPa) and (b) Tanδ, respectively, as functions of frequency (Hz).

The imaginary dissipative energy, related to the viscous component was evaluated at different frequencies (Fig. 4b). Significant increase in Tanδ was observed for OPAAF 25 at higher frequencies. This could be attributed to material fatigue, probably due to the strain used for the

mechanical characterization. Interestingly, the viscous component was less evident for OPAAF 38. In general, the elastic behavior of OPAAFs make them a suitable candidate as scaffolds for soft tissue engineering, where elasticity and adequate mechanical support influence morphology, orientation of cultured cells and induce changes in signal transduction system and secondary messengers, especially for certain types of soft tissues, as for example adipose tissue [37-40].

To evaluate the biological properties of OPAA hydrogel foams containing RGD-mimetic repeating units, the cell-scaffold interactions (cell adhesion, distribution and viability) were extensively studied. HUVECs growth on OPAAF 25 and OPAAF 38 was visualized over time by confocal laser scanning microscopy (CLSM) after live/dead staining. After 7 days of culture, cells were covering the complete surface and growing into the scaffold pores (Fig. 5 and 6). Imaging revealed layers of viable cells (green) and some dead cells (red) that can be discerned among predominantly viable cells. Cells were regularly distributed on scaffolds of both types, with uninterrupted cell layers on the OPAAF 38 (Fig. 6b). OPAAF 25 also exhibited continuous cell layers, although HUVECs did not grow on all edges of the scaffold pores (Fig. 6a). Moreover, the shape of primary HUVECs was more rounding, short-spindle, on OPAAF 25, while it was more flat, long-spindle, on OPAAF 38.

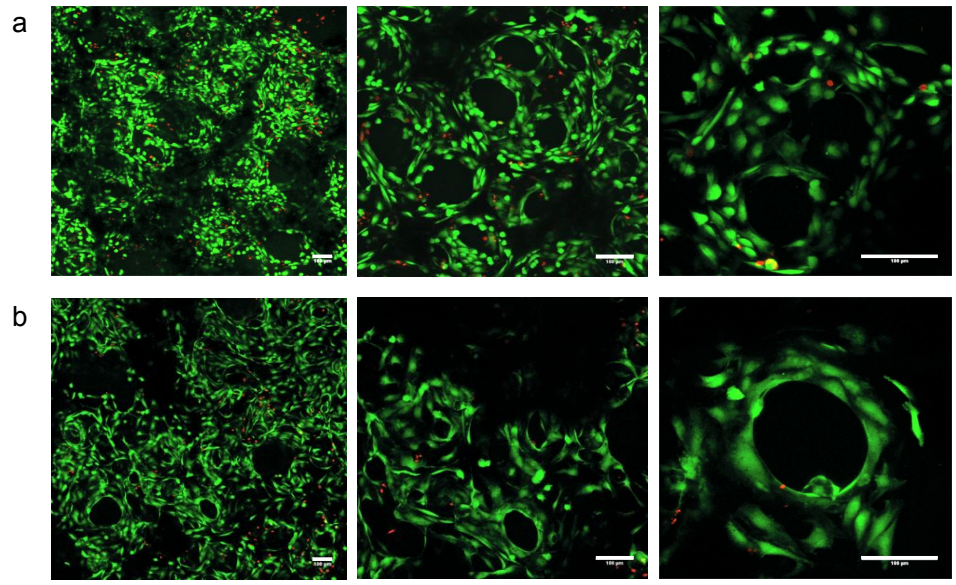

Figure 5. Confocal microscope images, live/dead assay for HUVECs seeded in OPAAF 25 (a) and OPAAF 38 (b) respectively, after 3 days of culture (scale bar, 100 μm).

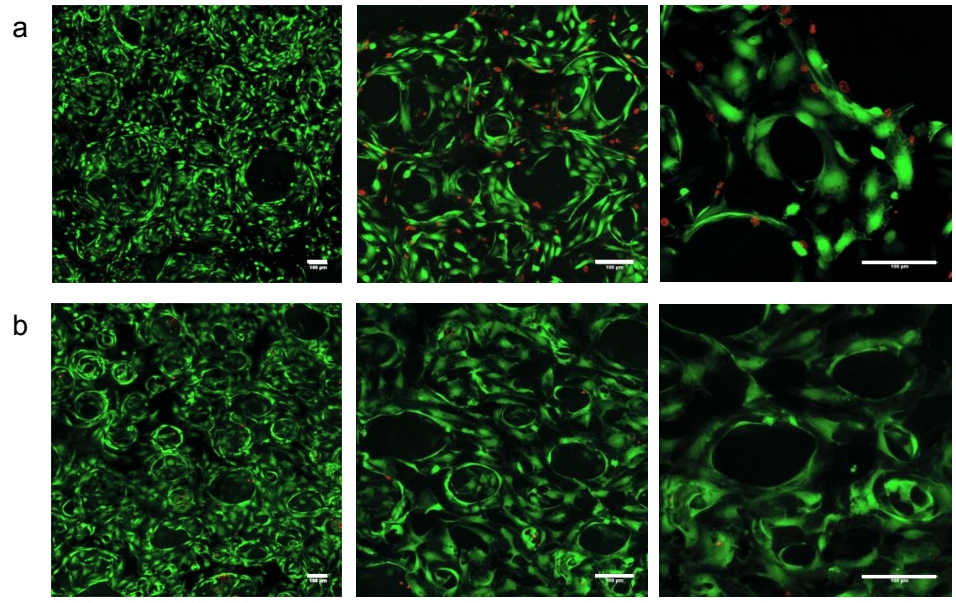

Figure 6. Confocal microscope images, live/dead assay for HUVECs seeded in OPAAF 25 (a) and 38 (b) respectively, after 7 days of culture (scale bar, 100 μm).

The assessment of *in vivo* biocompatibility of OPAA foams was performed in a mouse model with subcutaneous implant in the medial femoral region. All mice tolerated well the constructs and did not develop limitations in leg movement. Healing of incision site was achieved within 3 days, and all implants were retained until the end of the experiments. As a first gross evaluation during removal, both constructs appeared well integrated at the implantation site, and newly formed tissue was evident within the pores. After paraffin-embedding and HE staining, scaffolds were microscopically analyzed (Fig. 7).

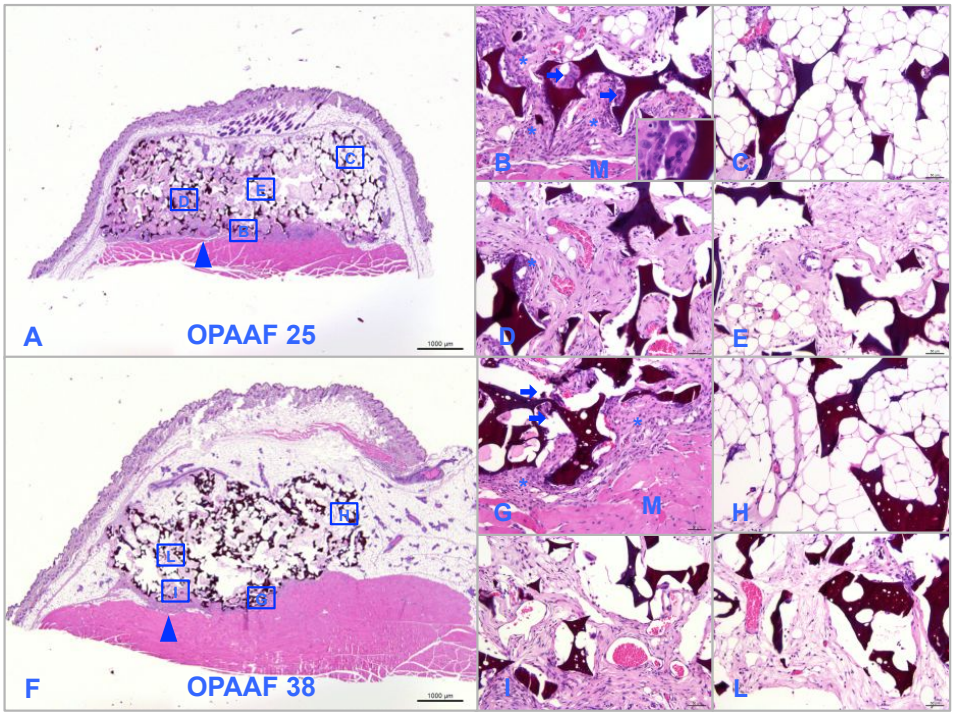

Figure 7. Histological examination of OPAA scaffolds after 51 days of implantation. A-E) OPAAF 25. F-L) OPAAF 38. Scaffolds were well integrated in the subcutaneous tissue, their overall porous structure was preserved, and infiltrating tissue filled the scaffold pores (A and F). Inflammation (*) was most prominent along the contact surface between the scaffold and underlying skeletal muscle (M) (B and G), multinucleated giant cells attempting to phagocytize the scaffold were found (arrows and insert). Infiltrating tissue was composed of vascularized adipose tissue (C and H), dense connective tissue (fibrosis) (D and I) and loose connective tissue (E and L). Arrowhead: femoral artery.

During sectioning, OPAAF 38 was difficult to cut given its stiffness, resulting in fragmentation of the scaffold in the histological sections. Both OPAA foams appeared dark-red to brown in HE stained sections. Both OPAAF 25 and OPAAF 38 had a homogenous structure containing unstained vacuoles, that were occasional and small-sized in OPAAF 25 and more numerous and variably sized in OPAAF 38. After 51 days of implantation, both scaffold types were well integrated in the murine subcutaneous tissue and their overall structure remained intact. Fibrous encapsulation was mild and incomplete around both scaffolds. Inflammation was overall mild, localized at the periphery of the scaffold, and composed of small to moderate numbers of macrophages, and lesser numbers of granulocytes (both neutrophils and eosinophils), lymphocytes, and foreign body multinucleated giant cells, in an attempt to phagocytize the implanted material. Slightly stronger host reaction was observed along the surface in contact with underlying skeletal muscles, while surrounding adipose tissue appeared almost unaffected by the presence of the scaffolds. As regards the tissue ingrowth, the pores of both scaffolds were infiltrated by adipose tissue and vascularized fibrous tissue (denser at the periphery and looser towards the center of the scaffold), growing over the surface of the material and occupying the cavity of pores. In OPAAF 25 there was more fibrosis compared to OPAAF 38. Overall, both scaffold types showed a good biocompatibility and tissue ingrowth, supporting their application in soft tissue engineering.

4. Conclusion

The increasing clinical demand for innovative therapeutic approaches able to improve patients' quality of life drove the scientists' attention toward regenerative medicine. This interest was catalyzed by its extraordinary

potential in volume and function compensation of damaged tissues, especially after trauma or tumor resection. Soft tissue engineering represents an important challenging field, where scaffolds morphology, biomechanics and cell-substrate interaction drastically influence the phenotype, signal transduction and cell differentiation of the regenerated tissue. The most studied biomaterials for soft tissue engineering are classified into natural origin and synthetic polymers. Problems related to natural origin polymers and expensive surface and chemical modifications of non-adhesive synthetic polymers motivated scientists to explore new functional classes of biomaterials, able to overcome drawbacks of the biomaterials cited above. Synthetic polymers containing RGD-mimetic repeating units, open new frontiers for the development of cell adhesive biomaterials in large scales. In this work we aimed at drawing the attention toward the potentials of synthetic RGD-mimetic poly(amido-amine)s polymers in tissue engineering.

Besides the excellent biological properties, RGD-mimetic PAA-based macro porous foams, are characterized by degradation kinetics and mechanical properties which match those required for soft tissue engineering scaffolds. The reported results have important implications for the design of scaffolds for soft, in particular adipose, tissue engineering. Successful adipose tissue engineering approaches rely on both adipose differentiation and the rapid recruitment of a vascular network to meet the metabolic requirements of the newly formed fat pad [41]. It may be possible to satisfy these biological design parameters by the development of scaffold composites controlling and guiding angiogenesis *in vivo*. Specifically, our results indicate that OPAAFs may be able to accelerate vascularization thanks to their ability to promote endothelial cell adhesion and proliferation in response to the elevated presence of RGD-mimetic sites. This process may be further enhanced,

because increased matrix rigidity promotes blood vessel formation by directly altering endothelial cell behavior [42]. This possible perturbation of blood vessels homeostasis represents an important issue, and better insight can help controlling and guiding angiogenesis and adipogenesis in a scenario where adipose tissue engineering is predominantly pursued for reconstruction therapies for breast cancer patients [43]. Future *in vivo* studies are required to specifically address these aspects.

References

[1] Langer R, Vacanti JP. (May 1993). Tissue engineering. Science 1993;260(5110):920–926

[2] Choi JH, Gimble JM, Lee K, Marra KG, Rubin JP, Yoo JJ, Vunjak-Novakovic G, Kaplan DL. Adipose tissue engineering for soft tissue regeneration. Tissue Eng Part B 2010;16(4):413-26.

[3] Patrick CW, Tissue engineering strategies for adipose tissue repair. Anat Rec 2001;263(4):361-366.

[4] Atala A, Lanza R, Methods of Tissue Engineering, San Diego, Academic Press; 2001.

[5] Lanza RP, Langer R, Vacanti JP. Principles of tissue engineering, San Diego: Academic Press; 2007.

[6] Hollister SJ. Porous scaffold design for tissue engineering. Nat Mat 2005;4:518-24.

[7] O'Brien FJ, Harley BA, Yannas IV, Gibson LJ. The effect of pore size on cell adhesion in collagen-GAG scaffolds. Biomaterials 2005;26:433–441.

[8] Drury JL, Mooney DJ. Hydrogels for tissue engineering: scaffold design variables and applications. Biomaterials 2003;24(24):4337–51.

[9] Gardel M, Schwarz U. Cell–substrate interactions. Journal of Physics: Condensed Matter 2010;22(19):190301.

[10] Lin CY, Li LT, Su WT. Study of subcellular dynamics on cell–substrate interactions by live cell imaging. Journal of Biomedical Materials Research Part A 2013;101(11).

[11] Hynes RO. Integrins: versatility, modulation, and signaling in cell adhesion. Cell 1992;69(1):11-25.

[12] Vogel V, Baneyx G. The tissue engineeting puzzle: a molecular perspective. Annu Rev Biomed Eng 2003;5:441-463.

[13] Hersel U, Dahmen C, Kessler H. RGD modified polymers: biomaterials for stimulated cell adhesion and beyond. Biomaterials 2003;24(24):4385-415.

[14] Choi WS, Bae JW, Lim HR, Joung YK, Park JC, Kwon IK, Park KD. RGD peptide-immobilized electrospun matrix of polyurethane for enhanced endothelial cell affinity. Biomed Mater 2008;3(4):044104.

[15] Lee YB, Shin YM, Lee JH, Jun I, Kang JK, Park JC, Shin H. Polydopamine-mediated immobilization of multiple bioactive molecules for the development of functional vascular graft materials. Biomaterials 2012;33(33):8343-52.

[16] Davis ME, Hsieh PC, Grodzinsky AJ, Lee RT. Custom Design of the Cardiac Microenvironment With Biomaterials. Circulation Research 2005;97(1):8-15.

[17] Hennessy KM, Clem WC, Phipps MC, Sawyer AA, Shaikh FM, Bellis SL. The effect of RGD peptides on osseointegration of hydroxyapatite biomaterials. Biomaterials 2008;29(21):3075-83.

[18] Yu J, Gu Y, Du KT, Mihardja S, Sievers RE, Lee RJ. The effect of injected RGD modified alginate on angiogenesis and left ventricular function in a chronic rat infarct model. Biomaterials 2009;30(5):751-756.

[19] Rosso F, Giordano A, Barbarisi M, Barbarisi A. From Cell–ECM interactions to tissue engineering. Journal of Cellular Physiology 2004;199(2):174–180.

[20] Benoit YD, Groulx JF, Gagné D, Beaulieu JF. RGD-Dependent Epithelial Cell-Matrix Interactions in the Human Intestinal Crypt. J Sign Transduction 2012;2012:248759.

[21] Doillon CJ, Silver FH, Berg RA. Fibroblast growth on a porous collagen sponge containing hyaluronic acid and fibronectin. Biomaterials 1987;8(3):195-200.

[22] Nazarov R, Jin HJ, Kaplan DL. Porous 3-D Scaffolds from Regenerated Silk Fibroin-Biomacromolecules 2004;5(3),718-726.

[23] Tripathi A, Kathuria N, Kumar A. Elastic and macroporous agarose–gelatin cryogels with isotropic and anisotropic porosity for tissue engineering. J Biomed Mater Res A 2009; 90(3):680-694.

[24] Mano JF, Silva GA, Azevedo HS, Malafaya PB, Sousa RA, Silva SS, Boesel LF, Oliveira JM, Santos TC, Marques AP, Neves NM, Reis RL. Natural origin biodegradable systems in tissue engineering and regenerative medicine: present status and some moving trends. J R Soc Interface 2007; 4(17):999-1030.

[25] Hu Y, Winn SR, Krajbich I, Hollinger JO. Porous polymer scaffolds surface-modified with arginine-glycine-aspartic acid enhance bone cell attachment and differentiation in vitro. Journal of Biomedical Materials Research Part A 2003; 64(3):583-590.

[26] Angelova N, Hunkeler D. Rationalizing the design of polymeric biomaterials. Trends in Biotechnology 1999;17(10):409-421.

[27] Blit PH, Shen YH, Ernsting MJ, Woodhouse KA, Santerre JP. Bioactivation of porous polyurethane scaffolds using fluorinated RGD surface modifiers. J Biomed Mater Res A 2010;94(4):1226-35.

[28] Kim TG, Park TG. Biomimicking extracellular matrix: cell adhesive RGD peptide modified electrospun poly(D,L-lactic-co-glycolic acid) nanofiber mesh. Tissue Engineering 2006;12(2):221-233.

[29] Guarnieri D, De Capua A, Ventre M, Borzacchiello A, Pedone C, Marasco D, Ruvo M, Netti PA. Covalently immobilized RGD gradient on PEG hydrogel scaffold influences cell migration parameters. Acta Biomater 2010;6(7):2532-39.

[30] Tanahashi K, Mikos AG. Protein adsorption and smooth muscle cell adhesion on biodegradable agmatine-modified poly(propylene fumarate-co-ethylene glycol) hydrogels. J Biomed Mater Res A 2003;67(2):448-457.

[31] Ferruti P, Bianchi S, Ranucci E, Chiellini F, Piras AM. Novel Agmatine-Containing Poly(amidoamine) Hydrogels as Scaffolds for Tissue Engineering. Biomacromolecules 2005;6(4):2229-35.

[32] Franchini J, Ranucci E, Ferruti P, Rossi M, Cavalli R. Synthesis, physicochemical properties, and preliminary biological characterizations of a novel amphoteric agmatine based poly(amidoamine) with RGD-like repeating units. Biomacromolecules, 2006;7(4):1215-22.

[33] Advanced Biomaterials Platform. Fondazione Filarete. 22/4 Viale Ortles Milan-Italy.

[34] Martello F, Tocchio A, Tamplenizza M, Gerges I, Pistis V, Recenti R, Bortolin M, Del Fabbro M, Argentiere S, Milani P, Lenardi C. Poly(amidoamine)-based Hydrogels with Tailored Mechanical Properties and Degradation Rates for Tissue Engineering. Acta Biomaterialia 2014;10(3):1206–1215.

[35] Ferruti P, Ranucci E, Trotta F, Gianasi E, Evagorou EG, Wasil M, Wilson G, Duncan R. Synthesis, characterisation and antitumour activity of platinum(II) complexes of novel functionalised poly(amido amine)s. Macromol Chem Phys 1999;200(7):1644-54.

[36] Murphy MB, Mikos AG. Polymer Scaffold Fabrication. Principles of Tissue Engineering. Third edition. Part V: Biomaterials in Tissue Engineering, 22:309-322.

[37] Samani A, Zubovits J, Plewes D. Elastic moduli of normal and pathological human breast tissues: an inversion-technique-based investigation of 169 samples. Physics in Medicine and Biology 2007;52(6):1565-76.

[38] Comley K, Fleck NA. A micromechanical model for the Young's modulus of adipose tissue. International Journal of Solids and Structures 2010;47(21):2982–90.

[39] Ingber D. Integrins as mechanochemical transducers. Current Opinion in Cell Biology 1991;3(5):841-848.

[40] Janmey PA, Weitz DA. Dealing with mechanics: mechanisms of force transduction in cells. Trends in Biochemical Sciences 2004;29(7):364-370.

[41] Patrick CW Jr. Adipose tissue engineering: the future of breast and soft tissue reconstruction following tumor resection. Semin Surg Oncol 2000;19(3):302-311.

[42] Mammoto A, Connor KM, Mammoto T, Yung CW, Huh D, Aderman CM, Mostoslavsky G, Smith LE, Ingber DE, Nature. 2009, 457(7233), 1103–1108.

[43] Patrick CW, Breast tissue engineering. Annual Rev Biomed Eng 2004;6:109-130.

Fabrication of branched vascular networks for large tissue engineering

Alessandro Tocchio[a,b,1] et al.

[a]Fondazione Filarete, Viale Ortles 22/4, 20139 Milano, Italy; [b]SEMM, European School of Molecular Medicine, Campus IFOM-IEO, Via Adamello 16, 20139 Milano, Italy;

Part of this chapter has been published: Tocchio A, Martello F, Lenardi C, Method for producing three-dimensional monolithic microfluidic devices, WO 2012 164512.

1. Introduction

The field of tissue engineering is dedicated to repair, restore or improve the functions of damaged or lost human tissues [1]. The aim of tissue engineering is to create functional tissues and organs *in vitro* and to use them as transplants or in vitro test systems [2]. Nevertheless, despite significant progresses have been achieved over the last 20 years, a number of challenges remain, preventing the widespread of tissue engineering clinical applications [3]. Perhaps the most important scientific issue hampering the development of tissue engineering technologies is the lack of a proper vascularization [4]. Nowadays only skin, cartilage and bladder grafts are successfully used in clinics [5–10] while cornea grafts are far ahead [11,12], mainly thanks to their low requirement for nutrients and oxygen that can be met by the host's vascularization. However, only few tissues can be successfully supplied

via diffusion from blood vessel systems that are further away [13,14]. In particular, this approach fails when applied to complex and large tissues [15]. This is due to the fact that the formation of new blood vessels is indeed a slow phenomenon and the deficiency of oxygen and nutrients supply rapidly causes widespread cell death in graft cores [16]. This is true also for large tissue-engineered constructs that are supplied with oxygen and nutrients *in vitro* by using perfusion bioreactors but after implantation *in vivo* they are supplied by diffusion only [17]. In fact, in the body most tissues rely on a highly branched system of multiscale blood vessels [18,19]. Living cells are generally found no more than 200 μm from the nearest capillary [20,17]. This spacing allows optimal diffusion of oxygen, nutrients, and removing of metabolic waste products to support and maintain viable tissues [21,22]. Likewise, any tissues grown in the laboratory, that is more than a few hundreds of microns thick, needs a vascular system and when this condition is not satisfied, cells quickly become irreparably damaged [23]. Diffusion limitation is the primary reason why the construction of tissues thicker than a few hundred microns is currently not practicable in vitro [22]. Overcoming the current inability to engineered tissue with blood vessel architecture is critical to create large and complex in vitro tissues and to transfer tissue engineered constructs to the clinic [15,18,24].

It is known that scaffold itself should be able to promote vascularization [25]. To date, several methods have been developed to generate engineered scaffold with perfusable vascular network. One of these methods to construct capillary networks is layer-by-layer assembly [26-29]. In brief open microfluidic channels are imprinted into one layer such that a second fabricated layer can then be aligned and bonded forming closed channels in an iterative manner. Layer-by-layer assembly requires a delicate and slow fabrication process of accurate stacking and

lamination of individual layers. It also imposes considerable design limitations on the materials and on the capillary architecture [30,31]. Bioprinting, is an alternative approach in which living as well as non-living materials with a precise 3D organization are patterned and assembled in a computer-aided printing processes [32]. Currently, this is a long process with strong limitations on resolution and printable materials [30].

In contrast to the methods described above, sacrificial templating provides a more scalable solution to rapidly and precisely construct vascular networks [33-35,19]. Molded gelatin was used as a sacrificial element to create microfluidic networks within collagen, fibrin, and matrigel. Alternatively sacrificial sugar structures were used to form a 3D fluidic vascular network with diameters and densities similar to those of capillaries. In this case a rigid 3D lattice of melt-spun sugar filaments have been casted in a polymeric matrix, and then sacrificed to create microfluidic architecture in the bulk. In a similar approach, 3D printed rigid filament networks of sugar glass were also used to generate perfusable cylindrical networks in cell-laden gels [19].

However, 3D sacrificial molding has so far been limited to specific casting material and to a narrow range of crosslinking and polymerization strategies. In this paper, we used a biocompatible sacrificial material, and a means to mold it, in the casting of branched 3D vascular networks for large engineered tissues. The polymer utilized in the fabrication of the sacrificial template is poly(vinyl alcohol) (PVA). PVA is a water-soluble synthetic thermoplastic polymer with sufficient rigidity [36] to support the weight of an open branched 3D microfluidic network and the ability to rapidly dissolve compatibly with living cellular environment [37]. The thermoplastic nature of PVA makes this material an ideal candidate for industrial production [38]. PVA is already suitable for the most common industrial fabrication technologies (e.g. injection and compression

molding) [38] and 3D printing [39]. This flexibility results in a great advantage in terms of process scalability and costs compared to the other sacrificial materials. We demonstrated that 3D molding based on PVA sacrificial structures is compatible with synthetic and natural biomaterials and with a wide variety of different crosslinking and polymerization strategies. In this work first we have generated branched microfluidic networks in biocompatible matrices and demonstrated that these networks are able to sustain the cell viability of murine embryonic fibroblast in the core of cell-laden constructs. Second we have seeded those microfluidic networks with primary endothelial cells and we have perfused them into a custom made bioreactor to form a one-layer tubular endothelium hierarchically branched as a vascular network.

2. Materials and Methods

All starting materials were purchased from Sigma Aldrich and used as supplied unless otherwise stated.

2.1 Fabrication of Plexiglas mold

Two different microfluidic patterns were designed and converted into STEP files using AutoCAD mechanical 2012. Both patterns were copied on a 10 mm Plexiglas sheet using a computer numerical control machine (Mikron HSM 600) with the aid of open-mind hyperMILL cad/cam software, producing an open microfluidic negative mold (Fig. 1b).

2.2 Casting of sacrificial templates

The mold was treated with a solution of castor oil and ethanol (15% w/w) to make it hydrophobic and non-adherent to the PVA solution.

Compressed air blowing was used to remove the excess hydrophobic solution. Then approximately 3 mm layer of aqueous PVA (Mowiol 4-88) solution (20% w/w) was casted on the mold and allowed to dry overnight (Fig. 1a). The dried PVA layer was leveled with a Teflon blade repeatedly wiped on the mold wetted with water. This iterative process efficiently removes the polymer excess out of the microfluidic track. The mold was then allowed to dry overnight and the sacrificial template was gently removed from the mold with tweezers (Fig. 2c). Some of the sacrificial templates were immersed in a 2% (w/w) solution of Poly(DL-lactide-co-glycolide) (PDLGA, 50:50 lactide/glycolide ratio) in chloroform, similarly as described in literature [19]. All PVA templates were stored at 20°C with calcium chloride until use to avoid the absorption of ambient moisture.

2.3 Glass slide silanization and mold fabrication

Glass slides were silanized to be used in the molds fabrication. In brief, glass slides were washed with acetone, activated by plasma oxygen (70 W, 70 s) and immersed in a trichlorododecylsilane (TCS) solution (5% v/v in petroleum ether) for 10 minutes. Afterwards, glass slides were washed in succession with petroleum ether and ethanol, dried with gentle air flow and stored at room temperature. The mold for microfluidic experiment was prepared using two preformed silicone spacers of 1 mm thickness, with a rectangular void area of 20X12 mm interposed between two silanized glass slides. The PVA sacrificial structure was placed in mold and pressed between the two silicone spacers. In this way, the sacrificial structure is suspended in the middle of the rectangular chamber (20X12X2 mm) created by the void parts of the silicone spacers. In case

of multilayer mold, multiple sacrificial structures were suspended in the mold simply by adding silicone spacers.

The mold for cellular experiments was fabricated in a similar manner, by using two custom-made PDMS silicone spacers of 1 cm thickness. Each one has a semicylindrical void area of 5 mm radius and 15 mm height. The sacrificial structure was placed and fixed between the two PDMS spacers and suspended in the middle of the cylindrical chamber created by the void parts of the PDMS spacers.

2.4 Fabrication of microfluidic hydrogels

To form a microfluidic gel, the liquid gel precursors, were injected into the mold, described in section 2.3, around the sacrificial template and solidified, making sure that the sacrificial structure remains completely immersed except for its ends (Fig. 3). Gel precursors used in the fabrication of microfluidic gels were hydroxyethyl methacrylate (HEMA), agarose and gelatin methacrylated (GelMA). Gels were prepared following the procedures described in detail in the sections 2.7, 2.8 and 2.9. Gelation was achieved in different ways depending on the specific precursor. HEMA gelation in poly(hydroxyethyl methacrylate) (PHEMA) was achieved by free radical polymerization initiated by APS/TEMED. GelMa hydrogels were obtained by exposing the pre-polymer solutions to a long wavelength UV lamp (B-100AP, UVP LLC, 365 nm, 10 mW/cm2) for 5 min. Agarose gel was let solidify at 4°C for 20 min. After gelation of the precursor, the sacrificial structure was removed by flushing with phosphate buffered saline (PBS) at 37°C. This procedure yields a microfluidic gel, with one hole at each end. Multilayered lattice were successfully fabricated in a similar manner by stacking different sacrificial structure separated by 1 mm (Fig. 4) For microfluidic study, the obtained

gels were perfused with 5-10% w/v aqueous solution of dyes (E122, E104, E131 and E142) and 0.5 μm fluorescent microspheres (Latex beads fluorescent red), using a micro pump (Mp-6 micropump, Bartels), connected to the gels trough silicon tubing (perfusion rate 0.6 mL/min) (Fig. 5,6).

2.5 Fabrication of microfluidic porous hydrogels.

Two different methods were used to prepare porous hydrogels, namely foaming and salt leaching. According to the first method, the polymeric precursor solution was prepared by mixing HEMA (35% w/w), poly(oxyethylene) (20) sorbitan monolaurate (Tween 20, 3% w/w), tetrametiletilendiamine (TEMED, 4% w/w) and ethylene glycol dimethacrylate (EGDMA, 2% w/w), as a crosslinking agent, in a mixture of ethylene glycol and water (1/3 w/w). According to the second method, 1 g of NaCl salt crystals were crushed using a mortar and a pestle, and then added to a 2 mL salt saturated polymeric precursor solution containing HEMA, TEMED and EGDMA with the same proportions described in the first method. Then, to induce the free radical polymerization, 21 μL of aqueous ammonium persulfate (APS) solution (20% w/w) was added to the hydrogel pre-polymer solution to start a free radical polymerization. The foaming solution was rapidly injected into a large cylindrical mold, similar to the one described in section 2.3, and vigorously shaken until stable foam is obtained. Unlike the previous the salt leaching precursors paste was manually placed in each mold halves and then compressed around the sacrificial template by closing the mold. After gelation the microfluidic porous gels were purified from solvent, unreacted monomers and porogen, together with sacrificial structure removal, by washing at 37°C with ethanol/water a solution (50% w/w)

under mechanical stirring. Washing cycles were performed every 8 hours for 3 days. Microfluidic porous gels were then washed in bi-distilled water for other 3 days using the same procedure.

2.6 Cell maintenance

NIH-3T3 murine embryonic fibroblasts (CRL-1658, ATCC, Manassas, USA) were kept at 37°C in 5% CO_2 95% air-humidified incubator. The cells were cultured in Dulbecco's Modified Eagle's Medium (DMEM) supplemented with 10% Fetal Bovine Serum (FBS), 2 mM L-Glutamine, 100 units/mL penicillin and 100 µg/mL–streptomycin. Once 80% confluent, the 25 cm^2 flasks were passaged (subculture ratio 1:4 for multiple flasks) every 2-3 days. Human umbilical vein endothelial cells (HUVECs) were obtained from PromoCell (Heidelberg, Germany). The cells were cultured in M199 medium supplemented with 2 mM L-Glutamine, 100 units/mL penicillin and 100 µg/mL streptomycin and freshly added with 20% of fetal bovine serum (FBS), 50 ng/mL β-endothelial cell growth factor (ECGF) and 100 µg/mL Heparin. During perfusion experiments in bioreactor, cells were perfused with endothelial cell growth media EBM-2 (Lonza) supplemented with EGM-2 singleQuot Kit Supplemets and Growth (Lonza), and they were used through passage 8.

2.7 Preparation of HEMA solution for microfluidic studies.

Ethylene glycol solutions containing 50% (w/w) of HEMA and 0.5% (w/w) EGDMA, as a crosslinking agent, were prepared. Irgacure 2959 (Ciba, 1000 mg/mL in dimethyl sulfoxide) was added to the hydrogel pre-polymer solution to yield final concentrations of 2% (w/w). After the gelation, the microfluidic gels were further purified from solvent or

unreacted monomers of reaction by washing at 37°C with ethanol/water a solution (50% w/w) under mechanical stirring. Washing cycles were performed every 8 hours for 3 days. Microfluidic porous gels were then washed in bi-distilled water for other 3 days using the same procedure.

2.8 Preparation of Agarose pre-polymer solution for cell viability studies.

Low-melting point agarose was dissolved in sterile PBS (pH 7.4) to yield a final concentration of 2.5% (w/v) and heated to 70°C. NIH 3T3 fibroblasts were trypsinized, counted and suspended within the agarose solution at 10 x 10^6 cells/mL that was cooled to ~42°C and pipetted to ensure even cell distribution. Agarose solution was replica molded to yield a microfluidic hydrogel as described in Section 2.4. Cylindrical cell laden hydrogel constructs, 10 mm in diameter and 15 mm in height, were placed in cell culture flask containing 10 mL of DMEM and used as static controls. Encapsulated cells were also cultured for 3 days in bioreactor under perfusion at a rate of 0.6 mL/min.

2.9 Preparation of GelMA hydrogel for endothelialized network formation.

Methacrylated gelatin (GelMa) was synthesized as described previously [40]. Briefly, type A porcine skin gelatin was solubilized at 10% (w/v) into Dulbecco's phosphate buffered saline (DPBS; GIBCO) at 60 °C. Methacrylic anhydride (MA) was added to the gelatin solution at a rate of 0.5 mL/min under stirring at 50 °C until the concentration of MA was up to 20% v/v. The MA was reached and allowed to react for 1 h then additional warm (40 °C) DPBS was added to stop the reaction. The mixture was dialyzed against distilled water using 12-14 kDa cutoff dialysis tubing for 1 week at 40 °C to remove salts and methacrylic acid. After lyophilization for 1 week, a white porous foam was obtained and

stored at -80 °C until further use. Freeze dried GelMA was dissolved in ethylene glycol at 60 °C, containing the photoinitiator (Irgacure 2959, 1000 mg/mL in dimethyl sulfoxide, 2% (w/w)), to yield a final concentration of 12% (w/v). GelMA pre-polymer solution was molded to yield a microfluidic hydrogel as described in Section 2.4. Microfluidic hydrogels were purified from solvent and exceeding initiator by washing with ethanol/PBS mixture (50% w/w, 40 mL) and then pure PBS. Washing cycles were performed every 8 hours for 6 days under mechanical stirring. The sacrificial structure was removed during washing. HUVECs were seeded in the vascular lumen by injecting the cells suspension ($5x10^6$ cells/mL) into the vascular architecture with a micropipette. Microfluidic hydrogels were then immersed in fresh medium where HUVECs were allowed to attach in static culture for 3 hour before introducing flow. Cylindrical hydrogel constructs were perfused at flow rates of 1.5 mL/hour in the bioreactor. Medium was replaced every 5 days.

2.10 Cell viability and vascular network imaging.

Murine fibroblasts viability was assessed by live/dead fluorescence assay (Calcein AM/Propidium Iodide, Life Technology). To this aim, 1 mm slices of microfluidic cell-laden hydrogel were imaged using a confocal microscope (Leica Microsystems, Leica SP5). Cross-section image montages of cell-laden hydrogels were composed using ImageJ. Similarly, HUVEC cells were visualized by applying a live/dead fluorescence assay to the microfluidic gel. Images were captured along the channel length by confocal microscopy. The autofluorescence background outside the microfluidic channels was removed using Adobe Photoshop.

2.11 Immunofluorescent staining of nuclei and the actin cytoskeleton

After 7 days in culture, cells were fixed *in situ* with 4% paraformaldehyde, rinsed with PBS, permeabilized with 0.1% Triton X-100, blocked with 2% BSA and then incubated with Alexa fluor 555 directly conjugated to phalloidin, 0,11uM, (Invitrogen, USA) for 40 min at room temperature for filamentous actin staining. After washing in PBS, cells were stained with 9.4μM of bisBenzimide H 33258 (Hoechst). Images were captured along the channel length and channel depth using a Leica SP5 confocal microscope. The autofluorescence background outside the microfluidic channels was removed using Adobe Photoshop.

2.12 Numerical analysis of the shear stress

In order to disclose appropriate microfluidic working conditions for vascular tissue-engineering experiments, a fluid-dynamic simulation was performed. A finite element model was built by using COMSOL Multiphysics platform (Comsol, USA). A three-dimensional model was developed to evaluate the shear stress inside the adopted microfluidic geometry. The mesh refinement was compliant with the achievement of reliable values of the observables, mainly shear stress and local flow rate. In particular higher number of elements is utilized in critical regions such as branches' bifurcation. The resulting mesh consists of 234401 tetrahedral elements. The wall of the calculation domain is set to be no-slip. It thereby causes a pressure drop from the inlet to outlet, while the fluid pressure at outlet is fixed as zero. The considered working fluid is water assumed incompressible and with uniform and constant physical properties. The used dynamic viscosity, at the working temperature of 37 °C, is according with the value reported in literature [41]. The inlet flow rate is the controllable input and its value is selected in order to

maintain the flow in the laminar regime. The mesh, the boundary conditions and the values of the input parameters are given in Table I.

2.13 Bioreactor

A modified version of U-Tube bioreactor [42] was designed for the perfusion of the microfluidic scaffold (Fig 1a). The bioreactor consists of three parts: the input reservoir, the scaffold chamber and the output reservoir. In particular, the scaffold chamber is designed in two parts: one open part housing the scaffold and the other used to press fit the scaffold (Fig 1b). These parts were fabricated by insertion of silicon pipe with crescent diameter and connected to the reservoir unit thanks to tube-to-tube connectors (Value Plastic, USA), and silicon tubing (VWR). Each 15 mL reservoir unit was made by one silicon tube with two tubing connector (Brand, Germany) at the extremities connected on the top to a syringe filter and at the bottom to T-valve. This configuration has the advantage to be adaptable to any scaffold size using silicon tubing with different diameters. This ability is crucial when dealing with soft hydrogel constructs. Moreover the bioreactor can be reused several times since every part is autoclavable. Once the input reservoir is filled with 15 mL of medium and the seeded scaffold is press-fit into the open chamber, with the help of the other part of the chamber, the bioreactor is ready to operate. The bioreactor was suspended vertically in the incubator to avoid cells from settling on the surface of the reservoir (Fig 1c). Flow of medium was induced and regulated with the use of a syringe pump (KDS 230 Multi syringe Infusion/Withdrawal) connected to the input reservoir by silicon tubing. After the initial perfusion of 10 mL, the flow was reversed continuously every 6 mL.

Theoretical basis	Fluid flow mechanics	Navier-Stocks equations
Fluid parameters	Density	1000 [kg/m^3]
	Dynamic Viscosity	6.9*10^{-4} [Pa•s]
	Compressibility	Incompressible flow
Environmental boundary conditions	Temperature	310.15 [K]
	Inflow rate	1.5 [ml/hour]
	Type of fluid flow	Laminar flow
	Boundary condition (outlet)	No pressure
	Boundary condition (wall)	No slip
Meshing	Type of mesh element	Tetrahedral
	Maximum mesh size	64.9 [μm]
	Minimum mesh size	7.0 [μm]

TABLE 1. Fluid properties and modeling set-up used in simulation.

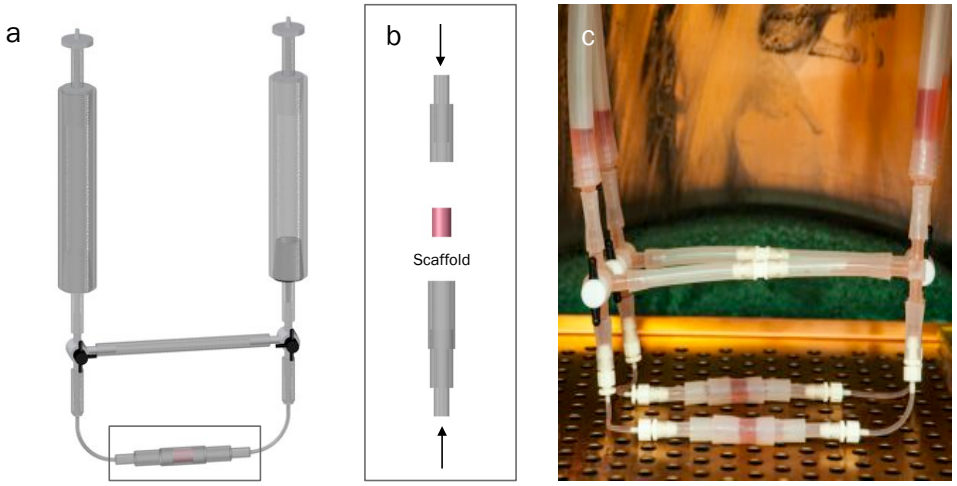

Figure 1. (a) Perfusion bioreactor scheme. The cellular medium oscillates between the two reservoir columns, flowing through the sample chamber, housing the scaffold. The direction of flow is reversed every 6 mL achieving continuous perfusion. (b) The chamber is made of one open part housing the scaffold and one used to press fit the scaffold. (c) Image showing the actual system during a perfusion experiment in standard incubator.

3. Result and discussion

3.1 Formation of sacrificial structures

Sacrificial templates were prepared by casting process according to two different patterns (Fig. 2c). The first one was designed to mimic branching capillaries and their fluidic features for cellular studies (right side of Fig. 2c). The second pattern was inspired to the work of King et al. [43] and intended for demonstrative purpose. Both the patterns were imprinted on plexiglas supports, to achieve negative molds. We demonstrate that the proportions of the sacrificial networks precisely replicate those of features on the casting mold (Fig 2b). In particular PVA meshes were characterized by a maximum features size of 500 μm and minimum dimension of 100 μm (Fig. 2c). Results show that our casting process allowed the generation of sacrificial template with predefined, multiscale, and reproducible patterns.

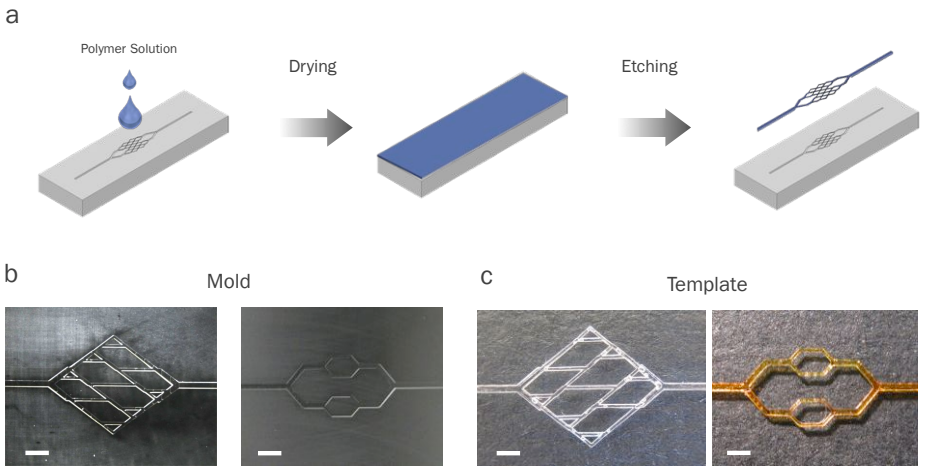

Figure 2. (a) Schematic diagram of sacrificial template fabrication. Aqueous PVA solution is casted on the mold and allowed to dry. Polymer excess out of the microfluidic track is removed by etching so that the sacrificial template can be demolded. (b) Images of Plexiglas mold (scale bars, 1 mm). (c) Top view of PVA sacrificial templates (scale bars, 1 mm).

PVA was chosen as sacrificial material because of its solubility in water as well as its mechanical properties. Indeed, PVA is a stiff and elastic at 25 °C, with Young's modulus 41.3 MPa, fracture strain of 41.3 MPa and maximum strain of 111% [36]. Furthermore the optical transparency [44] of the PVA solution allowed homogeneous photopolymerization of hydrogel precursors and do not affect after dissolution live imaging.

3.2 Fabrication of microfluidic gels

To fabricate hydrogel with interconnected microvascular networks, sacrificial elements were soaked in the precursor mixture except at their ends. Since the two ends of the template were not enclosed in the gel, they melted yielding openings at its extremities; flushing with aqueous solution through these openings rapidly removed the template. The process yields a monolithic gel with a vascular network matching the pattern of the sacrificial elements and therefore the features impressed on the original mold. Fig. 3b and 3c show examples of a microfluidic PHEMA gel that contained 200 μm wide channels. SEM cross-section images showed that the orthogonal profile of channel walls was preserved (Fig. 3d and 3e). In fact, the casting procedure used to create the sacrificial template stamp generates features with rectangular cross-sectional shapes. As expected, co-encapsulation and dissolution of three sacrificial templates produced microfluidic gels that contained three independent networks, as showed in Fig. 4d and 4e. It is worthy to note that channels were found to be smaller than the original features of the sacrificial template, which is probably due to sample shrinkage upon sample processing. Images of monolithic microfluidic gels confirmed that

the applied method is compatible with a wide range of materials (collagen and agarose), different precursors (i.e. HEMA and GelMA), different solvents (water, ethylene glycol and ethanol) and different crosslinking strategies (UV and free radical polymerization). The versatility of this approach is mainly due to properties of PVA. It is soluble in water, slightly soluble in ethanol, but insoluble in other organic solvents. Indeed, the PVA dissolution in dense aqueous media is slow enough to allow the matrix to be completely crosslinked before dissolution. PVA templates have shown to be compatible with either high and low molecular weight precursors thanks to its small pore size that prevents monomers from diffusing into the template during polymerization. When monomer diffusion occurs, as in the case of gelatin, the sacrificial structure becomes interpenetrated with hydrogel polymeric chain, thus occluding the microfluidic channels (data not shown).

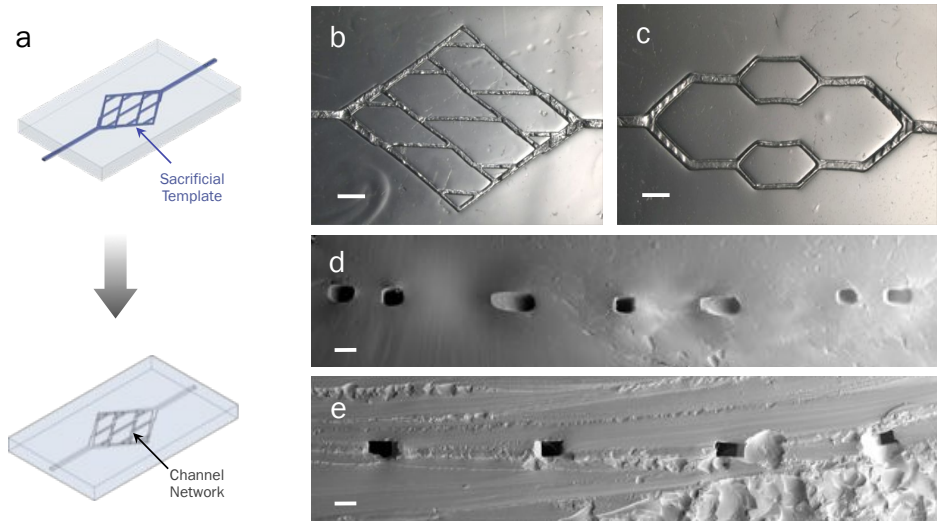

Figure 3. (a) Schematic fabrication diagram of microfluidic gels. (b,c) Optical images of microfluidic PHEMA hydrogels. Channels are slightly wider than the original template, due to the swelling of the hydrogels upon removal (scale bars, 1 mm). (d,e) SEM micrographs of multilayer microfluidic gel cross section (scale bar, 200 μm).

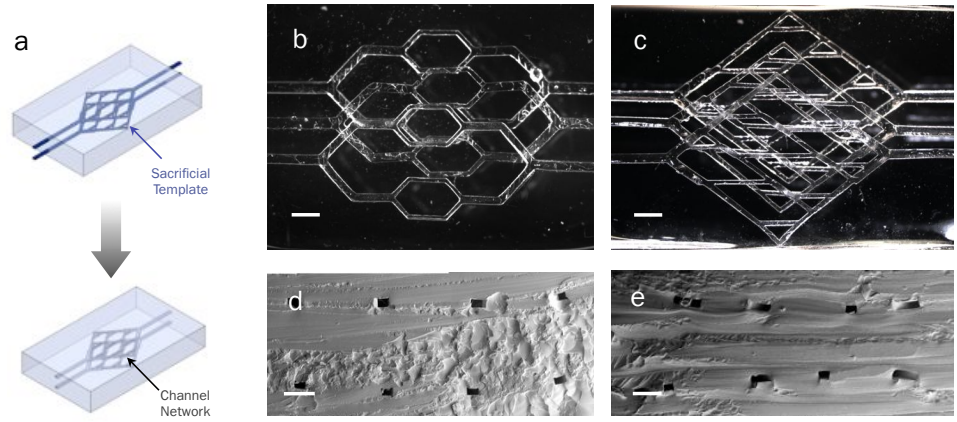

Figure 4. (a) Schematic diagram of fabrication of multilayers microfluidic gels. (b,c) Optical images of a multilayer microfluidic PHEMA gels (scale bars, 1 mm). (d,e) SEM micrograph of multilayer microfluidic gel cross sections (scale bar, 400 μm).

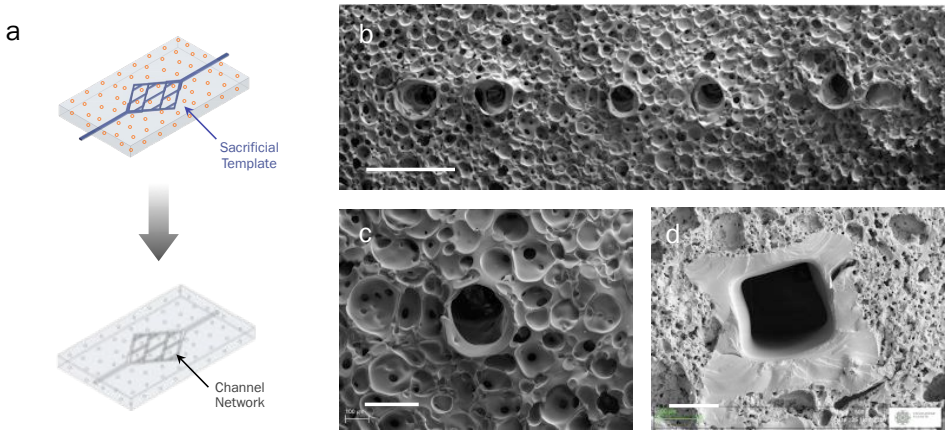

Figure 5. (a) Schematic diagram of fabrication process of microfluidic porous hydrogels. The sacrificial structure is encapsulated into the liquid hydrogel precursor together with a porogen material. After crosslinking the sacrificial template and porogen are removed by washing with water, yielding an open perfusable channel network in a porous matrix. (b) SEM micrograph showing the cross-section of porous scaffold produced by foaming with embedded microfluidic channels (scale bars, 500 μm). (c,d) SEM micrograph magnification showing the cross-sections of two porous scaffolds produced by foaming (c) and salt leaching (d). Cross sectional images show that the channels can be connected to (c) or isolated (d) from the hierarchical porosity of the scaffold, varying the reaction conditions (scale bars, 200 and 100 μm).

3.3 Fabrication of microfluidic porous scaffold

In order to demonstrate the integration between 3D sacrificial molding method and porous biomaterials we combined our method either with foaming or salt leaching techniques, that are commonly used to generate hierarchical porosity of tissue engineering scaffold. In brief the sacrificial structure was encased into the precursors mixture together with either a foaming solution or a porogen material. After the hydrogel crosslinking, both the sacrificial and the porogen elements were removed, leaving behind an interconnected microfluidic network within the porous matrix (Fig. 5a). The SEM images show the cross-sections of porous scaffolds with embedded microfluidic channels (Fig. 5b). We demonstrated the ability to generate microfluidic matrixes in which the fluidic pathways are connected (Fig. 5c) to or isolated (Fig. 5d) from the hierarchical porosity of the scaffold on both the porogen agent and monomer mixture. This results were possible thanks to the chemical and mechanical stability of the PVA sacrificial element. In fact, due to the low stiffness and thermal stability of the sacrificial material used so far, the sacrificial molding was not compatible with exothermic polymerization reaction [26], like those commonly used to generate porous matrices by foaming.

3.4 Microfluidic Study

To study the fluidic behavior of the gels, we placed a liquid solution at one extremity of the microfluidic network. This resulted in a convective flow of the solution through the channels, as shown by the delivery of 500 nm diameter fluorescent microspheres (Fig. 6 a,c). The mechanical resistance of the microfluidic network was assessed by perfusing them with an aqueous suspension of fluorescent microspheres at a rate of 0.6 mL/min. For these tests, microfluidic gel was connected to a micropump, as described in section 2.4. Under these conditions, we did not observed

any fracturing or deformation of fluidic features. This behavior can be ascribed to the monolithic nature of the gels as well as the lack of architectural seams, which make them suitable for non-leaking perfusion with laminar and turbulent flow. To establish whether microfluidic pathways increase the mass transport rate within the gels, we perfused them with a solution of azorubine at a rate of 0.6 mL/min (Fig. 6 b,d), and compared the diffusion of dye with that in bulk gels. Similarly, multilayer microfluidic gels were perfused using different dyes (Fig. 7 b,d). As expected, we noticed that the mass transport in a gel was enhanced by the presence of microfluidic networks and the PVA dissolution allows diffusive and connective transport into the bulk gel.

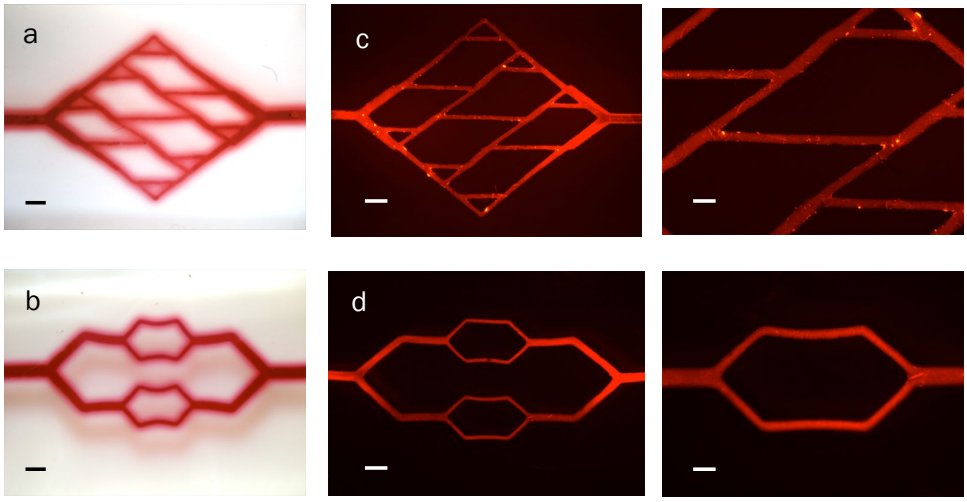

Figure 6. a). Optical images and enlargements of single layer microfluidic gel perfused with red dye solution (a,b) and fluorescent microspheres (b,d) (scale bars, 1 mm and 400 μm).

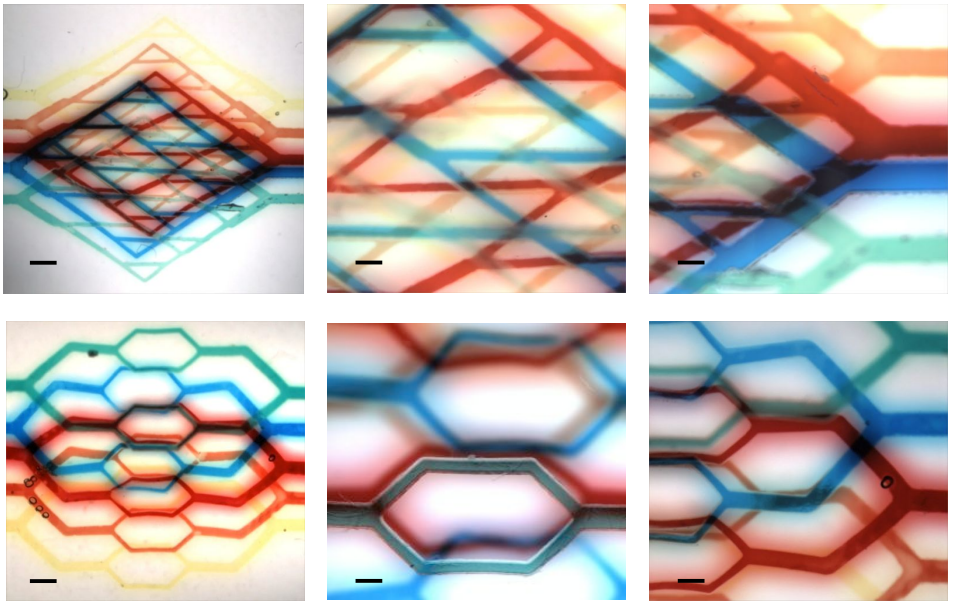

Figure 7. Optical images and enlargements representing a multilayers microfluidic networks in PHEMA gel perfused by different dye solutions (scale bars, 1 mm and 500 µm).

3.5 Cell viability study.

Cell-laden engineered constructs can develop a necrotic core due to lack of adequate mass transport. Therefore a major requirement of an engineered vasculature is to sustain cellular activity for extended time at physiological cell densities [19]. With the aim to demonstrate that our fabrication approach allow a greater nutrient mass transfer we generated a perfusable cylindrical cell-laden construct with a single layer of fluidic channels within its center, as described in the section 2.8. In this case the sacrificial structure was coated with PDLGA before casting in order to avoid the deformation of the sacrificial template during the slow agarose solidification. The coating is then gently removed with a tweezer to avoid reduction of nutrients transport into the hydrogel. In static conditions, live/dead fluorescence assay showed that the inner sections of cell-laden hydrogel follow a trend of decreasing cell viability that became

pronounced after 72 hours of static culture (Fig 8). Noteworthy, viability was higher in perfused microfluidic hydrogel than in static control, as previously demonstrated [45]. In particular, high cellular survival was evident at the gel perimeter and near perfused channels. The cell viability decayed radially from the perfused channels, as shown in Fig. 8a. These data can be explained by considering that perfused channels provide the gel with a continuous renewal of nutrient and removal of waste products that otherwise accumulate in static systems. Accordingly, microfluidic networks were found to sustain 3D cell culture with higher viability and greater proliferation compared to cells grown in bulk hydrogels. These results demonstrate that patterned perfusable architectures are able to provide effective mass transport throughout dense cell-laden construct, which is a fundamental requirement for the transition of implanted engineered tissues in the clinical practice.

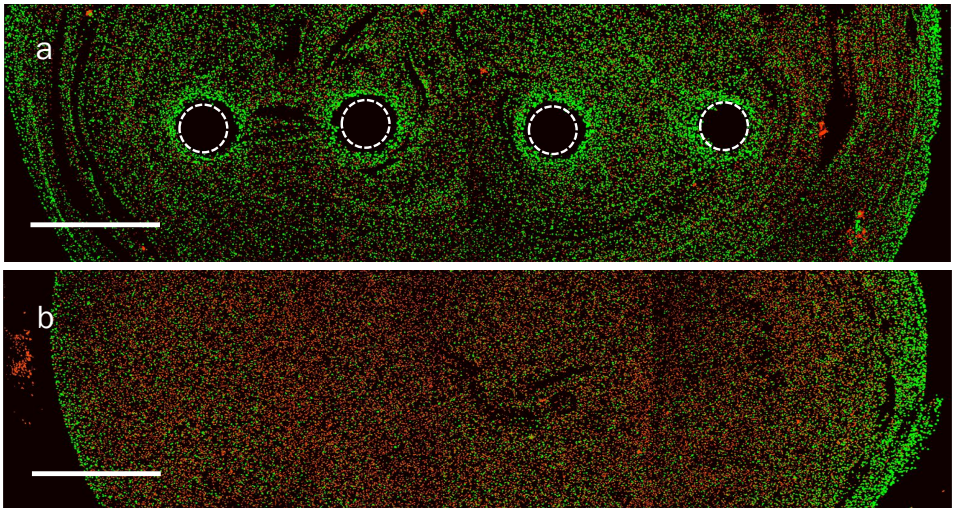

Figure 8. Cross-section images montages of cell laden agarose gels with (a) and without fluidic channels (b). NIH 3T3 murine fibroblasts (10^7 cells/mL) embedded in the gels were stained, after 72h of culture, with a fluorescent live/dead assay (green, Calcein; red, Propidium iodide). Cells survive at the gel perimeter and near perfused channels, and survival decayed radially deeper in the gels (scale bar, 1 mm).

3.6 Endothelialized network formation.

Endothelial cells were seeded as a dense suspension through one inlet of the microfluidic gel and quickly lined the walls of the entire branched vascular network. After perfusion for two days, cells still remain attached to the inner surfaces of the channels (Fig. 9a).

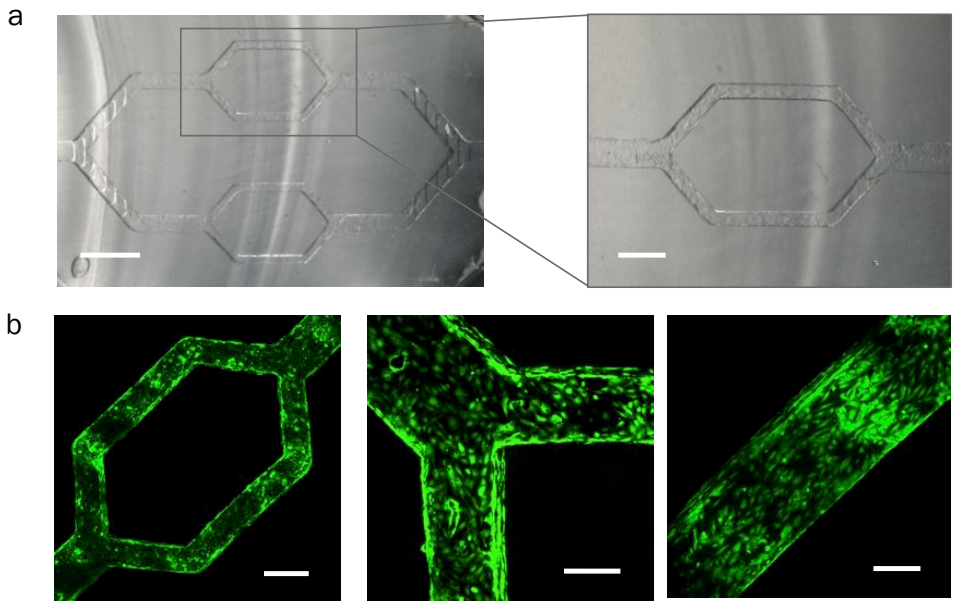

Figure 9. (a) Optical images of branched GelMA microfluidic network seeded with HUVEC cells after 7 days of perfusion in bioreactor (scale bars, 1 mm and 500 μm). (b) Live/dead fluorescent images showing different portions GelMA network coated on the walls by HUVECs (scale bars, 500 μm, 250 μm and 100 μm).

After 7 days, HUVECs formed confluent monolayers that conformed to the channel walls (Fig. 9 and 10) and thereby formed square endothelial lining, as confirmed by optical and immunofluorescence cross-sectional images (Fig. 10). HUVECs deformed the features of the microfluidics networks, so that the angles of squared section became noticeably rounded, as previously shown [26,46]. The cell-induced deformation leaves open the microfluidic networks and doesn't inhibit a continuous

perfusion of culture media. Both light microscopy and immunofluorescence imaging showed that most of the cells were aligned with the direction of the flow, as previously demonstrated [46].

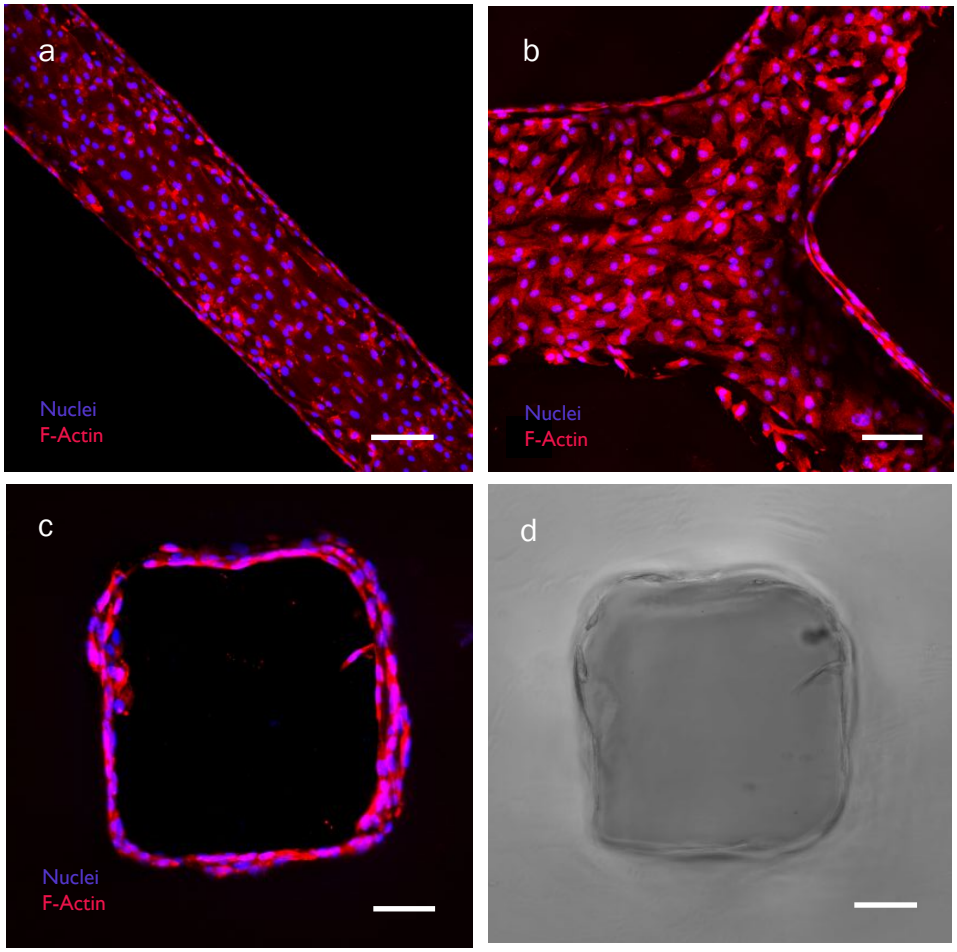

Figure 10. (a,b,c) Maximum intensity projection confocal images of HUVEC cells grown in microfluidic channels of GELMA hydrogel. The cytoskeleton actin and nuclei were stained with phalloidin (red), hoechst (blue), respectively. Cells form confluent monolayers on all channel walls in single (a) and branched channel (b). Fluorescent (c) and optical (d) cross-sectional images of three-dimensional reconstructions showing that HUVECs conform to the inner channel surfaces (scale bars, 100 μm for a,b and 50 μm for c,d).

Moreover, the organization of F-actin filaments was observed to change in response to shear stress. Depending on scaffold conditioning endothelial cells behavior and their angiogenic potential are altered, see Baiguera and Bagatti for a review [47], within this technique many factors and their combinations can be further studied. The formation of a confluent endothelial lining, regulating mass-transport exchange and controlling blood flow and vessel tone, is a fundamental requirement for vascularized living tissue.

3.7 Shear stress analysis.

Figure 11 shows the fluid flow velocity field as resulting from the simulation. The maximum locates inside the smallest branches of the microchannels. With a inlet flow rate of 1.5 (mL/h) the maximum flow velocity was calculated to be 6.005 (mm/s) and the corresponding Reynolds number 0.156. The latter value indicates that the flow regime is laminar, thus feed-backing the initial assumption on the fluid motion. Figure 12 shows the shear stress distribution. At the flow rates of 1.5 mL/h the estimated maximum shear stress was 0.988 dyne/cm^2 and localized at the channel walls. This value is comparable to those naturally sensed by vascular cells within the physiological conditions, which are in the range of 1–10 dyne/cm^2 [50,51]. From the computational simulation suitable experimental conditions for vascular tissue engineering are then established.

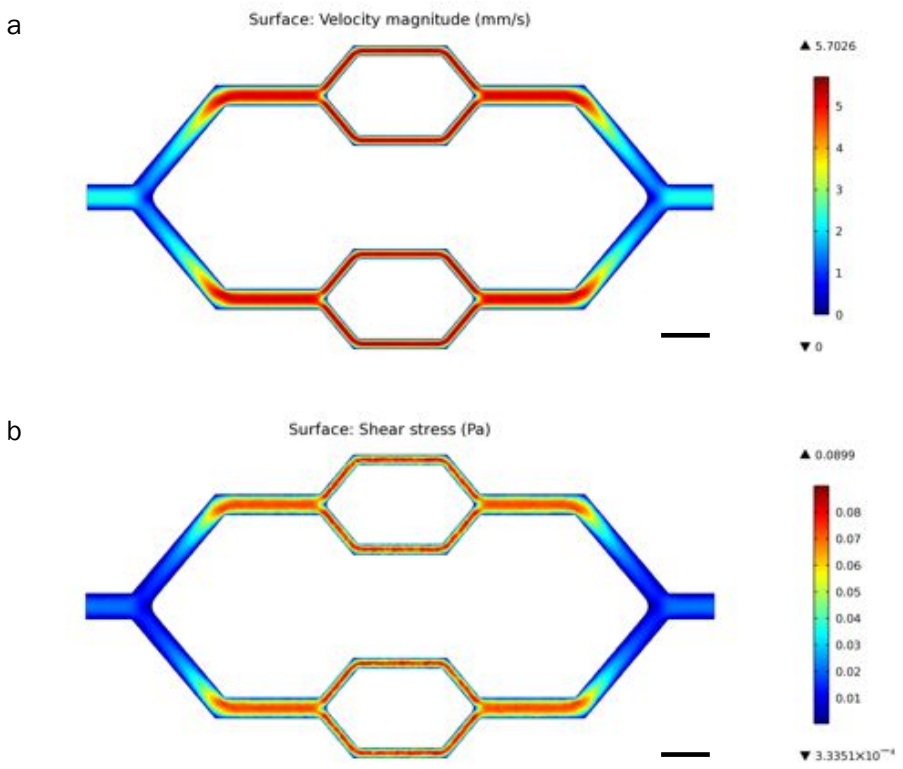

Figure 11. Fluid flow velocity field (a) and surface shear stress profile (b) of the internal walls of microfluidic gel perfused at 1.5 mL/hour rate (scale bar, 1 mm).

4. Conclusions

We have demonstrated a novel sacrificial templating approach by constructing robust, multilayer, microfluidic networks in hydrogel and shown that they can be reliably perfused without leaks or occlusions.

The obtained microfluidic networks have shown to provide effective nutrient and oxygen distribution throughout the hydrogel scaffold, resulting in cells with higher viability and greater proliferation as compared to cells grown in bulk gels. We also showed that PVA sacrificial molding is well suited for the creation of densely populated vital tissue

constructs with perfusable branching vascular channels. A key advantage of our method is that the perfusable scaffold is formed in a one step process simply by filling the empty volume around the template and by crosslinking the matrix. In fact it rapidity prevents the formation of a necrotic core in thick engineered construct. We expect that our method for controlled architecture of patterned fluidic networks coupled with further improvements in bioreactor technologies may enable the scaling of dense cellular constructs to large volume. Moreover, compared to other methods, it represents a progress in manufacturability and scalability, since it is compatible with a wide variety of synthetic and natural biomaterials, crosslinking strategies and polymerization reaction. The thermoplastic nature of the sacrificial element allows the use industrial processes (e.g. injection and compression molding) to manufacture it. This characteristic will allow rapid and reproducible mass production of multiscale microvascular architectures. Moreover, the chemical stability of sacrificial template guarantees a long-term storage and easy product distribution. We forecast that these characteristics will facilitate the adoption of the technology and its integration in many advanced therapies medicinal products.

However this approach is still limited to planar networks or their stacks, lacking the three-dimensional versatility of photolithographic methods, such as stereolithography. In order to overcome this limitation, a possible solution is the integration of 3D printing technology in the fabrication of the sacrificial template. This will allow to rapidly and reproducibly generate microvascular architectures voxel by voxel. We expect that this will require a limited effort considering that PVA is already used in 3D printing as support material [39]. Preliminary experiments are ongoing to test the feasibility of this approach.

References

[1] Langer R, Vacanti JP. (May 1993). Tissue engineering. Science 1993;260(5110): 920–926.

[2] Korossis SA, Bolland F, Kearney JN, Fisher J, Ingham E. Topics in Tissue Engineering In: Ashammakhi N, Reis RL; 2005. Volume 2, chapter 8.

[3] Khademhosseini A, Langer R, Borenstein J, Vacanti JP. Microscale technologies for tissue engineering and biology, Proc Natl Acad Sci USA 2006;103(8):2480-87.

[4] Lanza RP, Langer R, Vacanti JP. Principles of tissue engineering, San Diego: Academic Press; 2007

[5] MacNeil S. Progress and opportunities for tissue-engineered skin. Nature 2007;445(7130):874-880.

[6] MacNeil S. Biomaterials for tissue engineering of skin. Materials Today 2008;11(5):26–35.

[7] Clar C, Cummins E, McIntyre L, Thomas S, Lamb J, Bain L, Jobanputra P, Waugh N. Clinical and cost-effectiveness of autologous chondrocyte implantation for cartilage defects in knee joints: systematic review and economic evaluation. Health technology assessment 2005;9(47):1-82.

[8] Ruano-Ravina A, Jato Díaz M. Autologous chondrocyte implantation: a systematic review. Osteoarthritis Cartilage 2006;14(1):47-51.

[9] Safran MR, Seiber K. The evidence for surgical repair of articular cartilage in the knee. J Am Acad Orthop Surg 2010;18(5):259-266.

[10] Atala A, Bauer SB, Soker S, Yoo JJ, Retik AB. Tissue-engineered autologous bladders for patients needing cystoplasty. Lancet 2006;367(9518):1241-46.

[11] Parikumar P, John S, Senthilkumar R, Manjunath S, Baskar S, Haraguchi K, Abraham S. Successful transplantation of in vitro expanded human corneal endothelial precursors to corneal endothelial surface using a nanocomposite sheets. J Stem Cells Regen Med 2011;7(2):94.

[12] ClinicalTrials.gov Identifier: NCT01765244. Allogeneic Tissue Engineering (Nanostructured Artificial Human Cornea) in Patients With Corneal Trophic Ulcers in Advanced Stages, Refractory to Conventional (Ophthalmic) Treatment.

[13] Santos MI, Reis RL. Vascularization in bone tissue engineering: physiology, current strategies, major hurdles and future challenges. Macromol Biosci 2010;10(1):12–27.

[14] Lovett M, Lee K, Edwards A, Kaplan DL. Vascularization strategies for tissue engineering. Tissue Eng Part B Rev 2009;15(3):353-370.

[15] Atala A, Kasper FK, Mikos AG. Engineering Complex Tissues. Sci Transl Med 2012;4(160):160rv12.

[16] Radisic M, Yang L, Boublik J, Cohen RJ, Langer R, Freed LE, Vunjak-Novakovic G. Medium perfusion enables engineering of compact and contractile cardiac tissue. Am J Physiol Heart Circ Physiol 2004;286(2):H507-H516.

[17] Rouwkema J, Rivron NC, van Blitterswijk CA. Vascularization in tissue engineering, Trends Biotechnol 2008;26(8):434-441.

[18] Novosel EC, Kleinhans C, Kluger PJ. Vascularization is the key challenge in tissue engineering. Advanced Drug Delivery Reviews 2011;63(4-5):300–311.

[19] Miller JS, Stevens KR, Yang MT, Baker BM, Nguyen DH, Cohen DM, Toro E, Chen AA, Galie PA, Yu X, Chaturvedi R, Bhatia SN, Chen CS. Rapid casting of patterned vascular networks for perfusable engineered three-dimensional tissues. Nature Materials 2012;11(9):768-774.

[20] Muschler GF, Nakamoto C, Griffith LG. Engineering principles of clinical cell-based tissue engineering. J Bone Joint Surg Am 2004;86-A(7):1541-58.

[21] Jain RK, Au P, Tam J, Duda DG, Fukumura D. Engineering vascularized tissue. Nature Biotechnology 2005;23(7):821-823.

[22] Jain RK, Au P, Tam J, Duda DG, Fukumura D. Engineering vascularized tissue. Nat Biotechnol 2005;23(7):821-823.

[23] Khademhosseini A, Vacanti JP, Langer R. Progress in tissue engineering. Scientific American 2009;300(5),64-71.

[24] Laschke MW, Menger MD. Vascularization in tissue engineering: angiogenesis versus inosculation. Eur Surg Res 2012;48(2):85-92.

[25] Bae H, Puranik AS, Gauvin R, Edalat F, Carrillo-Conde B, Peppas NA, Khademhosseini A. Building Vascular Networks. Sci Transl Med 2012;4(160):160ps23.

[26] Golden AP, Tien J. Fabrication of microfluidic hydrogels using molded gelatin as a sacrificial element. Lab Chip 2007;7(6):720-725.

[27] Ling Y, Rubin J, Deng Y, Huang C, Demirci U, Karp JM, Khademhosseini A. A cell-laden microfluidic hydrogel. Lab Chip 2007;7(6):756-762.

[28] Choi NW, Cabodi M, Held B, Gleghorn JP, Bonassar LJ, Stroock AD. Microfluidic scaffolds for tissue engineering. Nature Mater 2007; 6(11):908-915.

[29] Cuchiara MP, Allen AC, Chen TM, Miller JS, West JL. Multilayer microfluidic PEGDA hydrogels. Biomaterials 2010;31(21):5491-97.

[30] Bettinger CJ, Borenstein JT, Langer R. in Nanotechnology and Tissue Engineering: The Scaffold. Micro- and Nanofabrication of Biodegradable Materials for Tissue

Engineering. In: Laurencin CT, Nair LS, editors. CRC Press, Boca Raton, FL, USA; 2008.

[31] Huang GY, Zhou LH, Zhang QC, Chen YM, Sun W, Xu F, Lu TJ. Microfluidic hydrogels for tissue engineering. Biofabrication 2011;3(1):012001.

[32] Visconti RP, Kasyanov V, Gentile C, Zhang J, Markwald RR, Mironov V. Towards organ printing: Engineering an intra-organ branched vascular tree. Exp Opin Biol Therapy 2010;10(3):409-420.

[33] Therriault D, White SR, Lewis JA. Chaotic mixing in three-dimensional microvascular networks fabricated by direct-write assembly. Nature Mater 2003;2(4):265-271.

[34] Bellan LM, Singh SP, Henderson PW, Porri TJ, Craigheada HG, Spectorb JA. Fabrication of an artificial 3-dimensional vascular network using sacrificial sugar structures, Soft Matter 2009;5:1354-57.

[35] Wu W, Hansen CJ, Aragón AM, Geubelle PH, Whitebd SR, Lewis JA. Direct-write assembly of biomimetic microvascular networks for efficient fluid transport. Soft Matter 2010; 6:739-742.

[36] Chen C, Torrents A, Kulinsky L, Nelson RD, Madou MJ, Valdevit L, LaRue JC, Mechanical characterizations of cast Poly(3,4-ethylenedioxythiophene): Poly(styrenesulfonate)/Polyvinyl Alcohol thin films. Synthetic Metals 2011;161(21–22): 2259–67.

[37] DeMerlis CC, Schoneker DR. Review of the oral toxicity of polyvinyl alcohol (PVA).,Food Chem Toxicol 2003;41(3):319-326.

[38] Mowiol® Polyvinyl Alcohol, Clariant GmbH Division CP 1999.

[39] Visser J, Peters B, Burger TJ, Boomstra J, Dhert WJ, Melchels FP, Malda J. Biofabrication of multi-material anatomically shaped tissue constructs. Biofabrication. 2013 Sep;5(3):035007.

[40] Nichol JW, Koshy ST, Bae H, Hwang CM, Yamanlar S, Khademhosseini A. Cell-laden microengineered gelatin methacrylate hydrogels. Biomaterials 2010; 31(21):5536-44.

[41] Aleksandrov AA, Trakhtengerts MS. Viscosity of water at temperatures of −20 to 150°C. Journal of engineering physics 1974;27(4):1235-39.

[42] Wendt D, Marsano A, Jakob M, Heberer M, Martin I. Oscillating Perfusion of Cell Suspensions Through Three-Dimensional Scaffolds Enhances Cell Seeding Efficiency and Uniformity. Biotechnology and bioengineering 2003;84(2):205-14.

[43] King KR, Wang CCJ, Kaazempur-Mofrad MR, Vacanti JP, Borenstein JT. Biodegradable Microfluidics. Adv Mater 2004;16(22):2007-12.

[44] Mahendia S, Tomar AK, Chahal RP, Goyal P, Kumar S. Optical and structural

properties of poly(vinyl alcohol) films embedded with citrate-stabilized gold nanoparticles. J Phys D Appl Phys 2011;44:205105.

[45] Song YS, Lin RL, Montesano G, Durmus NG, Lee G, Yoo SS, Kayaalp E, Haeggström E, Khademhosseini A, Demirci U. Engineered 3D tissue models for cell-laden microfluidic channels. Anal Bioanal Chem 2009;395(1):185-193.

[46] Esch MB, Post DJ, Shuler ML, Stokol T. Characterization of In Vitro Endothelial Linings Grown Within Microfluidic Channels. Tissue Eng Part A 2011;17(23-24):2965-71.

[47] Baiguera S, Ribatti D. Endothelialization approaches for viable engineered tissues. Angiogenesis 2013;16(1):1-14.

[48] Black AF, Berthod F, L'heureux N, Germain L, Auger FA. In vitro reconstruction of a human capillary-like network in a tissue-engineered skin equivalent. FASEB J 1998;12(13):1331–40.

[49] Chen X, Aledia AS, Ghajar CM, Griffith CK, Putnam AJ, Hughes CC, George SC. Prevascularization of a Fibrin-Based Tissue Construct Accelerates the Formation of Functional Anastomosis with Host Vasculature. Tissue Eng Part A 2009;15(6):1363–71.

[50] Resnick N, Yahav H, Shay-Salit A, Shushy M, Schubert S, Zilberman LC, Wofovitz E. Fluid shear stress and the vascular endothelium: For better and for worse. Prog Biophys Mol Biol 2003;81(3):177–199.

[51] Wang S, Tarbell JM. Effect of fluid flow on smooth muscle cells in a 3- dimensional collagen gel model. Arterioscler Thromb Vasc Biol 2000;20(10):2220–25.

Chapter 6

Conclusions and Perspectives

Alessandro Tocchio[1,2]

[1]Fondazione Filarete, Viale Ortles 22/4, 20139 Milano, Italy; [2]SEMM, European School of Molecular Medicine, Campus IFOM-IEO, Via Adamello 16, 20139 Milano.

In this PhD thesis we have developed a technology platform towards the design of vascularizable scaffolds for large tissues engineering.

To this aim we have designed a series of biodegradable and biomimetic poly(amidoamine) based hydrogels. In order to improve the mechanical and degradation properties of this class of materials, we investigated several key parameters of the synthesis reaction, such as monomer ratio, reaction time and introduction of acrylic chains. This approach allowed to achieve a variety of hydrogels and eventually resulted in the optimization of both the chemical and biophysical properties as a function of the biological response. Thanks to these studies we developed a versatile biomaterials platform with tailorable physico-chemical and biological properties suitable both for *in vitro* culture and *in vivo* tissue engineering applications.

In particular, this biomaterials library was further investigated to design a novel photopolymerizable matrix for three-dimensional cell encapsulation and microfluidic applications needed for later stages of this work. To this aim, RGD-mimic diacryl amide-terminated PAA oligomers were conjugated with Jeffamine® . The novel triblock copolymer obtained was able to

promote high surface cell adhesion and proliferation and sustained cell viability in 3D. Further, high pattern fidelity and resolution were demonstrated in the fabrication of perfusable endothelialized microfluidic channels. These studies support the use of PAA-based hydrogels as tunable and inexpensive biomaterials for the creation of complex cell-laden microengineered constructs.

In order to match the requirements of hierarchical porosity and roughness, mimicking the complexity of the *in vivo* milieu, we developed macroporous PAA hydrogel foams. PAA foams were able to promote cell adhesion and enhance three-dimensional endothelial cell growth in vitro. Biocompatibility and the capacity to promote cell migration within OPAA foams were demonstrated through subcutaneous implant in murine model. *In vivo* results indicate that PAA foams have the potential to induce vascularization thanks to their RGD-mimicking sites, which are able to promote endothelial cell adhesion and proliferation. The extensive investigation of both the physico-chemical behavior and biological response demonstrated that PAA foams are able to provide appropriate scaffolding to support and guide soft tissue growth.

Despite significant successes have been achieved in the field of tissue engineering, insufficient mass transport is still limiting the size of the engineered tissues to smaller than clinically relevant dimensions. Novel solutions are required to reduce the gap between the nutrient diffused region in the scaffold and the desired construct size. To this aim, we developed an innovative fabrication approach to engineer porous and cell-laden hydrogel scaffolds with a perfusable microfluidic network. This approach was demonstrated to be suitable for the creation of densely populated vital tissue constructs with perfusable branching endothelialized channels. *In vitro* perfusion was efficiently performed using a customized bioreactor, specifically developed for the perfusion of

soft hydrogel scaffolds. One key advantage of this technology is that the perfusable scaffold is formed in a one step process simply by filling the empty volume around the sacrificial template, crosslinking the matrix and then dissolving the template. This rapid method prevents the formation of a necrotic core in thick cellular construct, indicating that this technology could provide a solution to scale current engineered tissue to clinically relevant dimensions.

Overall, the reported results have important implications in soft tissue engineering, especially in the design of vascularizable scaffolds for adipose tissue regeneration. Current approaches in this field rely on both controlling and recruiting of a vascular network. These constraints could be satisfied leveraging our technology platform in order to design scaffold composites able to control and guide angiogenesis both *in vitro* and *in vivo*. To achieve this goal and optimize the techniques described in this thesis, different challenges still remain. One of the main challenges resides in the optimization of the microstructural parameters of the scaffold to fine-tune the fluids and biomolecules dynamics within the scaffold. This optimization, so far hampered by design limitations, would allow: i) to mimic the natural tissue growth *in vitro*, providing suitable conditions for vascularization; ii) to enable *in vivo* angiogenesis, enhancing vessels ingrowth within the scaffold and favoring the anastomosis with the host vasculature.

Nanotechnology in medicine: from inception to market domination

Alessandro Tocchio[1,2] and Valentina Morigi[3] et al.

[1]Fondazione Filarete, Viale Ortles 22/4, 20139 Milano, Italy; [2]SEMM, European School of Molecular Medicine, Campus IFOM-IEO, Via Adamello 16, 20139 Milano, Italy; [3]The Methodist Hospital Research Institute (TMHRI), Houston, TX, U.S.A.

This chapter has been published: Morigi V, Tocchio A, Pellegrini CB, Sakamoto JH, Arnone M, Tasciotti E, Nanotechnology in medicine: from inception to market domination. Journal of Drug Delivery 2012; Volume 2012, Article ID 389485

1. Introduction

Globally defined as the application of nanotechnology to the clinical arena, nanomedicine has its roots in the same basic concepts and principles of nanotechnology, i.e. materials with the nano-scale features present unique characteristics, otherwise absent at a macroscopic level [1]. Just as nanotechnology benefits from mathematics and engineering, nanomedicine too has a multidisciplinary nature involving notions and techniques borrowed from biology, chemistry and physics [2]. As a result of this successful marriage, nanostructure materials display emerging functions that have exceptional benefits when applied to medical devices.

The success of nanotechnology in the healthcare sector is driven by the possibility to work at the same scale of several biological processes, cellular mechanisms and organic molecules; for this reason, medicine

has looked at nanotechnology as the ideal solution for the detection and treatment of many diseases. One of the many applications of nanotechnology to the medical sector is in the field of drug delivery. The advent of protocols and methods for the synthesis, functionalization, and use of nanoparticles and nano-carriers has flooded the scientific and clinic community with new therapeutic approaches from molecular targeting to radiofrequency ablation, from personalized therapies to minimally invasive techniques.

While most members of the investment community are able to grasp the meaning of nanotechnology and can expertly launch and manage a viable product into the market, they are limited in their conceptual understanding of this scientific discipline and the intricate inner workings behind the product's functionality. [3] On the contrary, those involved in the scientific research recognize that nanomedicine is an expansion of nanotechnology, but have very little understanding of the business expertise required to develop their technologies into a commercial product. [3] Cooperation is therefore needed between the two factions in order to lead nanomedicine-based inventions to a successful market position.

2. Nanomedicine Market

With 76% [4] of the publications and 59% [4] of the patents, drug delivery is the market segment that dominates the nanomedicine sector. In vitro diagnostics represent the second leading field, contributing with 11% [4] of the publications and 14% [4] of the patent filings. According to the European Commission [4] in a global vision, clustering the publications in the three geographical areas USA, Europe and Asia (Japan, China, South Korea, Taiwan, Singapore and India) Europe is leading with 36% [4] of the worldwide publications, followed by the USA with 32% [4] and Asia with

18%. [4] Considering all patent applications in the different fields of nanomedicine, USA hold a share of 53%, [4] Europe has 25% [4], and Asia 12%. [4] Biopharmaceutical and medical devices companies are well aware of the potential applications of nanotechnology to the healthcare sector, as demonstrated by the increasingly growing partnerships between these enterprises and nanomedicine start-ups.

According to a research report from Business Communications Company (BCC) Research, despite the catastrophic consequences of the 2008-09 crisis on capital markets, the global nanomedicine sector, which was worth $53 [5] billion in 2009, is projected to grow at a compound annual growth rate (CAGR) of 13.5%, surpassing $100 billion in 2014 (See Figure 1a) [5]. One of the largest segments of this market is represented by anticancer products. Valued about $20 billion [5] in 2009, it is expected to reach $33 billion [5] in 2014, growing at a CAGR of 11% [5] (see Figure 1b.).

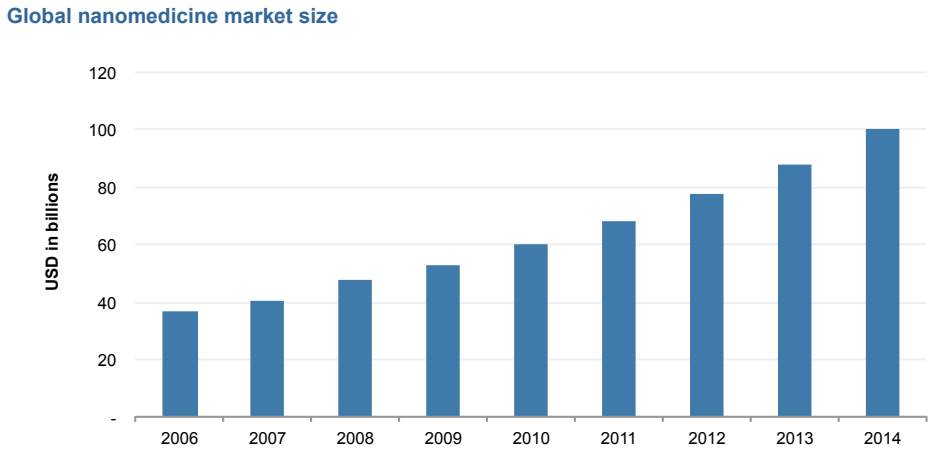

Figure 1a. This graph shows the global nanomedicine market size, measured in terms of revenues, such as sales revenues, grants revenues and milestones. From 2006 to date, a steady growth has occurred, which is expected to continue through 2014, at a CAGR of 13.5% [5].

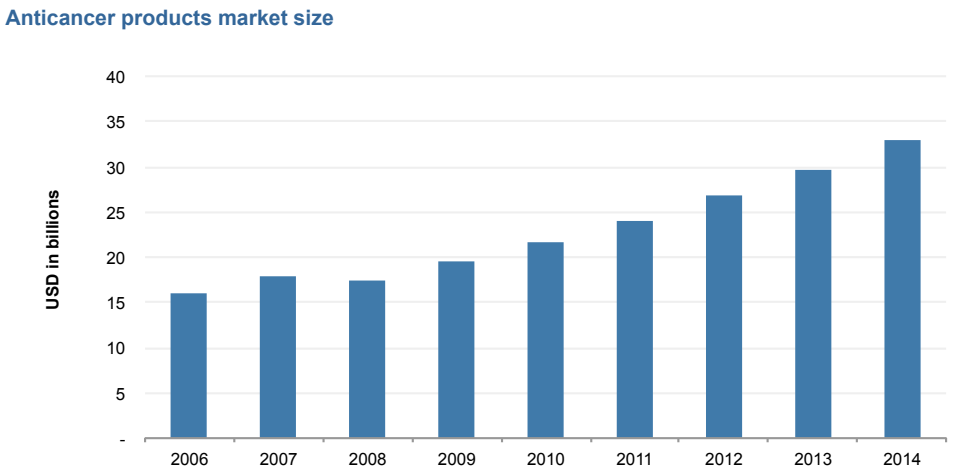

Figure 1b. The graph illustrates the market size for the anticancer applications segment. Except for a slight decrease in 2008, the market has and it is predicted to expand, by a factor of steady growth [5].

3. Financing of Nanomedicine

3.1. Common issues in the investments on innovation

In The primary output of innovation is obtaining the know-how, which the inventor initially possesses. Unfortunately, the confidentiality of this knowledge can be breached and its use by one company cannot preclude the use of the same by another one. Therefore, investors approaching novel projects are aware of the fact that they will not be able to easily appropriate the total returns of the investment undertaken. As a consequence, there is a lack of attractiveness in financing innovative projects. In fact, from the perspective of economic theory, it is complex to find funding for innovative ideas in a competitive market place. [6] Even in large firms, there is evidence of shortages in resources to spend on the innovative projects that the managers would like to undertake. [6] There are a number of reasons for this phenomenon: low expected returns due to an incapacity to capture the profits from an invention, the

exaggerated optimism in undertaking an investment on breakthrough projects and most notably the uncertainty and risk associated with these projects. Technology-based companies can also consider imitating the inventions developed by competitors. However, Mansfield et al [7], using survey evidence, found that imitating is not costless, and could result in expenses equal to 50% [7] to 75% [7] of the cost of the original invention, not eliminating the underinvestment problem. Policymakers are trying to change the funding situation, by facilitating the invention process, rationalizing the interventions through government encouragement of innovative activities, sustaining the intellectual property system, allowing Research & Development tax incentives, and supporting research collaborations. Nonetheless, the path that leads the nano-scale outcome from the laboratory to the marketplace is long and expensive, putting the inventor in a position of disadvantage.

3.2. Asymmetric information, credibility and commitment

The financing and management of innovative products in nanomedicine – like many young and innovative multi-sectoral fields – happens in a context of both financial and product markets failures. These make the financing and management of innovation a particularly complex process, which is also reflected in the corporate governance structure of innovative firms.

Asymmetric information, transaction costs, intangible goods, credibility and commitment issues, jointly with high and unique risks, make it impossible for traditional financial institutions to be part of the picture, paving the way for angel investors, seed and venture capital investors, or other forms of non-traditional financial institutions.

The asymmetric information issue is partly due to the different information set in the hands of the innovator as opposed to that of the possible provider of funds (Admati and Pfleiderer 1994) [8], which gives rise to a "two-sided incentive problem" (Hellmann 1998) [9]: the best incentive to reconcile the conflicting behavior of entrepreneur (unobservable efforts) and venture capitalist (monitoring costs) is multi-stage financing. In an alternative approach, staged financing solves the lack of credibility and of an adequate commitment technology on the part of the entrepreneur.

The credibility and commitment issues arise because the entrepreneur possesses a "unique human capital" (Neher 1994) [10]: once the Venture Capital has provided financing, the entrepreneur can decide to withdraw and, therefore, hold the VC hostage of his/her decisions. In such conditions, the VC would not provide financing, as the entrepreneur cannot make a credible commitment not to withdraw. The solution in this case is the "staged capital commitment" similar to Hellmann (1998) [9] with a different rationale: the unique human capital of the entrepreneurs must be blended with the firms in various sequential stages. This leads to a progressive increase in the expected value of the firm (in terms of a future Initial Public Offering), so that the initial investments become the collateral (the firm itself) for the VC, providing the right incentive to continued financing.

The two approaches also require both the entrepreneur and the VC to participate in the ownership of the firm (as financing happens with shares), and therefore an evolving strategic and managerial relationship between the two parties in an evolutionary view of the firm (Arnone and Giacometti 1999) [11]. Often the VC possesses very good managerial skills, due to its experience in dozens of start-ups, while the innovating entrepreneur has little or none. Against this backdrop, the staged

financing with shares (i.e., joint ownership) also helps addressing the key issue of management decisions: at the beginning of the 'relationship', the entrepreneur has the most detailed technical knowledge and almost complete managerial powers to set up all the technical work that needs to be embodied into the firm. As this knowledge is transferred to the firm other managerial aspects take priority (e.g. competition, finance and governance) where the VC has better skills. By increasing VC ownership in stages, management powers can be transferred to VC-appointed managers, with specific skill in running an evolving start-up firm and take it adequately to the market, usually with an IPO.

Due to significant concern and disapproval for fundraising in support of innovation, fledgling nanomedicine companies, do not have an endless number of financial options. Therefore, in order to establish start up companies, co-funders generally commit their own money and expertise into it. This is one aspect that represents the internal capital of the start-up, as opposed to the external one, which has to be collected from other sources. At this stage start-up companies turn towards government and foundations' grants (i.e. the National Institutes of Health, and the National Science Foundation programs), in order to finance the research and development of their innovative products. These funds are also intended to protect the intellectual property of these novel discoveries and to attract professional investors.

In order to expand and sustain their business, nanomedicine start-ups usually begins by turning to angel investors - private financiers who provide seed fundings - then to Venture Capitalists (VCs). The interaction and support of these professional investors is essential to assess whether a market entry is possible and to decide which market share managers can realistically achieve at different time horizons. In fact VCs enter at a specific moment of the life of the company when it is still in an

early stage, but has already strongly proved its value and perspective. According to Paul A. Gompers and Yuhai Xuan, the general role of VCs is to alleviate asymmetric information between private venture capital-backed targets and the public acquirers, building a bridge between the two parts [12]. These funds plan investment decisions in order to decrease possible agency costs that afflict young entrepreneurial companies. Venture capitalists usually add value to companies in which they invest beyond pure financing, providing managerial expertise, industrial experience, contacts and – not least – momentum. [12] There is strong evidence of VCs involvement in the management of the financed nanotechnology companies as they often have higher costs and longer development times compared to an equivalent information technology business. Furthermore, Backer and Gompers [13], asserted that venture capital-backed firms have better boards of directors compared to those not financed by VCs. This evidence confirms the crucial role played by VCs in the economic success of nanomedicine-based products.

Corporate finance literature has devoted a meaningful stream of research to the relevance of board composition as a useful tool against different typologies of asymmetric information and agency costs. Literature has clearly underlined the existence of a connection between firms' performances and board composition. However, notwithstanding these important results, there is not a universally accepted evidence about the optimal board composition that allows the minimization of the above mentioned agency costs. In the VC literature evidence, a board composed by internal, external and instrumental (Baysinger and Butler 1985) [14] should achieve the result of the minimization of agency costs that is a propaedeutic step for a feasible way out for VC investors.

3.3. Landscape

In 2007 investment in nanotechnology by VCs was US $702 million [15], involving 61 deals. 27% [15] went to healthcare and life science, 31% [15] to energy and environment, and 42% [15] to electronics & IT. Two years later, nanotechnology market captured US $792 million from VCs. [15] Of these, the largest share (51%) [15] went to healthcare and life sciences, followed by energy and environment, and electronics & IT, with 23% and 17%, respectively. [15] Doubling the funds invested in the healthcare segment in just two years, the VC industry has demonstrated a clear interest in investment opportunities in the nanomedicine field (See Figure 2.a and 2.b).

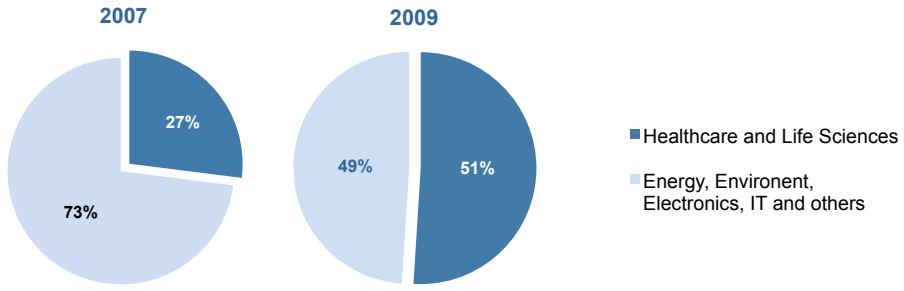

Figure 2. VC funding of nanotechnology in 2007 (a) and 2009 (b). The pie charts demonstrate the attractiveness of nanomedicine market for venture capital investors. Captivated by the great potential of future development, in only two years VCs have shifted their focus on the 'science of the tiny things', nearly doubling investments in this sector.

Although venture capital investors want to continue to be involved in the science & technology of the small scale, they are extremely cautious about large investments in nanotechnology and nanomedicine, as positive returns on investments are expected only in the long term, especially for nanomedicine. [3] VCs and private investors are still burned by the sub-prime crisis of 2008 [16], which took a serious toll on their

assets, causing catastrophic losses to the whole financial community and restricted access to funds. However, the decline of fundraising might also be a result of ordinary funding cycles, with several VCs having already raised enough resources for the short term. [17] Experts see the Wall Street's crisis of 2008, as a possible regime-change [16], rather than a temporary market malfunctioning. After four decades of fairly straightforward access to relatively inexpensive capital, capital markets are currently undergoing major changes. [16] According to the National Science Foundation, innovation is an essential source of competitiveness for economy [18] and represents an excellent opportunity to sustain the economic recovery after the 2008 crisis. As usually happen after a crisis, investors become risk adverse, adopting more rigid risk-cover policies, but there is evidence that the nano-business seems to be too attractive not invest in.

4. Business Strategies

The main business area characterizing a nanomedicine company, as well as pharmaceutical and biotechnology industries, is the research and development (R&D). Choosing the R&D strategy, managers evaluate two possible options. The first is based on the idea to perform the entire process inside the company, composing a highly experienced team of scientists. The second option is based on universities or research institutes and is founded on the reliance on leading academic laboratories created over time by "scientific stars". This second possibility will certainly reduce company costs as these academics frequently co-found the companies based on their discoveries and become part of the scientific boards. We have gathered strong evidence of this second option for the R&D strategy in the companies we analyzed. The commercialization of the research-based product might represent

another business area of the nanomedicine company. However, the typical option considered and adopted by managers is to license out the manufacturing and commercialization of the nanomedicine-based product to larger companies. If this is the case, the business model pursued will not include commercialization, and the company will be technology and research based.

The commercialization of the nanomedicine products/technologies is currently driven by start-ups and Small-medium enterprises (SMEs) [4] and it is performed through three types of business models:

1. The development of a nanotechnology platform that can be used to add value to second-party products: this business model seems to be particularly attractive for drug delivery companies, which typically license their particular technologies out to pharmaceutical industries. Otherwise the drug delivery system is tailored and applied to a specific drug complying the particular instructions of the larger company. [4]

2. The development and manufacturing of high-value materials for the medical device and pharmaceutical industry: several start-ups and SMEs merely provide nanomaterials for the manufacture of medical devices or nanotechnology-enhanced drugs. [4]

3. The development of nanotechnology improved medical devices or pharmaceuticals: companies adopting this business model intend to develop a proprietary product pipeline as well as trying to bring to the market place new or standard drugs delivered with a drug delivery system or else to develop, for example, a new diagnostic platform based on nanotechnologies. [4]

5. Regulatory Risk

The U.S. Food and Drug Administration's long approval procedure and regulations make nanomedicine products different from those of other industries using nanotechnologies with no limitations due to regulatory bodies. As a consequence, the expenditure to bring a nanomedical product to the marketplace is so huge that pharmaceutical and biotechnology industries have no alternative but focus on the blockbusters that can please the stockholders. [3] Nanoparticles are not inevitably hazardous, but they have unique properties that question their safety. It is reasonable to presume that nanomaterials are 'new for safety evaluations purposes' [3], and therefore they merit careful regulatory oversight by FDA both before and after entering the marketplace. In this arena, federal agencies like the FDA and the U.S. Patent and Trade Mark Office (PTO), impose a sort of order, for the protection of the population safety, while encouraging the development of these products.

The advent of nanomedicine, besides causing changes in the biopharmaceutical industries' business model and value chain, brought two crucial regulatory issues: difficulties in product classification and a lack of scientific expertise on the part of the FDA. [19]

On the basis of the product's principal method of action the FDA classifies nano-products as drugs, devices, or combination thereof. For regulatory purposes the FDA applies the same requirements to each part of the combination product and verifies whether the manufacturer gave the correct definition to the product. The definition becomes extremely ambiguous novel for nano-based drug delivery devices as they can be considered either devices (carriers) or drugs (effectors). [20] [21] The FDA will face exceptional challenges in efficiently regulating such products. In order to successfully do so, a strong scientific knowledge of

the field is essential together with a better understanding of the potential risk associated to the exposure of patients to nanomedical products. [21]

6. Best practices in the Clinic

Bringing new products to the market has always represented a great challenge, especially when it comes to highly innovative products with high risk/high return. Despite the numerous entry barriers of the nanomedicine market, there are some noteworthy examples of nano-based, FDA-approved products that successfully reached the market, impacting medicine and anticipating a change in the healthcare arena.

Within the anticancer products segment, DoxilTM and AbraxaneTM are two main examples of success in the clinic. Sequus Pharmaceutical was the first company to sell Doxil, the liposomal formulation of Doxorubicin, a powerful but toxic chemotherapic, initially approved for treatment of Kaposi's sarcoma in the USA in 1995. [22] Sequus was then acquired in 1998 by ALZA Pharmaceutical for US $580 millions [23], which subsequently merged with Johnson and Johnson in 2001 in a US $12.3 billions deal. [23] The other approved nano therapeutic agent, Abraxane, instead, was originally sold by Abraxis Biosciences, which was acquired in June 2010 by Celgene Corporation for US $2.9 billions. [24] Granted by the orphan drug designation in January 2005 by the FDA, this product consists of albumin nanoparticles containing paclitaxel, and is indicated for the treatment of breast cancer [22]. Conventional chemotherapies consist of injections of cytotoxic drug intravenously, which indiscriminately kill both healthy and tumor cells. The clinic success of Doxil™ and Abraxane™ was driven by their ability to concentrate preferentially in tumors, because of the gaps (otherwise called endothelial fenestrations) characterizing the blood vessels that supply the cancerous mass. Nanoparticles of the right size can penetrate these "gates" and passively

diffuse into the tumors. [25] Thanks to this generation of chemotherapies, patients are now benefiting from new treatment strategies for delivering drugs through nanotechnology carriers with lower systemic toxicity and improved therapeutic efficacy. [22]

The economic success of these nanomedical products is driven by an urgent demand of new anticancer therapies able to better fight this highly aggressive and increasingly frequent disease. In fact, the FDA problematic regulatory process, the unsteady funding situation, and the expensive and lengthy R&D process did not thwart the development and success of Doxil™ and Abraxane™.

Despite being the most profitable, anticancer delivery systems are not the only clinically approved nanomedical products. In fact, advances in nanomedicine are bringing breakthroughs in other problematic areas of medicine. Following are some examples of successful nano-enabled biomedical products currently on the market.

The first successful application of nanoparticles in the clinic was Omniscan™, the leading injectable paramagnetic resonance product of Amersham. This contrast agent was approved for Magnetic Resonance Imaging (MRI), launched in 1993, and utilized ever since both in neurology, to detect strokes and brain tumors, as well as in cardiology. This contrast agent - originally developed by Salutar – has prolonged half-life in patients with renal insufficiency. After the conduction of pre-clinical testing, Salutar was acquired by Nycomed, which in turn purchased Amersham International, in 1997. Currently, Amersham and its rights on Omniscan are propriety of General Electric Healthcare. The deal was closed in 2003 for US $9,5 Billions on an all-stock transaction. According to G.-P.Yan et al. (2007) [26] and as confirmed by Spiess (2011) [27], there are 12 different MRI contrast agents currently on the market. [28]

Magnevist™ was marketed by Bayer Schering Pharma as their first intravenous contrast agent employed in the clinic. In 2004, the company demonstrated that the product safely and effectively eases the visualization of cranial and vertebral anatomy among cancers and wounds and since then it is diffused worldwide with that specification of use. [29]. Another competitor is OptiMARK™, a gadolinium-based contrast agent (the only FDA-approved for administration by power injection) for MRI of brain, liver and spine. [30] Produced by Mallinckrodt, it allows the visualization of lesions with atypical vascularity. Finally, Multihance™ is the first extracellular fluid contrast agent to posses interaction with plasma proteins. Bracco Group produces this contrast agent – an Italian company specialized in diagnostic imaging, drugs and devices – and is utilized in diagnostic MRI of the liver and Central Nervous System (CNS). It was launched in Europe in 1998, and received the FDA approval for market the product in the United States in 2004. [31]

Returning to the segment of the pharmaceutical applications of nanomedicine, it is important to remember the two FDA-approved nanoparticles-based drugs applied for the treatment of severe fungal infections: AmBisome™ (liposome for injection), sold by Gilead Sciences and Fujisawa Healthcare and Abelcet™,(lipid complex), marketed by Elan Corporation. Liposomal formulation of amphotericin B (AmBisome™, in its trade name) was originally one of the income-making drugs of NeXstar Pharmaceuticals. The company, along with its products portfolio, was then acquired by Gilead in March 1999. For what concern Abelcet™ (the conventional amphotericin B), its North America rights were acquired by Enzon Pharmaceuticals in 2002, in an operational and profitable deal of $360 million (including facilities and operating assets related to the development, production and sale of the drug). The drug was employed in the treatment of patients with aggressive fungal infection associated to

cancer, organs transplantation and other postsurgical complications. [32] We wanted to emphasize theses two specific products also because they have been subject of a "pharmacoeconomic study". As a result of the analysis, that involved the two drugs in the empirical treatment of persistently febrile neutropenic patients with presumed fungal infection, AmBisome™ was found to be more cost-effective compared to Abelcet™. [33]

RenaZorb™, sold by Spectrum Pharmaceuticals, represents another case of a nano-enabled product, which fruitfully reached the marketplace for the treatment of Hyperphosphatemia in End Stage Renal Disease (ESRD) and potentially Chronic Kidney Disease (CKD). RenaZorb™ is a lanthanum-based phosphate-binding agent currently in clinical trial, utilizing Spectrum's proprietary nanoparticle technology. [34] The economic and clinical success of this nanoparticle is mainly driven by the clinical scenario. According to the National Kidney Foundation., only in the U.S are estimated to be more than 20 million people with CKD with numbers expected to double over the next decade. These patients live on kidney dialysis, and are potential candidates for phosphate binder therapy. [35]

In the light of all this overview of the best practices in the clinic, anticancer remains the biggest share of the nanomedicine market, besides for number of publications and patents, also for number of commercialized products. Increasing acceptance with the general public of the employment of nanotechnologies in the clinic, along with popular widespread sensitivity for the aggressiveness of cancer can be considered strong drivers for the commercial success of this segment. Furthermore, the first tangible considerable returns due to commercial triumphs, represent an undoubted source of attraction for investors. On their part, financiers must realize the importance of providing the

substantive funds, necessary to gain the solid results and successful drugs as well as devices and therapies the market requires. The effective investments on Doxil™, Abraxane™, as well as on the other mentioned successful products are prime examples of this practice.

7. Conclusions and Future Promises

Despite the issues nanomedicine still has to face, investments in this market are predicted to increase. New applications of nanomedicine have been demonstrated and the resulting expansion of the potential market makes the risk more appealing. Ferocious financial collapse elevated sunk costs of the essential R&D process, tricky access to funds, uncertainty of expected returns, and the extremely meticulous and lengthy FDA regulatory process have not deterred the investors' community. On the other hand, the promises of great future potential developments in the different market segments and high returns connected to the high risk of the innovation investments make this market still considerably attractive. Compared to the 2007 benchmark, VCs in 2009 decided to double their investments in this sector, at the expenses of the information technology market. The fact that nanomedicine dominates the VC fundings in the healthcare market is surely a good predictor of the bright future landscape of expansion of this promising area of research.

Moreover, good returns could even be the result of more accurate assessments of the investments' risks. A pharmacoeconomic analysis would allow the efficient allocation of the monetary resources and the maximization of the highest health return at the lowest costs. A cost-effectiveness analysis (CEA) is structured with a comparison of the costs and effects of two or more treatments, which are under examination. Whereas in the very early stage of the drug development cycle the high failure rate for novel drug molecules is largely due to a not adequate

therapeutic index, in the clinical development phase, this rate originates from economic reasons. Therefore, the development of unsuccessful drugs has to be abandoned very fast, in order so save resources for more promising compounds. This saving is obtained through an accurate economic evaluation performed in the early stages of the development process. The benchmark is represented by life-years saved by the investigated nanotherapeutic; if a nano-enabled therapy does not save sufficient life-years to break-even, it should not be developed further. [36]

The major limit to the success of this kind of analysis is given by the scarcity of clinical data concerning nanomedicine. The best solution to this issue is collaboration. According to Bosetti and Vereeck, [36] economists and investors specialized in health market should work closely with healthcare providers, researchers, patients associations, doctors and technologists of all kinds, to creating a shared platform able to facilitate communication between parties with the ultimate aim to reduce the high risks associated to investments in nanomedicine. As a result, also patients will benefit from these investments, in terms of innovative techniques, therapies, devices and drugs designed to extend and improve their lives.

References

[1] Bethesda NC. National Cancer Institute. NCI Alliance for Nanotechnology in Cancer: Understanding Nanotechnology. In Learn About Nanotechnology ed. Institute, 2010.

[2] Pitzer JW, Sun S, Kumar S, Valluri V. Nanotechnlogy 2.0. Credit Suisse Report; 2008.

[3] Flynn T, Wei C. The pathway to commercialization for nanomedicine. Nanomedicine 2005;1(1):47-51.

[4] Wagner V, Hüsing B, Gaisser S. Nanomedicine - Drivers for Development and possible impacts. In: BOCK Anne-Katrin, editors. Joint Research Centre, European commission; 2008.

[5] Nanotechnology in Medical Applications: The Global Market, BCC Research Report; 2010

[6] Lerner J, Hall BH. The Financing of R&D and Innovation. In: Hall, BH, Rosenberg R editors. Handbook of the Economics of Innovation. Elsevier; 2010.

[7] Mansfield E, Schwartz M, Wagner S. Imitation Costs and Patents: An Empirical Study. Economic Journal 1981; 91: 907-918.

[8] Admati AR, Pfleiderer P. Robust financial contracting and the role of venture capitalist. Journal of Finance 1994;49(2).

[9] Hellmann T. The Allocation of control rights in venture capital contracts. The Rand Journal of Economics 1998;29(1):57-76.

[10] Neher DV. Essay on entrepreneurial finance: venture capital, financial contracting and the structure of investment. Ph.D. Dissertation, Princeton University 1994.

[11] Arnone M, Giacometti U. Crescita, innovazione tecnologica e mercato dei capitali: il ruolo del Venture Capital. Quaderno Istituto Regionale di Ricerca della Lombardia (IRER), Collana Sintesi, n.18; 2000.

[12] Gompers PA, Xuan Y. Bridge Building in Venture Capital-Backed Acquisitions. Harvard Business School; 2009.

[13] Baker M, Gompers PA. The Determinants of Board Structure at the Initial Public Offering. Journal of Law and Economics 2003;46(2):569-598.

[14] Baysinger BD, Butler HN. Corporate Governance and the board of directors: performance effects of changes in board composition. Journal of Law, Economics and Organization 1985;1(1):101-124.

[15] Nano Materials Intelligence - Nanotechnology Corporate Strategies. Lux Research Inc Report 2008.

[16] Burrill GS. Analysis for PhRMA based on publicly available data. Burrill and Company Report; 2009.

[17] Spinverse Capital and Consulting. Venture Capital in Nanotechnology. Observatory Nano, Economic Report; 2010.

[18] Thornton E, Jespersen F. Drug, Biotech Research Spending Hangs Tough. Business Week 2009,

[19] Sanhai WR, Sakamoto JH, Canady R, Ferrari M. Seven challenges for nanomedicine, Nat Nanotechnol, 2008;3(5):242-244.

[20] Food and Drug Administration, classification of nano-products, www.fda.gov.

[21] Miller J. Beyond Biotechnology: FDA Regulation of Nanomedicine. Columbia Sci Technol Law Rev 2003;4:E5.

[22] Sakamoto JH, van de Ven AL, Godin B, Blanco E, Serda RE, Grattoni A, Ziemys A, Bouamrani A, Hu T, Ranganathan SI, De Rosa E, Martinez JO, Smid CA, Buchanan RM, Lee SY, Srinivasan S, Landry M, Meyn A, Tasciotti E, Liu X, Decuzzi P, Ferrari M. Enabling individualized therapy through nanotechnology. Pharmacological Research 2010;62(2):57-89.

[23] Alza Boots Oncology with $580M Sequus Acquisition, Press Release.

[24] Celgene Corporation (CELG) to acquire Abraxis BioScience Inc. (SBIX) for $2.9 Billion, Press Release.

[25] Ferrari M. Beyond Drug Delivery. Nature Nanotechnology 2008;3:131-132.

[26] Yan GP, Robinson L, Hogg P. Magnetic resonance imaging contrast agents: Overview and perspectives. Radiography 2007;13(1):e5ee19.

[27] Spiess R. Magnetic nanoparticles as contrast agents for MRI; 2011.

[28] Companies histories and profiles. Amersham, PLC, Available at www.fundinguniverse.com.

[29] Gadopentetic acid, Definition available on wikipedia.com.

[30] The buyer's guide for medical professionals, Optimark. Available at: Medcompare.com.

[31] Bracco Diagnostic, Inc. and health trust purchasing group sign a three-year agreement for contrast media. Business Wire; 2007. Published on AllBusiness.com.

[32] ENZON Pharmaceuticals, Press Releases; 2002.

[33] Gilead Press Releases. Available at the company's web site: www.gilead.com.

[34] Spectrum. Product pipeline, RenaZorb. Available at: www.sppirx.com/renazorb.

[35] National Kidney Foundation, Available at www.kidney.org.

[36] Bosetti R, Vereeck L. Future of nanomedicine: obstacles and remedies. Nanomedicine 2011;6(4):747-755.

General Summary

Alessandro Tocchio[1,2]

[1]Fondazione Filarete, Viale Ortles 22/4, 20139 Milano, Italy; [2]SEMM, European School of Molecular Medicine, Campus IFOM-IEO, Via Adamello 16, 20139 Milano.

In this work, customizable biocompatible hydrogels were combined with innovative fabrication approaches to engineer scaffolds with controlled chemical, mechanical and biological features and a hierarchical three-dimensional architecture. The abilities of these scaffolds to supply nutrient perfusion and mass transport, and to promote in vitro vascularization in large constructs are evaluated and discussed in detail.

An introduction to the thesis and the relevant scientific background regarding this study is given in the **Chapter 1.**

In **Chapter 2** the design of novel biocompatible poly(amidoamine) (PAA) based hydrogels with wide and controlled degradation rate and improved mechanical and biological properties for biomedical applications is presented. Poly(amidoamine) (PAA) hydrogels containing the 2,2-bisacrylamidoacetic acid-4-amminobutyl guanidine monomeric unit have a known ability to enhance cellular adhesion by interacting with the RGD-binding $\alpha V\beta 3$ integrin, expressed by a wide number of cell types. The scientific interest on this class of materials has been traditionally hampered by their poor mechanical properties and restricted range of degradation rate. Here, we present the design of novel biocompatible,

RGD-mimic PAA-based hydrogels with wide and tunable degradation rate as well as improved mechanical and biological properties for biomedical applications. This is achieved by radical polymerization of acrylamide-terminated PAA oligomers (OPAA) both in presence and absence of 2-hydroxyethylmethacrylate (HEMA). The degradation rate is precisely tunable by adjusting the PAA oligomer molecular weight and the acrylic comonomer concentration in the starting reaction mixture. Cell adhesion and proliferation tests on Madin-Darby Canine Kidney (MDCK) epithelial cells show that PAA-based hydrogels have the capacity to promote cell adhesion up to 200% compared to the control. Mechanical tests show higher compressive strength of hydrogels containing acrylic chain compared to traditional PAA hydrogels. The results presented in this study indicate that these PAAs hydrogels are excellent biomaterials for the fabrication of tissue engineering scaffolds.

PAA hydrogels were further investigated in **Chapter 3** to design a novel photopolymerizable matrix for three-dimensional cell encapsulation and microfluidic applications, needed for later stages of this work. To this aim a novel triblock copolymer (OAPAO) is synthesized by conjugating Jeffamine® and RGD-mimic diacryl amide-terminated poly(amidoamine) oligomers (OPAA), described in Chapter 2, through a simple polyaddition step. The hydration, mechanical and degradation properties of OAPAO were demonstrated to be tunable through modification of macromonomers' molecular weight and concentration. OAPAO bulk hydrogels were tested with NIH 3T3 murine fibroblast and human umbilical vein endothelial cells (HUVECs), showing the ability to strongly promote cell adhesion and proliferation. OAPAO hydrogel was used for encapsulation of murine fibroblasts to form cell-laden hydrogels. Encapsulated cells showed viability and proliferation similar to the one embedded in agarose gels. High pattern fidelity and resolution of OAPAO

were demonstrated in the fabrication of perfusable microfluidic channels. Overall, these studies support the use of OAPAO hydrogels as tunable and inexpensive biomaterials for the creation of complex cell-laden microengineered constructs.

In order to recreate the complex microarchitecture of natural extracellular matrix, open cell macro porous foams of PAA hydrogels were fabricated, as described in **Chapter 4**. RGD-mimic OPAA oligomers, described in Chapter 2 and 3, were cross linked via free radical polymerization, using ammonium persulfate as initiator, and ammonium bicarbonate as foaming agent, obtaining solid scaffolds with optimal hierarchical porosity and roughness. The capacity of PAA foams to promote cell adhesion and proliferation in 3D-cell culture has been evaluated in vitro for HUVECs. Biocompatibility and the capacity to promote cell migration inside OPAA foams were demonstrated through subcutaneous implant in murine model. The extensive screening of the biological, chemical and mechanical properties demonstrated that OPAA foams are able to support and enhance three-dimensional cell growth and can be considered an optimal scaffold for soft tissue engineering.

In **Chapter 5** the development of innovative fabrication approaches to engineer scaffolds with a perfusable microfluidic network is presented. Branched microfluidic networks were embedded within hydrogel matrices through an innovative method based on sacrificial templates. Results demonstrated that perfused microfluidic networks are able to sustain the cell viability of murine fibroblasts in the core of hydrogel cell-laden constructs. These microfluidic networks, when seeded with endothelial cells and perfused in customized perfusion bioreactor are able to form one-layer tubular endothelium hierarchically branched as a vascular network. This innovative approach was demonstrated to be suitable for the creation of densely populated vital tissue constructs with perfusable

branching vascular channels. Compared to other methods, it represents a progress in manufacturability and scalability, being compatible with a wide range of synthetic and natural biomaterials, crosslinking strategies and polymerization reaction.

In **Chapter 6**, there is a general review of the results obtained in this work. In this chapter we conclude that combination of customizable PAA hydrogels with innovative fabrication approaches, to control the 3D scaffold architecture and mass transport dynamics, create a technological platform able to give a viable solution to the vascularization problem in tissue engineering, as originally aimed in this thesis work. We forecast that this combined strategy will allows new scenarios towards the engineering of thick and complex soft tissues.

APPENDIX A explores issues involved in technology transfer of nanomedicine products. A detailed analysis of market, competitors and investors in the sector has been performed, further supported by one-to-one interviews to both American and European market experts. This overview aims to help scientists, startup mangers and investors to understand the key dynamics and successful cases in the transfer of nanotechnology in medicine.

Acknowledgments

Resume

Alessandro Tocchio was born on the 30th of March 1982, in Milan (Italy). His educational background includes a Bachelor and a Master of Science in Physics Engineering from the Politecnico of Milan, with focus on nanotechnology, completed with final dissertation on magnetic nanoparticles for biomedical applications, prepared at the CVUT in Prague. Before completing his academic career, Alessandro also worked as a junior investment analyst at a private equity firm in Milan, to explore the financial milieu. Since 2009, he is working as a researcher at Fondazione Filarete in Milan, developing innovative technologies for regenerative medicine applications. From January 2010 he is attending a PhD program in medical nanotechnology of the European School of Molecular Medicine (SEMM). During his Ph.D. study, Alessandro worked under the supervision of Prof. Paolo Milani and Cristina Lenardi. The results of his research are presented in this thesis.

During his scientific career, Alessandro published three peer-reviewed scientific articles and he currently has two patents. In summer 2012, he attended the Graduate Study Program of Singularity University at the NASA - AMES Research Center in California, sponsored by the University itself. In 2012, Alessandro founded Tensive, as a spin-off of Fondazione Filarete. Tensive exploit the know-how and the technologies presented in this work to develop innovative prosthesis for the treatment of large human tissue defects. Tensive have been awarded with several prizes. Among others there are the Best business idea of the Milan area and in Life Sciences at Start Cup Milano Lombardia (2011) and the First Place (Hardware and Computing) at Intel Global Challenge 2013, held at the Haas School of Business - UC Berkeley.